WASHINGTON UNIVERSITY

SEVER INSTITUTE OF TECHNOLOGY

HEAT AND MOMENTUM TRANSFER FROM COMPRESSIBLE TURBULENT JETS OF HOT AIR IMPINGING NORMALLY ON A SURFACE

BY

John Frederick Tomich

Prepared under the direction of Professor E. Weger

A dissertation presented to the Sever Institute of Washington University in partial fulfillment of the requirements for the degree of

DOCTOR OF SCIENCE

January, 1967

Saint Louis, Missouri

WASHINGTON UNIVERSITY

SEVER INSTITUTE OF TECHNOLOGY

ABSTRACT

HEAT AND MOMENTUM TRANSFER FROM COMPRESSIBLE TURBULENT JETS OF HOT AIR IMPINGING NORMALLY ON A SURFACE

by JOHN FREDERICK TOMICH

ADVISOR: E. WEGER

January, 1967

Saint Louis, Missouri

The results of an analytical and experimental study of the heat transfer from the normal impingement of compressible, turbulent jets are presented. A technique for calculating heat flux distributions in the impingement region has been developed, and the calculated results are compared with the measured experimental data. The theory for heat transfer from uniform impinging flows has been adapted to calculate heat fluxes in the stagnation area of an impinging jet, and a solution of the integral momentum boundary layer equation has been used for the calculation of heat fluxes in the remainder of the impingement region. The solution is general enough so that compressible

flows with variable wall surface temperatures can be treated. The static pressure distribution and boundary layer thickness in the impingement region have also been calculated. Calculated heat flux and static pressure distributions agree well with the experimental data of the present study.

Since knowledge of the free jet velocity and temperature variation is needed for the impingement region calculations, and since no general computational techniques were available for free jet calculations, a finite difference technique has been developed to obtain a general solution which eliminates the need for the simplifying assumptions required in previous investigations. The jet Mach number and jet temperature ratio have been found to be the only two initial jet properties which are necessary to characterize the dimensionless velocity and temperature variation in the free jet. Modifications of "dynamic eddy transfer coefficients" given in the literature are used in this free jet solution. The numerical solutions of the turbulent, free jet conservation equations have been found to agree well with experimental data of the present study and those of previous investigations.

An experimental program was carried out to obtain data on the free jet velocity and temperature variation, on the impingement region heat flux and static pressure distributions, and on the wall jet velocity and temperature variation, as few data had been obtained in these areas by previous investigators.

TABLE OF CONTENTS

TABLE OF CONTENTS
(continued)

TABLE OF CONTENTS
(continued)

TABLE OF CONTENTS
(continued)

LIST OF TABLES

LIST OF FIGURES

LIST OF FIGURES
(continued)

LIST OF FIGURES
(continued)

HEAT AND MOMENTUM TRANSFER FROM COMPRESSIBLE TURBULENT JETS OF HOT AIR IMPINGING NORMALLY ON A SURFACE

1. INTRODUCTION

1.1 GENERAL

A good calculational method for estimating the impingement region heat flux to the surface upon which a jet of hot or cold gas impinges is greatly needed since jets are used in many heat transfer applications to provide high heat fluxes. The use of jets is attractive because they are low in cost and easy to control. Applications of impinging jets include their use in paper drying, tempering of glass, heating metal ingots, and annealing non-ferrous sheet metals. Jets are also important in aerospace technology, and methods for accurately predicting the characteristics of both free and impinging jets are needed for such applications as the testing of heat shield materials, the contacting of gas streams for the purpose of energy, momentum, or mass exchange, and calculation of the region occupied

by jet or rocket exhausts. While some research has been done on the prediction of heat fluxes from low temperature, low speed, impinging jets, almost no work has been done on the estimation of heat fluxes from high temperature, compressible jets. Methods of calculating heat fluxes from impinging jets have suffered from the lack of a good general calculational technique for describing compressible free jet characteristics. Therefore, any analysis of the compressible impinging jet must include a good computational method for predicting velocity and temperature distributions in compressible free jets.

In the impinging jet flow considered here, the flow from the cylindrical nozzle impinges normally on the flat plate. This is shown schematically in Figure 1; the nomenclature is listed in Appendix 9.1. The flow field can be considered as consisting of three separate flow regions -- the free jet region, the impingement region, and the wall jet region.

The free jet region is the region where the flat plate has no disturbing effect on the flow. In the free jet region, the static pressure is, for subsonic jets, very nearly equal to the ambient pressure (1)*. The second

*The numbers in parentheses indicate references in the Bibliography.

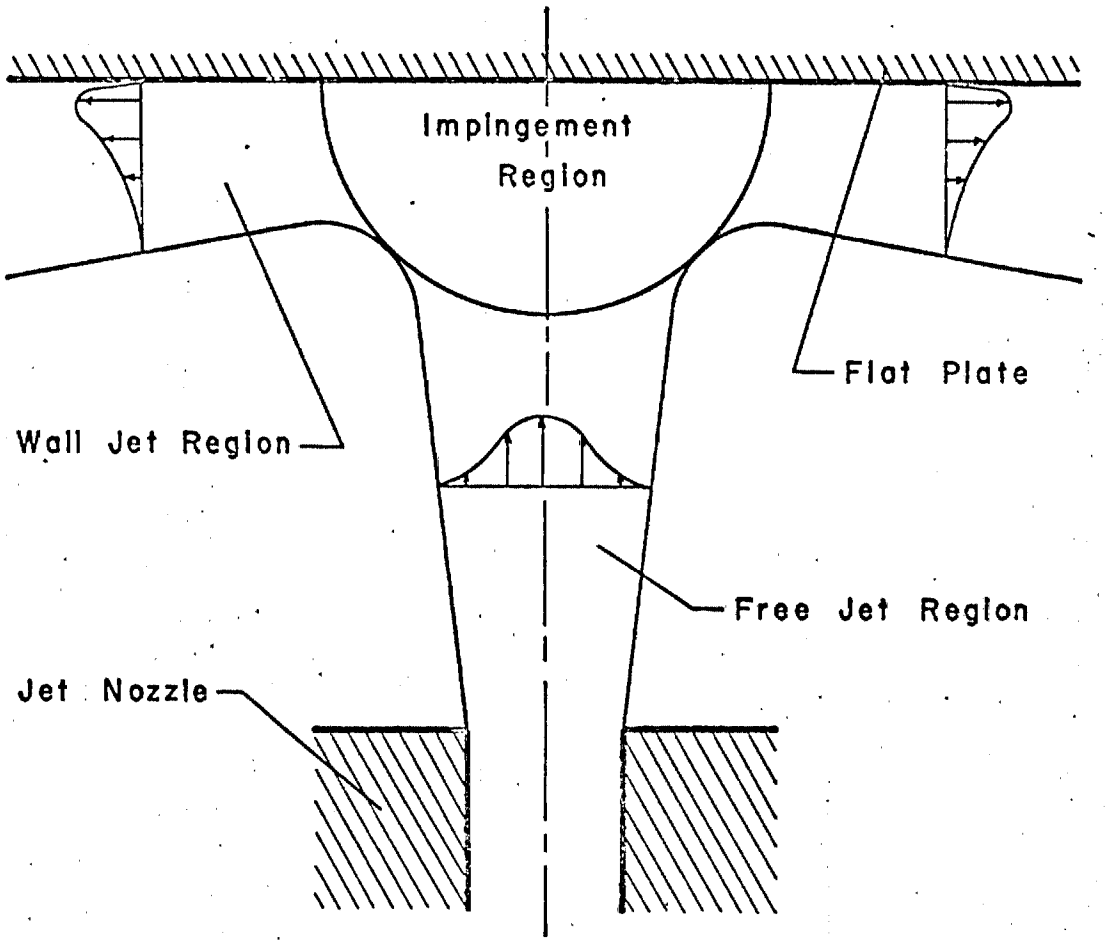

Figure 1

SCHEMATIC DIAGRAM OF IMPINGING JET

flow region is the impingement region. In this region, the flow properties are determined primarily by the direct interaction of the jet and the flat plate. The impingement region is a region where the static pressure is greater than the ambient pressure and where the flow direction changes rapidly. When the flow streamlines are approximately parallel to the surface of the flat plate and the static pressure is again very nearly equal to the ambient pressure, the flow has entered the wall jet region. In this region the flow is essentially that of a radial wall jet. Thus an impinging jet may be considered to be a free jet transforming into a wall jet in the impingement region.

1.2 RESEARCH OBJECTIVES

The primary objective of the present study was to develop a calculational method for the prediction of impingement region heat transfer from high temperature, turbulent, impinging jets. In order to achieve this objective, it was necessary to determine the velocity and temperature variation of compressible free jets. Therefore, a second objective was to develop a calculational technique for a simple yet very general solution to the boundary layer conservation equations for a compressible, turbulent, free

jet. A third objective was to design and build the equipment for an extensive experimental study of compressible impinging jets of high temperature and Mach number and to obtain the experimental data required to evaluate the results of the analysis. In addition, experimental data were to be taken on the velocity and temperature variation in the wall jet region.

2. THE FREE JET REGION ANALYSIS

2.1 INTRODUCTION

In order to predict heat fluxes in the impingement region of a compressible, axially symmetric, turbulent impinging jet, it was necessary to first develop a good, general solution for velocity and temperature variation in the free jet. This free jet solution was then used as a starting point for the analysis of the impingement region.

A computational technique, based on finite difference solutions of the boundary layer forms of the momentum and energy conservation equations, was developed to calculate both the axial velocity and temperature decay and the radial variation of velocity and temperature. It is of a more general form than those obtained previously, and its use can be extended to a variety of boundary conditions different than the ones which were applicable in the present work. Good agreement between the calculated results and experimental data from previous investigations as well as the present one has been obtained.

The structure of the compressible, axially symmetric free jet can be described in terms of three flow regions (see Figure 2). The potential core region extends to the

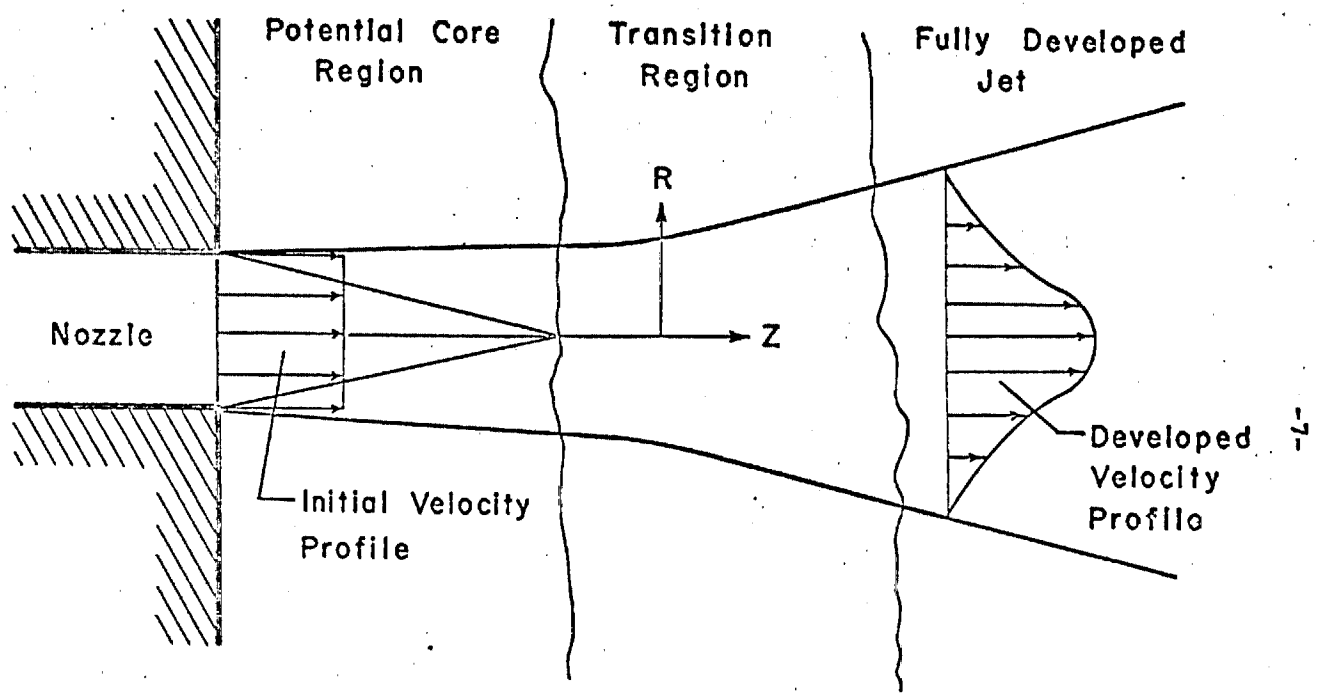

Figure 2

SCHEMATIC SKETCH OF FREE JET

point where the turbulent mixing region reaches the jet axis. This region is, of course, not necessarily identical for velocity and temperature. The next region is a transition region where the spread of the jet in the radial direction and the axial decay of the center-line properties are very rapid. This is followed by the fully developed region where the radial spread of the jet is nearly linear with respect to axial distance. The greater the compressible effects, the greater is the deviation from linearity.

There are many problems which arise in connection with any numerical approach to the problem of solving for temperature and velocity as a function of position in the compressible free jet. One is the non-existence of similarity (2) in the profiles (as distinct from the case for incompressible flow). The model must also take into account the fact that the free jet only becomes fully-developed a certain number of nozzle diameters downstream from the nozzle. Therefore, a complete treatment must include the potential core region and the transition region, as well as the fully developed portion of the jet. The boundary conditions are also a source of difficulty. These include the prescribed conditions at the nozzle (i.e. flat or other types of profiles) and the conditions at an infinite radial

distance (i.e. whether the jet is exhausting into a moving gas stream or into quiescent surroundings).

Because of these problems, most of the available calculational techniques have had to make use of various simplifying assumptions which has limited their usefulness. Much of the work has been restricted to the problem of axial velocity and temperature decay, while the question of the radial variation of these quantities has not been dealt with extensively. Another limitation in previous work has been that, even when non-isothermal systems were being studied, the range of temperatures used in the experimental studies was usually too small to bring out variations in the eddy-transfer coefficients with density. It was the intent of the present study to overcome some of these limitations.

2.2 REVIEW OF THE LITERATURE

Hinze and van der Hegge Zijnen (3), Tollmien (4), Schlichting (5), and others have obtained solutions to the problem of determining the velocity and temperature profiles in incompressible, turbulent free jets. These solutions, however, are somewhat limited in that they do not apply to the region near the nozzle. Solutions for the velocity and temperature profiles in compressible, turbulent jets have been much less numerous than the solutions

for the incompressible case, and they have been just as limited.

Kleinstein (6) presented solutions for the velocity, temperature, and concentration profiles in the fully developed region of a compressible, turbulent free jet. He used the approximate technique of linearizing the boundary layer equations in the plane of the von Mises variables (the stream function and axial distance are the coordinates of the von Mises plane) and then solving these linearized equations. Kleinstein incorporated in his solution a new formulation for the eddy viscosity of a compressible free jet. The solution agreed well with experimental data (2), (7) for the axial decay of axial velocity and temperature. Radial distributions of velocity and temperature, however, were not shown or compared with experimental data. Kleinstein's solution was also restricted to jet flows where the initial velocity and temperature profiles could be represented by step functions.

Pai (8) solved the boundary layer equations in the plane of the von Mises variables by using a finite difference technique. This solution was restricted to a turbulent Prandtl number of unity and the case of a free jet exhausting into a moving external stream. No comparison

was made between the solution and experimental data, probably due to the lack of data for this type of flow.

Warren (7) solved for the axial variation of velocity and temperature in a compressible turbulent free jet exhausting into a media at rest using an integral method. He used "universal" profiles to describe the radial variation of axial velocity in the potential core region and the fully developed jet. Warren also proposed a formulation for the eddy viscosity of a compressible free jet. The solution, which also was restricted to a turbulent Prandtl number of one, agreed fairly well with experimental data except for the transition region.

Szablewski (9) developed an analysis of the core region of a compressible free jet. He used a "similarity" parameter and numerical integration of the boundary layer equations to obtain velocity and temperature profiles, but the solution was restricted to the potential core region. Other investigators have also treated various aspects of the compressible jet problem (1), (10).

2.3 NUMERICAL SOLUTION

In the present investigation, no transformations are made. The solution of the boundary layer equations is obtained by using a variation of a finite difference technique

due to Abbott (11). Solutions are obtained for free jet injection into a medium at rest where initial free jet velocity and temperature profiles are assumed to be step functions. "Dynamic eddy transfer coefficients" are defined for the turbulent compressible flow. These transfer coefficients are modifications of those introduced by Kleinstein (6) and are functions of axial position only.

Although the solution presented here is somewhat restricted because it is derived for specific application to the impinging jet problem, the finite difference technique can be used to describe jets exhausting into a uniform external stream, jets with initial profiles of velocity and temperature of an arbitrary shape, and jets with variable fluid properties. Also, concentration profiles can be obtained, and, as more is learned about the structure of free turbulent shear flows, this finite difference technique can accommodate more advanced formulations of the eddy transfer coefficients which may be functions of both axial and radial position.

A schematic diagram of the free jet showing the coordinate system used is shown in Figure 2. The boundary layer equations for the conservation of mass, momentum, and energy in the turbulent, compressible, axially symmetric free jet

(derived in Appendix 9.2) are:

$$\frac{\partial}{\partial z}(\rho v_z) + \frac{1}{r}\frac{\partial}{\partial r}(r\rho v_r) = 0 \qquad (1)$$

$$\rho v_z \frac{\partial v_z}{\partial z} + \rho v_r \frac{\partial v_z}{\partial r} = \frac{1}{r}\frac{\partial}{\partial r}\left[(r\rho\epsilon_v)\frac{\partial v_z}{\partial r}\right] \qquad (2)$$

$$\rho v_z C_p \frac{\partial t}{\partial z} + \rho v_r C_p \frac{\partial t}{\partial r} = \frac{1}{r}\frac{\partial}{\partial r}\left[(rK)\frac{\partial t}{\partial r}\right] + \rho\epsilon_v\left(\frac{\partial v_z}{\partial r}\right)^2 \qquad (3)$$

The heat capacity and the static pressure are assumed to be constant in the above equations. The assumption of constant static pressure has been shown to be a valid assumption for subsonic free jets (1). All densities, velocities, and temperatures have been time-smoothed for turbulent flow. The boundary conditions for this free jet flow are:

At $z=0$,	$v_z = v_{z_j}$	$r < \frac{D}{2}$
	$t = t_j$	
	$v_r = 0$	
	$v_z = 0$	$r \geq \frac{D}{2}$
	$t = t_a$	
	$v_r = 0$	
At $r=0$,	$\frac{\partial v_z}{\partial r} = 0$	All z
	$\frac{\partial t}{\partial r} = 0$	
	$v_r = 0$	

$$\text{As } r \to \infty, \quad \left.\begin{array}{l} V_z \to 0 \\ t \to t_a \\ V_r \to 0 \end{array}\right\} \text{ All } z$$

Making Equations (1)-(3) dimensionless, they become:

$$\frac{\partial}{\partial Z}(PV_z) + \frac{1}{R}\frac{\partial}{\partial R}(RPV_R) = 0 \tag{4}$$

$$PV_z\frac{\partial V_z}{\partial Z} + PV_R\frac{\partial V_z}{\partial R} = \frac{1}{v_{zj}D}\frac{1}{R}\frac{\partial}{\partial R}\left(RP\epsilon_v\frac{\partial V_z}{\partial R}\right) \tag{5}$$

$$PV_z\frac{\partial T}{\partial Z} + PV_R\frac{\partial T}{\partial R} = \frac{1}{\rho_j v_{zj} D}\frac{1}{R}\frac{\partial}{\partial R}\left(R\frac{K}{C_p}\frac{\partial T}{\partial R}\right) + \frac{v_{zj}}{D(t_j - t_a)C_p}P\epsilon_v\left(\frac{\partial V_z}{\partial R}\right)^2 \tag{6}$$

The transformed boundary conditions are:

$$\text{At } Z = 0, \quad \left.\begin{array}{l} V_z = 1.0 \\ T = 1.0 \\ V_R = 0 \end{array}\right\} R < \frac{1}{2}$$

$$\left.\begin{array}{l} V_z = 0 \\ T = 0 \\ V_R = 0 \end{array}\right\} R \geqslant \frac{1}{2}$$

$$\text{At } R = 0, \quad \left.\begin{array}{l} \frac{\partial V_z}{\partial R} = 0 \\ \frac{\partial T}{\partial R} = 0 \\ V_R = 0 \end{array}\right\} \text{All } Z$$

$$\text{As } R \to \infty, \quad \left.\begin{array}{l} V_z \to 0 \\ T \to 0 \\ V_R \to 0 \end{array}\right\} \text{All } Z$$

For incompressible jets, expressions for the eddy kinematic viscosity have been obtained semi-empirically in terms of parameters of the main jet flow using either Prandtl's constant exchange coefficient theory, von Karman's hypothesis, or Taylor's vorticity theory (5). Solutions incorporating these expressions have agreed well with experimental data. Therefore, the expressions for eddy kinematic viscosity derived using these theories have become generally accepted for the solution of incompressible free jet flows.

For compressible free jet flows, however, the mechanism of the transport phenomena has not been semi-empirically determined, and few empirical formulations have resulted in solutions which compare well with experimental data. Kleinstein (6) has stated that a "dynamic eddy transfer coefficient", $\rho\epsilon_v$, must be used as a measure of the transport phenomena for compressible flows. Furthermore, Kleinstein, using an empirical approach to deduce this result, states that this transfer coefficient is a function of axial

position only. Kleinstein's momentum transfer coefficient is as follows:

$$\rho\epsilon_v = 0.0183\ P_a^{1/2}\ v_{zj}\ \frac{D}{2} \tag{7}$$

Warren (7) in his analysis of the compressible free jet, proposed two expressions for the eddy kinematic viscosity, one for the potential core region and another for the fully developed jet. These expressions were similar to Prandtl's constant exchange coefficient. Warren found, however, that the experimentally determined constant in Prandtl's constant exchange coefficient should be a linear function of the Mach number at the nozzle exit. Warren's momentum transfer coefficients are as follows:

Core region:

$$\epsilon_v = (0.0434 - 0.0069\,M)(r_{1/2} - r_i)\,\frac{v_{zi}}{2} \tag{8}$$

Fully developed jet:

$$\epsilon_v = (0.0434 - 0.0069\,M)\,r_{1/2}\,\frac{v_{zm}}{2} \tag{9}$$

In the present approach, Kleinstein's eddy transfer coefficient has been modified slightly to provide a better agreement with experimental data. The eddy transfer coefficient for momentum is:

$$P\epsilon_v = F(M)\, P_a^{1/2}\, P_m\, v_{zj}\, D\, f_v(Z) \qquad (10)$$

where $F(M) = 0.00954 - 0.00782M + 0.00325M^2$

$$f_v(Z) = 0.2 \text{ for } Z \leqslant Z_{cv}$$

$$= 1.0 \text{ for } Z > Z_{cv}$$

$$Z_{cv} = 4.73\, P_a^{-1/2}$$

Also, if the turbulent Prandtl number is only a function of axial position, the eddy thermal conductivity may be expressed as

$$\kappa = F(M) C_p P_a^{1/2} P_m \rho_j v_{zj} D\, f_t(Z)/N_{Pr}^{(t)} \qquad (11)$$

where $f(t) = 0.2$ for $Z \leqslant Z_{ct}$

$$= 1.0 \text{ for } Z > Z_{ct}$$

$$Z_{ct} = 3.43\, P_a^{-1/2}$$

$$N_{Pr,\,Air}^{(t)} = 1.0 \text{ for } Z \leqslant Z_{ct}$$

$$= 0.715 \text{ for } Z > Z_{ct}$$

These transfer coefficients differ from those of Kleinstein's analysis (6) by the inclusion of P_m, $f_v(Z)$, $f_t(Z)$, and $F(M)$. Kleinstein's coefficients, when used in

the finite difference calculations, result in a solution which does not agree well with data for the axial decay of velocity and temperature. Although Kleinstein defined the extent of the core regions for velocity and temperature (Z_{cv} and Z_{ct} respectively), it is evident that his transfer coefficients are much too large in the core regions, which he did not treat in his analysis. Therefore, $f_v(Z)$ and $f_t(Z)$, which modify the transfer coefficients for the fully developed jet to obtain "average eddy transport coefficients" for the core regions, are included to provide better agreement with axial decay data. Note also that the turbulent Prandtl number in the temperature core region is unity, indicating equal turbulent transport rates of momentum and energy. The turbulent Prandtl number for the remainder of the flow field has been found to be roughly constant and very nearly equal to the laminar Prandtl number (2), (6). An analysis of the shape of the axial decay data showed that the addition of P_m would provide an improved axial variation of velocity and temperature. Warren (7) stated that a function of Mach number must be included in the transfer coefficient expressions if agreement with data over a wide Mach number range is desired. Thus, the best value of F(M) was found for each experimental Mach

number, and a least squares method was then used to obtain F(M) as a second order polynomial in Mach number.

Substituting Equations (10) and (11) into Equations (5) and (6), we have

$$\underline{PV_z}\,\frac{\partial V_z}{\partial Z} + \underline{PV_R}\,\frac{\partial V_z}{\partial R} = A_v\,\frac{1}{R}\,\frac{\partial}{\partial R}\left(R\,\frac{\partial V_z}{\partial R}\right) \tag{12}$$

where

$$A_v = \frac{P e_v}{V_{zj} D} = F(M)\,P_a^{1/2}\,P_m\,f_v(Z) \tag{13}$$

$$\underline{PV_z}\,\frac{\partial T}{\partial Z} + \underline{PV_R}\,\frac{\partial T}{\partial R} = A_t\,\frac{1}{R}\,\frac{\partial}{\partial R}\left(R\,\frac{\partial T}{\partial R}\right) + N_{Ec}\,A_v\left(\frac{\partial V_z}{\partial R}\right)^2 \tag{14}$$

where

$$A_t = \frac{K}{C_p \rho_j V_{zj} D} = F(M)\,P_a^{1/2}\,P_m\,f_t(Z)/N_{Pr}^{(t)} \tag{15}$$

$$N_{Ec} = \frac{V_{zj}^2}{C_p(t_j - t_a)} \tag{16}$$

The finite difference solution used here is a variation of the fully implicit method of Abbott (11) for constant temperature, incompressible, axially symmetric flows. The following finite difference approximations for derivatives at $(Z+\Delta Z, R)$ were used:

$$\frac{\partial V_z}{\partial Z} = \frac{V_z(Z+\Delta Z, R) - V_z(Z,R)}{\Delta Z} \tag{17}$$

$$\frac{\partial V_z}{\partial R} = \frac{V_z(Z+\Delta Z, R+\Delta R) - V_z(Z+\Delta Z, R-\Delta R)}{2\Delta R} \tag{18}$$

$$\frac{\partial^2 V_z}{\partial R^2} = \frac{V_z(Z+\Delta Z, R+\Delta R) - 2V_z(Z+\Delta Z, R) + V_z(Z+\Delta Z, R-\Delta R)}{\Delta R^2} \tag{19}$$

Similar expressions were used for the derivatives of radial velocity, temperature, and density. Another radial derivative form, which was used in the continuity equation in order to make the application of the boundary conditions easier, is as follows:

$$\frac{\partial V_R}{\partial R} = \frac{V_R(Z+\Delta Z, R) - V_R(Z+\Delta Z, R-\Delta R)}{\Delta R} \tag{20}$$

The finite difference approximations were substituted into Equations (4), (12), and (14), which, along with Equations (13), (15), and (16), the equation of state, and the boundary conditions, comprise the system of nonlinear algebraic equations to be solved at each point in the finite difference network (see Figure 3). Also, it is obvious that some radial position, at which velocities and temperatures are essentially equal to those at an infinite radial distance, must be chosen to represent an infinite radial distance in the numerical calculations. This radial position, which varied from 1.25 nozzle diameters near the nozzle exit to

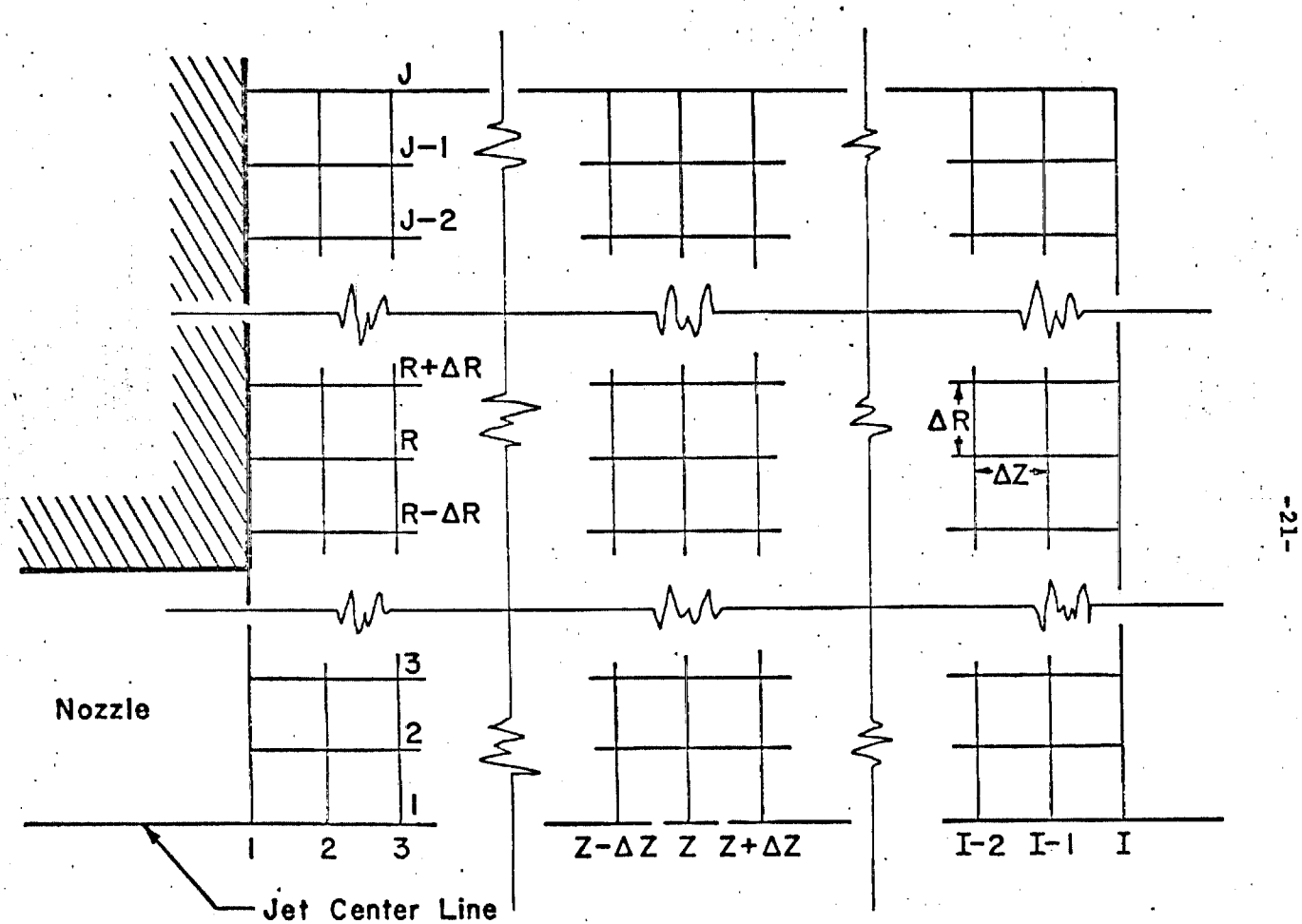

Figure 3

THE FINITE DIFFERENCE NETWORK

25 nozzle diameters for the fully developed jet, was determined by the capabilities of the available computer, an IBM 7072.

The system of algebraic equations was linearized by taking the coefficients (shown as the underlined coefficients in Equations (12) and (14)) of the nonlinear terms at their known value on the previous line of the network or at Z. The resulting system of linear, algebraic equations was solved using Thomas' method (12) for initial values of V_Z, V_R, and T at each point of the line $Z+\Delta Z$. The computational accuracy was then improved using an iterative procedure, and the solution was carried downstream to $Z+2\Delta Z$, etc. Wegstein's method (13) was used to accelerate the convergence of this iterative process.

Near Z=0 smaller step sizes were required (14) to converge to the correct solution than were required further downstream where the gradients were much smaller. The step sizes were increased downstream in order to speed up the numerical solution. The finite difference network in Figure 3 shows only the section of the finite difference network containing the smallest step sizes. A description of the free jet calculational procedure, including the computer program listing, are given in Appendix 9.3.

3. THE IMPINGEMENT REGION ANALYSIS

3.1 INTRODUCTION

A technique for estimating the heat flux distribution in the impingement region of a compressible, turbulent, impinging free jet was developed. In addition, the static pressure distribution on the plate, the thickness of the boundary layer in the impingement region, and the velocity at the edge of the boundary layer were calculated. Although the flow outside the boundary layer is not a uniform flow, the boundary layer concept remains valid since the flow over the plate can be divided into regions: a very thin boundary layer near the wall where friction plays an essential part, and the remaining region outside this layer, where friction may be neglected. The solutions for the compressible, turbulent, free jet were used as a starting point for the computations and the plate surface temperature distribution was used as a boundary condition. Although the number of heat flux measurements in the impingement region was limited by the size of the experimental system, the calculated heat flux distributions agreed well with these measurements. Also, the shape of the heat flux distribution curves agreed with those obtained by previous investigators.

The impingement region can be described in terms of two areas. The stagnation area is the area around the stagnation point where the heat flux is approximately constant. The other area, which comprises the remainder of the impingement region, is characterized by a heat flux which rapidly decreases with increasing radial distance.

The solution for the heat flux distribution in the impingement region is a very difficult problem which could not have been solved without several simplifying assumptions. Even a numerical solution of the partial differential equations describing the flow is not possible without the development of new numerical techniques. Previous solutions have been generally limited to either incompressible flows, constant wall temperatures, or jets with uniform velocity profiles at the entrance of the impingement region. There have also been several attempts to develop expressions containing dimensionless groups to correlate heat flux data. An attempt was made in the present work to make as few assumptions as possible. This will make the technique more generally applicable and useful.

3.2 REVIEW OF THE LITERATURE

Perry (15), Vickers (16), and others have attempted to correlate heat flux data resulting from the impingement of

jets on flat surfaces by using expressions containing dimensionless groups. Although these expressions seem to correlate their data fairly well, their results are only valid for similar experimental systems, and, hence, are quite specific. Perry (15), who studied the impingement of high temperature, turbulent jets, did find evidence of a stagnation area in which the heat flux was approximately constant.

Kezios (17) and Schauer and Eustis (18) have published the only calculational methods for estimating heat flux distributions from impinging jets. Kezios solved the problem of determining the heat flux distribution resulting from the impingement of a cold axially symmetric jet of air on a hot, constant temperature plate. The temperature difference between the plate and the air was of the order of 130°F, and the impinging jet was assumed to have uniform velocity and temperature profiles entering the impingement region. Kezios obtained his solution by using a potential flow solution for impingement region velocity, and then transforming the heat transfer results of two-dimensional, flat plate flows to the axially symmetric case and applying them to the impinging jet flow for equal values of certain dimensionless parameters. Kezios both measured and

predicted a stagnation area in which the heat flux was actually around 5% higher at the outer edge than at the center (the stagnation point).

Schauer and Eustis (18) calculated the heat flux distribution resulting from the impingement of an incompressible, two-dimensional free jet for two separate cases. In the first case, the initial free jet temperature was equal to the ambient temperature, but the plate temperature was not, and in the second case, the plate temperature was equal to the ambient temperature but the jet temperature was not. The linearity of the energy equation in temperature, allowed superposition of these heat transfer solutions. This enabled Schauer and Eustis to obtain a heat flux distribution for the step surface temperature distribution problem. The solution of Schauer and Eustis was restricted to low temperature flows with temperature differences of 20 to 30°F. The incompressible free jet solution of van der Hegge Zijnen (19) was used as a starting point for the heat transfer solution. An analysis, based upon conduction through the laminar sublayer near the wall, was used for the stagnation area. An integral solution of the boundary layer equations combined with Reynold's analogy and a Blasius expression was used for the region outside the stagnation area. Schauer and Eustis'

solution indicated the presence of a stagnation area which was not so sharply defined as those indicated by Perry (15) and Kezios (17).

Several investigators have calculated either the pressure distribution on the flat plate or the potential flow velocity distribution in the impingement region. Snedecker and Donaldson (20) have measured pressure distributions resulting from the impingement of incompressible free jets and correlated parameters of the pressure distributions with free jet data. Strand (21), Slezkin (22), Leclerc (23), Schrader (24), and Tani and Komatsu (25) have obtained potential flow solutions for the impingement of jets with uniform velocity distributions on flat plates.

Kemp, Rose and Detra (26), Fay and Riddell (27) and Lees (28) have solved the laminar boundary layer equations for the stagnation point heat flux resulting from a uniform impinging flow. The results can be applied to the problem of stagnation point heat transfer in dissociated air. Kemp, Rose and Detra and Lees went a step further and used the concept of "local similarity" to obtain solutions in regions away from the stagnation point. The concept of "local similarity" is essentially the joining together of solutions of

the laminar boundary layer equations, each of which is valid over a limited region.

3.3 COMPUTATIONAL TECHNIQUE

In the present investigation, the static pressure distribution on the surface of the plate is calculated by equating the momentum of the free jet with the force exerted on the plate by the pressure distribution. Then, the heat transfer in the stagnation area is calculated by adapting the solution of Kemp, Rose and Detra (26) for heat flux distributions resulting from uniform impinging flows to the case of impinging jets. The velocity at the edge of the boundary layer is calculated from the calculated pressure distribution. Also, the boundary layer thickness is determined by solving the integral momentum equation. The calculated boundary layer thickness and the assumption of similar dimensionless temperature profiles in the boundary layer are then used to calculate the heat flux distribution in the remainder of the impingement region.

3.3.1 The Static Pressure Distribution on the Plate

A schematic diagram of the impingement region showing the coordinate system used is shown in Figure 4.

In order to calculate the static pressure distribution on the surface of the plate, the static gauge pressure at

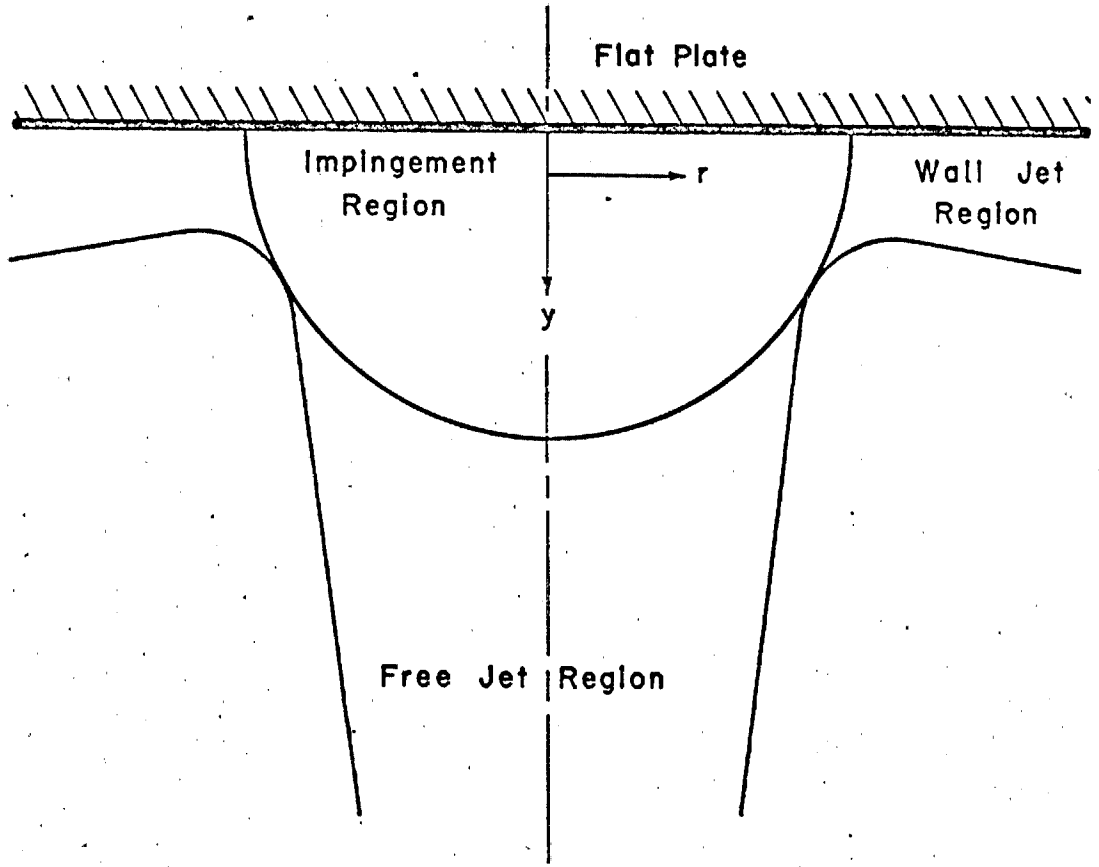

Figure 4

SCHEMATIC DIAGRAM OF IMPINGEMENT REGION

the stagnation point is taken as being equal to the total velocity head pressure that the free jet flow would have at the position of the stagnation point of the plate, or

$$\Delta p_s = \frac{\rho v_z^2}{2 g_c}\Big]_{\substack{y=0 \\ r=0}} = \frac{\rho_j v_{zj}^2}{2 g_c} P V_z^2\Big]_s \tag{21}$$

where P and V_z are obtained from the numerical solution of the free jet flow. Also, note that $y=0$ is equivalent to $z=H$, since $y=H-z$.

Now, a y-direction momentum balance is made over the impinging jet. It should be mentioned that the axial component of the momentum of the free jet flow does not vary with axial distance (2), so that the axial component of the momentum at any axial position is equal to the momentum of the jet at the nozzle exit. Therefore, we have

$$\frac{\rho_j v_{zj}^2}{g_c} \frac{\pi D^2}{4} = 2\pi \int_0^\infty \Delta p \, r \, dr$$

$$= 2\pi r_s^2 \int_0^\infty \Delta p(\xi) \xi \, d\xi \tag{22}$$

where

$$\xi = \frac{r}{r_s} \tag{23}$$

Also, from the experimental measurements, it was determined that the impingement of a fully developed free jet on

a flat plate produced a static pressure distribution which could be correlated by the following expression.

$$\frac{\Delta p}{\Delta p_s} = \exp(-0.694\,\xi^2) \tag{24}$$

The quality of this correlation is shown in Figure 5.

Substituting Equation (24) into Equation (22), we have

$$\frac{\rho_j v_{zj}^2}{g_c}\frac{\pi D^2}{4} = 2\pi r_s^2 \Delta p_s \int_0^\infty e^{-0.694\xi^2}\,\xi\,d\xi \tag{25}$$

The evaluation of the integral and rearranging of the equation gives the following equation for the "half-width" of the pressure distribution.

$$\frac{r_s}{D} = \sqrt{\frac{1.388\,\rho_j v_{zj}^2}{8\,g_c\,\Delta p_s}} \tag{26}$$

With Equations (24) and (26), the static pressure distribution has been predicted entirely from free jet information.

3.3.2 Stagnation Area Heat Flux Distribution

The solution of the laminar boundary layer equations of Kemp, Rose, and Detra (26) for the stagnation area heat flux from uniform impinging flows will now be adapted to the case of an impinging jet.

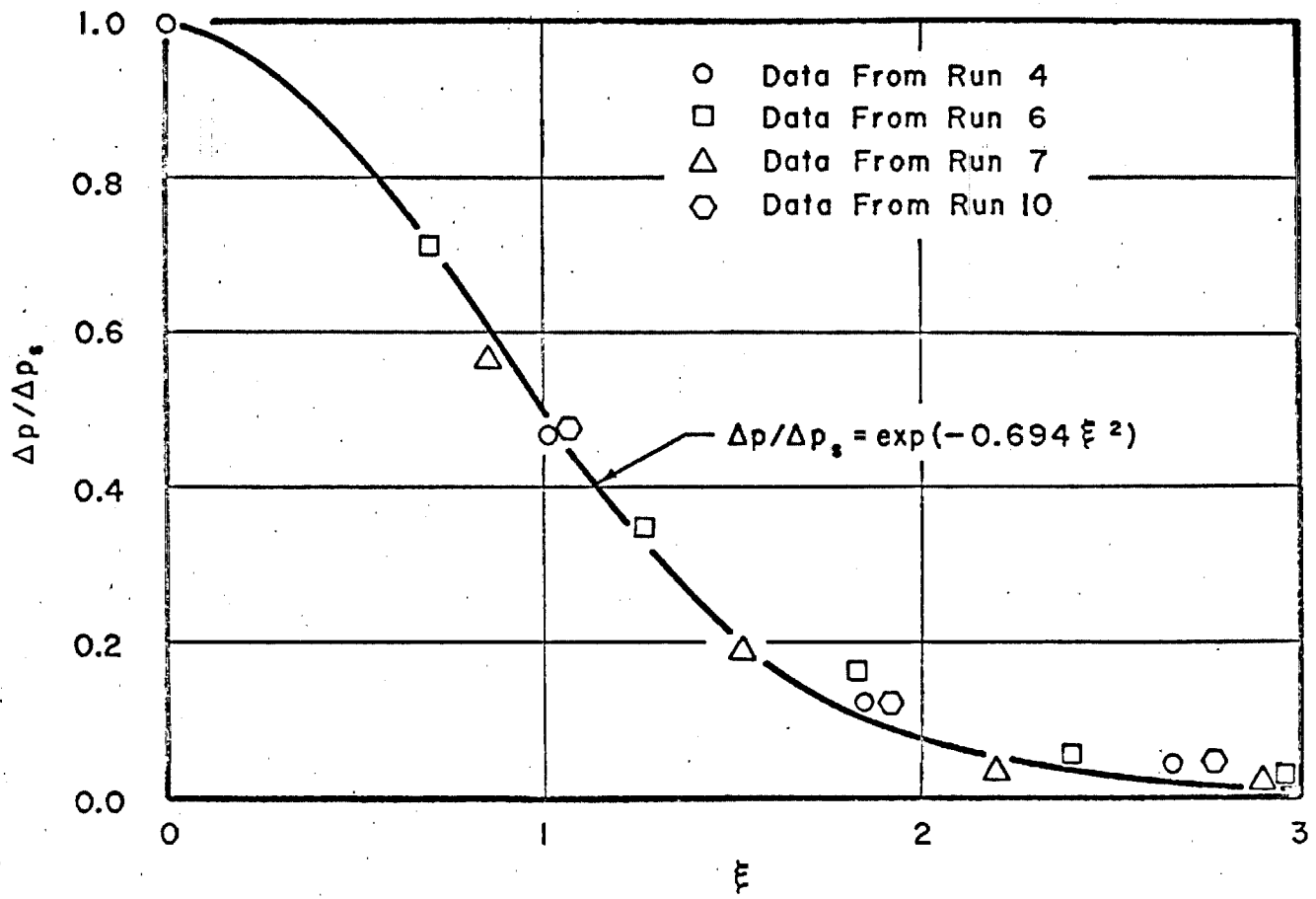

Figure 5

THE CORRELATION OF PRESSURE DISTRIBUTION DATA

Writing the radial component of the momentum equation for the edge of the impingement region boundary layer and neglecting frictional forces, which are small at the edge of the boundary layer, we have

$$\frac{\rho_e V_{re}}{g_c}\frac{dV_{re}}{dr} = -\frac{dp}{dr} \tag{27}$$

Note that we have made the standard boundary layer assumption that the pressure does not vary over the thickness of the boundary layer. Differentiating Equation (27) yields

$$\frac{d^2p}{dr^2} = -\frac{\rho_e V_{re}}{g_c}\frac{d^2V_{re}}{dr^2} - \frac{\rho_e}{g_c}\left(\frac{dV_{re}}{dr}\right)^2 - \frac{V_{re}}{g_c}\frac{d\rho_e}{dr}\frac{dV_{re}}{dr} \tag{28}$$

However, at the stagnation point, we have the condition that

$$V_{re} = 0 \tag{29}$$

Evaluating Equation (28) at the stagnation point, it becomes

$$\left.\frac{d^2p}{dr^2}\right]_s = -\frac{\rho_{es}}{g_c}\left[\left(\frac{dV_{re}}{dr}\right)_s\right]^2 \tag{30}$$

Equation (30) can also be written in terms of the gauge pressure.

$$\left.\frac{d^2\Delta p}{dr^2}\right]_s = -\frac{\rho_{es}}{g_c}\left[\left(\frac{dV_{re}}{dr}\right)_s\right]^2 \tag{31}$$

Or, solving for $\left(\frac{dv_{re}}{dr}\right)_s$, we have

$$\left(\frac{dv_{re}}{dr}\right)_s = \sqrt{-\frac{q_c}{\rho_{es}} \left[\frac{d^2\Delta p}{dr^2}\right]_s} \tag{32}$$

The differentiation of Equation (24) at the stagnation point gives

$$\left[\frac{d^2\Delta p}{dr^2}\right]_s = \frac{-1.388\,\Delta p_s}{r_s^2} \tag{33}$$

Substituting Equation (33) into Equation (32), the derivative of the velocity at the edge of the boundary layer at the stagnation point is

$$\left(\frac{dv_{re}}{dr}\right)_s = \sqrt{\frac{1.388\,\Delta p_s\, q_c}{\rho_{es}\, r_s^2}} \tag{34}$$

At this point, two assumptions will be made. First, it will be assumed that, in the impingement region, the momentum and thermal boundary layer thicknesses are equal. This is essentially stating that both the laminar and turbulent Prandtl numbers are one in this region. Secondly, it will be assumed that the stagnation temperature along the edge of the boundary layer is constant, and is equal to the stagnation temperature of the free jet solution at a position corresponding to the position of the stagnation point

of the plate. This is essentially stating that the flow along the streamline at the edge of the boundary layer is adiabatic. Moreover, because the Mach number at the edge of the boundary layer is relatively small for the calculations to be made, the stagnation temperature at the edge of the boundary layer differs from the static temperature by no more than 20 to 30 degrees F. Therefore, the static temperature will be used in place of the stagnation temperature in these calculations.

Because of the latter assumption, ρ_e can be replaced with ρ_{es} in Equation (27), and the equation becomes

$$\frac{dp}{dr} = -\frac{\rho_{es} v_{re}}{g_c} \frac{dv_{re}}{dr} \tag{35}$$

Writing Equation (35) in terms of the gauge pressure, we have

$$\frac{d\Delta p}{dr} = -\frac{\rho_{es} v_{re}}{g_c} \frac{dv_{re}}{dr} \tag{36}$$

Integrating Equation (36) with the initial condition that, at $r=0$, $v_{re}=0$ and $\Delta p=\Delta p_s$, yields

$$\frac{\rho_{es} v_{re}^2}{2 g_c} = \Delta p_s - \Delta p \tag{37}$$

Substituting Equation (24) into Equation (37) and rearranging, we obtain an expression for the velocity at the edge of the boundary layer versus radial position.

$$V_{re} = \sqrt{\frac{2 g_c \Delta p_s \left[1 - \exp(-0.694 \xi^2)\right]}{\rho_{es}}} \tag{38}$$

The expression developed by Kemp, Rose, and Detra (26) for the heat transfer rate in the stagnation area of a uniform flow impinging on a surface, written for impingement on a flat plate, is as follows.

$$q_w = C_1 \left[1 + 0.096 \sqrt{\beta(r)}\right] \left(\frac{\rho_s \mu_s}{\rho_w \mu_w}\right)^{0.438} \sqrt{\rho_w \mu_w \left(\frac{dV_{re}}{dr}\right)_s} \left[\frac{(h^\circ - h_{ws})}{N_{Pr}}\right] \tag{39}$$

where

$$\beta(r) = 2 \frac{d(\ln V_{re})}{d(\ln \eta)} = 2 \frac{\eta}{V_{re}} \frac{dV_{re}}{d\eta} \tag{40}$$

$$\eta(r) = \int_0^r \rho_w \mu_w V_{re} r^2 \, dr \tag{41}$$

$$C_1 = 0.648$$

In order to adapt this equation to the stagnation area heat flux distribution resulting from the impingement of free jet flows, three quantities in Equation (39) must be determined. First, it is necessary to use Equations (40) and (41) to determine $\beta(r)$. Also, h° is defined as the stagnation point enthalpy of the uniform flow in the solution of Kemp, Rose, and Detra. Since the velocity and temperature on the center-line of the free jet are continually decaying, the stagnation enthalpy of the free jet flow at some specific axial position must be chosen to represent h° in the computations. Finally, the best numerical value of C_1 must be determined for the impinging jet case.

The calculation of $\beta(r)$ is made by making the integration indicated in Equation (41), numerically, using Simpson's Rule (28) to obtain $\eta(r)$. Then, differentiating Equation (38) gives $\left(\frac{dv_{re}}{dr}\right)$.

$$\frac{dv_{re}}{dr} = \sqrt{\frac{2 g_c \Delta p_s}{\rho_{es}}} \; \frac{0.694 \frac{r}{r_s} \exp(-0.694 r^2/r_s^2)}{r_s \sqrt{1 - \exp(-0.694 r^2/r_s^2)}} \qquad (42)$$

Also, Equation (40) may be written in the following manner.

$$\beta(r) = 2 \frac{\eta}{v_{re}} \frac{dv_{re}}{dr} \frac{dr}{d\eta} \qquad (43)$$

Also, from Equation (41) we have

$$\frac{dr}{d\eta} \quad \frac{1}{\rho_w \mu_w V_{re} r^2} \tag{44}$$

Therefore, substituting Equations (38), (42), and (44) into Equation (43), we have an equation for $\beta(r)$.

$$\beta(r) = \sqrt{\frac{\rho_{es}}{2 g_c \Delta p_s}} \frac{1.388 \exp(-0.694 r^2/r_s^2)\ \eta(r)}{[1-\exp(-0.694 r^2/r_s^2)]^{3/2} r r_s^2 \rho_w \mu_w} \tag{45}$$

The substitution of the numerically calculated values of $\eta(r)$ into Equation (45) gives $\beta(r)$.

The value of h° chosen for the calculations was the stagnation enthalpy at a height above the plate equal to the radial length of the impingement region, or at $y = 3.16 r_s$. The radial length of the impingement region is the radial distance where the gauge static pressure is 0.1% of the gauge static pressure at the stagnation point. Choosing the value for h° as the stagnation enthalpy at this height above the plate is essentially assuming that the region of increased static pressure is a hemisphere with the center of its plane circular surface located at the stagnation point. The value of C_1 was determined by minimizing the deviations between calculated and measured heat fluxes and was found

to be 0.703. Now all the quantities needed to calculate the heat flux distribution in the stagnation area are known, and the calculations can be performed by substituting these quantities into Equation (39). Computer programs written to make these computations and a description of the computations are given in Appendix 9.4.

3.3.3 Impingement Region Turbulent Boundary Layer Thickness

The integral momentum equation for the impingement region boundary layer is

$$v_{re}\frac{d}{dr}\left\{\int_0^{\delta_v} r\rho v_r\,dy\right\} - \frac{d}{dr}\left\{\int_0^{\delta_v} r\rho v_r^2\,dy\right\} = rg_c\tau_w + r\delta_v g_c\frac{dp}{dr} \tag{46}$$

The derivation of this equation is given in Appendix 9.5. We now assume a power profile for v_r,

$$\frac{v_r}{v_{re}} = \left(\frac{y}{\delta_v}\right)^{\frac{1}{n}} \tag{47}$$

and a Blasius type wall shear stress relationship

$$\frac{g_c\tau_w}{\rho_w} = 0.025\,v_{re}^2\left(\frac{\nu}{v_{re}\delta_v}\right)^{1/4} \tag{48}$$

For lack of more detailed information, it will be assumed that ρ is only a function of radial position and is equal to ρ_w. Although this is not correct, the error which is

introduced is quite small. The value of both of the integrals in Equation (46) increases about 10 to 15 per cent because of this assumption, but the left side of the equation changes by only 3 to 4 per cent.

Substituting Equations (47) and (48) into Equation (46) and integrating, we obtain

$$\left(\frac{n}{n+1}\right) v_{re} \frac{d}{dr}\left[r \rho_w v_{re} \delta_v\right] - \left(\frac{n}{n+2}\right) \frac{d}{dr}\left[r \rho_w v_{re}^2 \delta_v\right]$$

$$= 0.025 \rho_w r v_{re}^2 \left(\frac{\nu}{v_{re} \delta_v}\right)^{1/4} + r \delta_v g_c \frac{dp}{dr} \qquad (49)$$

The boundary conditions for the calculation of the turbulent boundary layer thickness are that, at the stagnation point ($r=0$), $\delta_v = 0$ and $v_{re} = 0$. These boundary conditions are such that Equation (49) cannot be solved numerically by the Runge-Kutta method (29) in its present form. Although the boundary conditions used are approximations for turbulent flow, their use has been shown to give good agreement in predicting turbulent boundary layer growth (30). Manipulating Equation (49) and defining a new variable,

$$Q = r \rho_w v_{re} \delta_v \qquad (50)$$

we obtain the following ordinary differential equation.

$$Q^{1/4}\frac{dQ}{dr} = (n+1)\frac{Q^{5/4}}{V_{re}}\frac{dV_{re}}{dr} + 0.025\frac{(n+1)(n+2)}{n}\rho_w^{5/4} r^{5/4} V_{re}\nu^{1/4} + \frac{(n+1)(n+2)}{n}\frac{Q^{5/4}}{\rho_w V_{re}^2} g_c \frac{dp}{dr} \quad (51)$$

Reducing the equation still further, we obtain

$$\frac{dW}{dr} = \frac{5}{4}\left\{(n+1)\frac{W}{V_{re}}\frac{dV_{re}}{dr} + 0.025\frac{(n+1)(n+2)}{n}\rho_w^{5/4} r^{5/4} V_{re}\nu^{1/4} + \frac{(n+1)(n+2)}{n}\frac{W}{\rho V_{re}^2} g_c \frac{dp}{dr}\right\} \quad (52)$$

where

$$W = Q^{5/4} \quad (53)$$

Now, Equations (50), (53), (42), (38) and (24) are used in conjunction with a Runge-Kutta numerical solution of equation (52) to obtain the turbulent boundary layer growth in the impingement region. The value used for "n" was determined by Schauer and Eustis (18) to be 3.55. The computer program used to make these calculations and details of the calculations are given in Appendix 9.6.

3.3.4 The Heat Flux Distribution in the Remainder of the Impingement Region

For lack of more explicit knowledge of the location of

the transition from laminar to turbulent flow, the assumption is now made that this transition takes place near the outer edge of the stagnation area. Using this assumption, the growth of the turbulent boundary layer, which was just calculated, will apply in the area of the impingement region outside the stagnation area. Also, retaining the assumption that the momentum and thermal boundary layers coincide in the impingement region, we will assume a power profile for temperature in the impingement region.

$$\frac{t-t_w}{t_e-t_w} = a\left(\frac{y}{\delta_v}\right) + b\left(\frac{y}{\delta_v}\right)^2 + c\left(\frac{y}{\delta_v}\right)^3 + \cdots \qquad (54)$$

If Fourier's heat conduction law is used for the heat flux into the plate, we have

$$q_w = -k \frac{dt}{dy}\Big]_{y=0} \qquad (55)$$

If Equation (55) is written for two radial positions (positions 1 and 2), and if Equation (54) is substituted, the ratio of the two heat fluxes will be as follows.

$$\frac{q_{w1}}{q_{w2}} = \frac{\delta_{v2}}{\delta_{v1}} \frac{(t_e - t_w)_1}{(t_e - t_w)_2} \qquad (56)$$

Now, we will take q_{w2} to be the heat flux at the outer edge of the stagnation area (calculated using Equation (39)) and q_{w1} to be the heat flux at any radial position in the impingement region outside of the stagnation area. It should also be noted here that the extent of the stagnation area remains undetermined at present. Therefore, designating the outer edge of the stagnation area by the subscript "c", the following equation can be written for the heat flux.

$$q_w = q_{wc} \frac{\delta_{vc}}{\delta_v} \frac{(t_e - t_w)}{(t_e - t_w)_c} \tag{57}$$

Using Equation (57), the measured wall temperature distribution, and the calculated boundary layer thicknesses, the extent of the stagnation area was determined, by minimizing deviations from measured heat flux data, to be

$$0 \leqslant \xi < 1.15$$

Schauer and Eustis (18) indicated the extent of the stagnation area to be

$$0 \leqslant \xi < 1.29$$

for their two-dimensional impinging jet solution.

These heat flux calculations were made by the same computer program used for the boundary layer thickness calculations. This program and details of the computations are found in Appendix 9.6.

4. EXPERIMENTAL PROGRAM

4.1 REVIEW OF THE LITERATURE

4.1.1 Free Jet Studies

Velocity and temperature distributions in incompressible, turbulent free jets have been measured by many investigators including Föerthmann (31), Reichardt (32), and Hinze and van der Hegge Zijnen (3). However, there is a lack of experimental data on the variation of velocity and temperature in hot gases at high subsonic Mach numbers. Corrsin and Uberoi (2) obtained experimental data for moderately high temperature, low Mach number flows; while Warren (7) experimentally studied high speed (both subsonic and supersonic) flows at relatively low temperatures. Snedecker and Donaldson (20) have also measured velocity profiles of free jets of cold air at high subsonic and supersonic speeds.

4.1.2. Impinging Jet Studies

Experimental studies of the heat transfer from impinging jets have been fairly numerous. The investigators include Anderson and Stresino (33); Gardon and Akfirat (34); Kezios (17); Perry (15); Schauer and Eustis (18); Smirov, Verevochkin, and Brdlick (35); and Vickers (16). A variety of impinging flows ranging from room temperature laminar

flows through high temperature turbulent flows have been studied. Some investigations have even been concerned with impinging flame fronts or the impingement of arrays of jets. In many instances, the experimental data from these investigations have been presented in the form of heat transfer coefficients whose definition is either not given or depends upon the particular experimental system used. Also, many investigators have utilized such specific experimental conditions that the results of their studies cannot be extrapolated to other physical systems. Finally, very few studies have been concerned with the distribution of point heat fluxes, and even fewer have presented data on the distribution of point heat fluxes resulting from the impingement of a high temperature, turbulent free jet.

4.2 THE EQUIPMENT

A picture of the equipment which was designed and built to obtain the required experimental data is shown in Figure 6. A schematic sketch is shown in Figure 7. For ease of discussion, the equipment will be grouped into four basic sections -- the flow system, the flat plate, the various stagnation temperature and total head probes, and the auxiliary equipment.

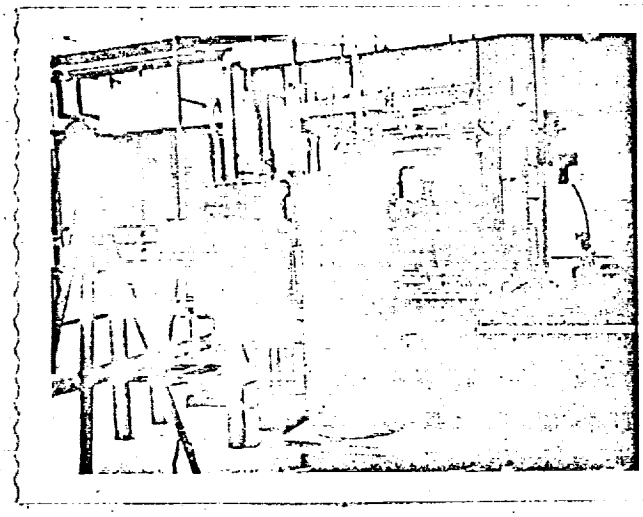

Figure 6

THE EQUIPMENT
FOR THE IMPINGING JET STUDY

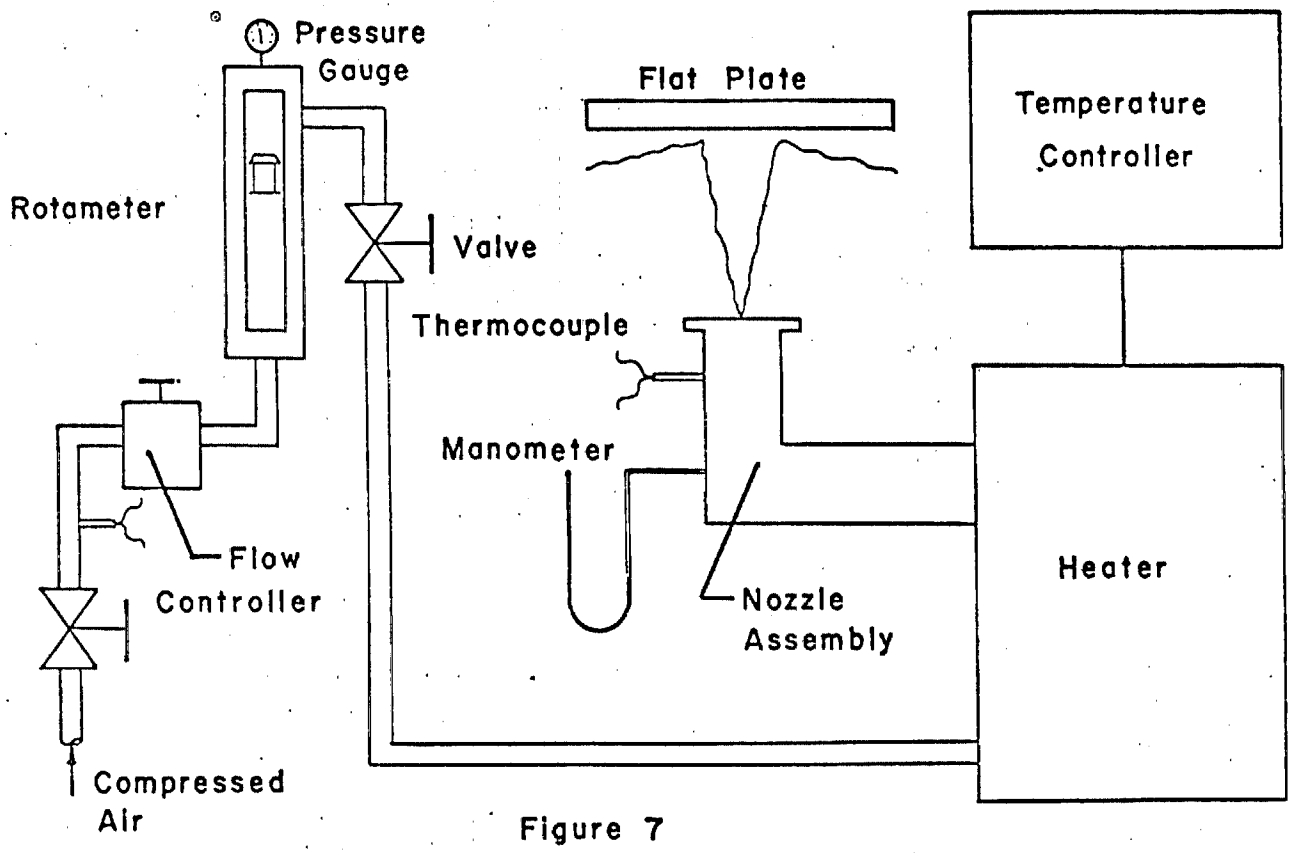

Figure 7

SCHEMATIC SKETCH OF EQUIPMENT

4.2.1 The Flow System

The air for the jet was taken from the tank of a laboratory air compressor. The air flowed through a pressure regulator which maintained a constant pressure for the air supplied to the experimental system. The flow rate of the air was controlled by a diaphragm-type flow controller and measured by a metering rotameter. The temperature and pressure of the air were measured, prior to its entrance into the heater, by a thermocouple and a pressure gauge. The air flow rate was extremely steady and did not vary noticeably during the course of an 8 to 10 hour experimental run.

The air then passed into a 10 kilowatt electrical resistance heater. The air temperature at the outlet of the heater was controlled by using on-off pyrometer regulation of one of the heater's two electrical circuits. The high temperature air then entered the stainless steel nozzle assembly. Although the maximum temperature of the air leaving the heater was 1600^{o}F, the maximum air temperature at the nozzle was only about 1300^{o}F. The difference was due to heat losses from the insulated pipe which carried the air between the heater and the nozzle.

The nozzle assembly consisted of a plenum chamber with three removable sections of fine screening (50 and 100 mesh

screening was used) to provide as uniform velocity and temperature profiles as possible at the nozzle exit, and a circular convergent nozzle with a short constant area throat. The throat was short in order to prevent the build-up of a thick boundary layer. Also, the assembly was designed to accommodate interchangeable nozzles 1/4 and 3/8 inches in diameter. The plenum chamber was designed with a large enough cross-section for flow so that the Mach number in the chamber was essentially zero; this made possible the measurement of the stagnation air temperature at that point. A schematic sketch of the nozzle assembly with the nozzle in place is shown in Figure 8.

Although the temperature of the air was only controlled at the outlet of the heater, the air temperature at the nozzle never varied more than 2 degrees F. This was due partly to the damping action of the large heat capacity of the insulation around the heater and piping. On the other hand, this large heat capacity made necessary a 5 to 8 hour period prior to an experimental run during which the outlet air attained a steady-state temperature. Also, an annular piece of flat stainless steel was placed in the plane of the nozzle exit to prevent entrainment of ambient

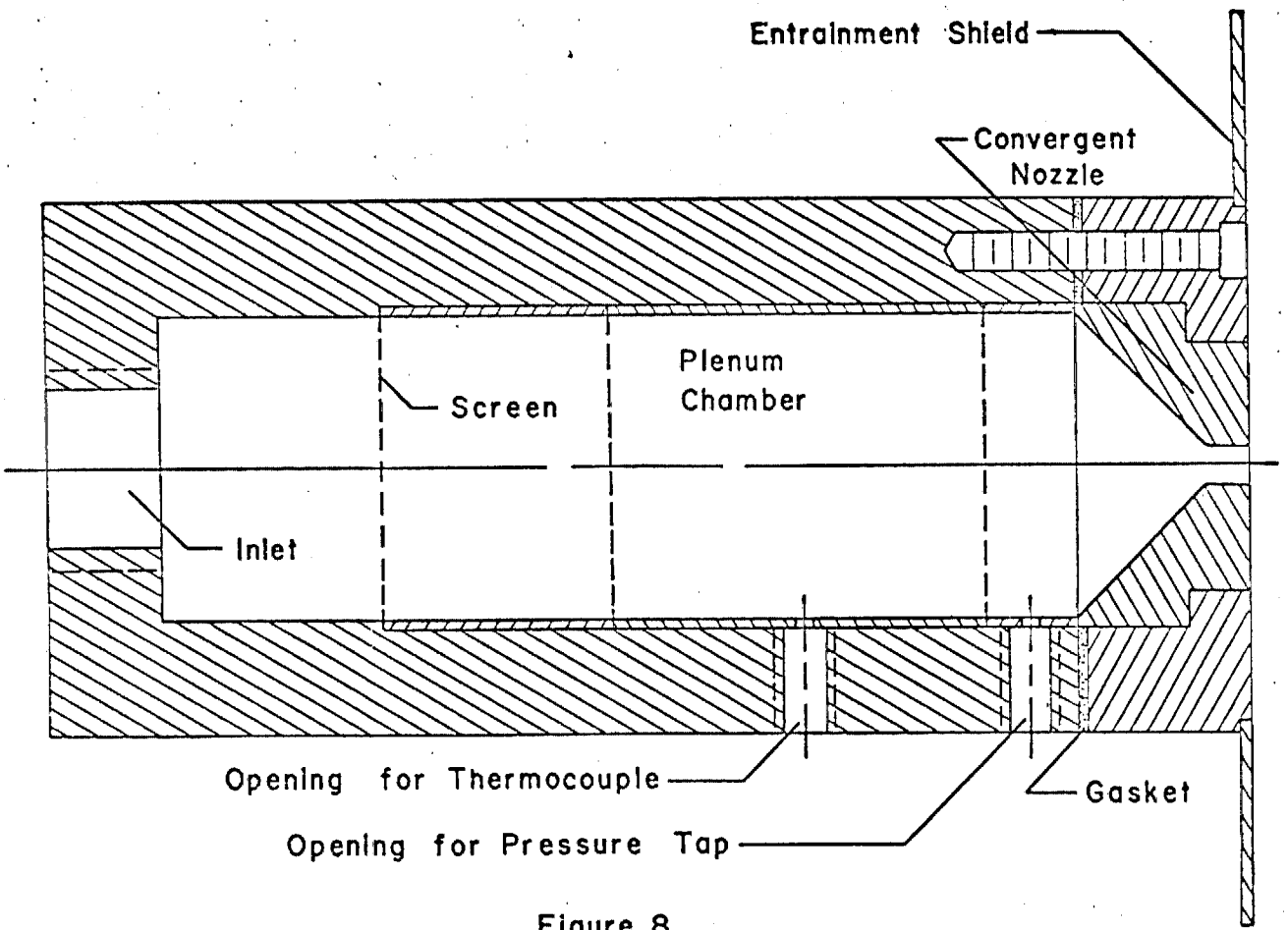

Figure 8
SCHEMATIC SKETCH OF NOZZLE ASSEMBLY

air from behind the nozzle. This insured the assumed condition of a jet ejecting into stationary air.

Flexible stainless steel pipe was used between the heater and the nozzle to eliminate changes in nozzle position caused by thermal expansion effects. The nozzle always moved during the transient heating period. Therefore, the nozzle assembly was attached to the base table by three leveling legs incorporating turnbuckles with two different thread sizes so that a fine leveling adjustment could be performed after steady-state conditions were reached. The position of the nozzle was checked optically using two transits. The flexible pipe, the nozzle assembly, and the heater were all well insulated to reduce heat losses.

4.2.2 The Flat Plate

The high temperature air of the jet impinged on a flat plate held normal to the axis of the jet 8 to 20 nozzle diameters downstream of the nozzle. The flat plate was a 2 feet by 2 feet by ½ inch thick piece of annealed Inconel 600 alloy which was instrumented for measurement of pressures, temperatures, and heat flux distributions on its surface. The back of the plate served as a water tank to stabilize the heat flux and temperature distributions. The size of the plate was large enough so that the flow was

essentially that of a free jet impinging normally on an infinite plane surface.

Temperature gradient probes were designed to measure the heat flux at various points on the surface of the plate. These probes consisted of ½ inch long, ¼ inch diameter rods with thermocouples along their axial length. Seven probes were embedded in the flat plate at various radial positions (measured from the stagnation point) so that their axes were perpendicular to the surface of the plate and their ends were flush with the surface. Two of the probes were located at the same radial position to check the assumed condition of axial symmetry. The probes were insulated from the remainder of the plate with thin rings of cast ceramic cement in order to obtain a close approximation to one-dimensional heat transfer at these points. Care was taken so that the probes, the plate, and the ceramic cement formed a smooth flat surface.

The thermocouple junctions were located in the rod at the surface of the plate, 1/8 inch below the surface, and 3/8 inch below the surface. The thermocouples at the surface were used to measure the surface temperature distribution of the plate.

The probes were also made of Inconel 600 annealed alloy since it was desirable to have as homogeneous a plate as possible. Inconel 600 annealed alloy was selected as the material of construction because it had a low enough thermal conductivity to insure an easily measureable temperature gradient and to reduce heat transfer along the plate, and a high enough thermal conductivity so that reasonably high heat transfer rates could be obtained through the plate. Also, the thermal conductivity as a function of temperature of this type of Inconel was readily available (36). Knowledge of the thermal conductivity of the probes and measured temperature gradients made possible the determination of the heat flux through them. A schematic sketch of a heat flux probe is shown in Figure 9.

There were 10-1/64 inch diameter static pressure taps in the plate situated at various radial positions. The pressure taps were countersunk with an included angle of 82° to a depth of ½ their diameter as recommended by Rayle (37) to eliminate errors introduced by their presence. A schematic sketch of the plate is shown in Figure 10. The positions of the heat flux probes and static pressure taps are given in Table 1.

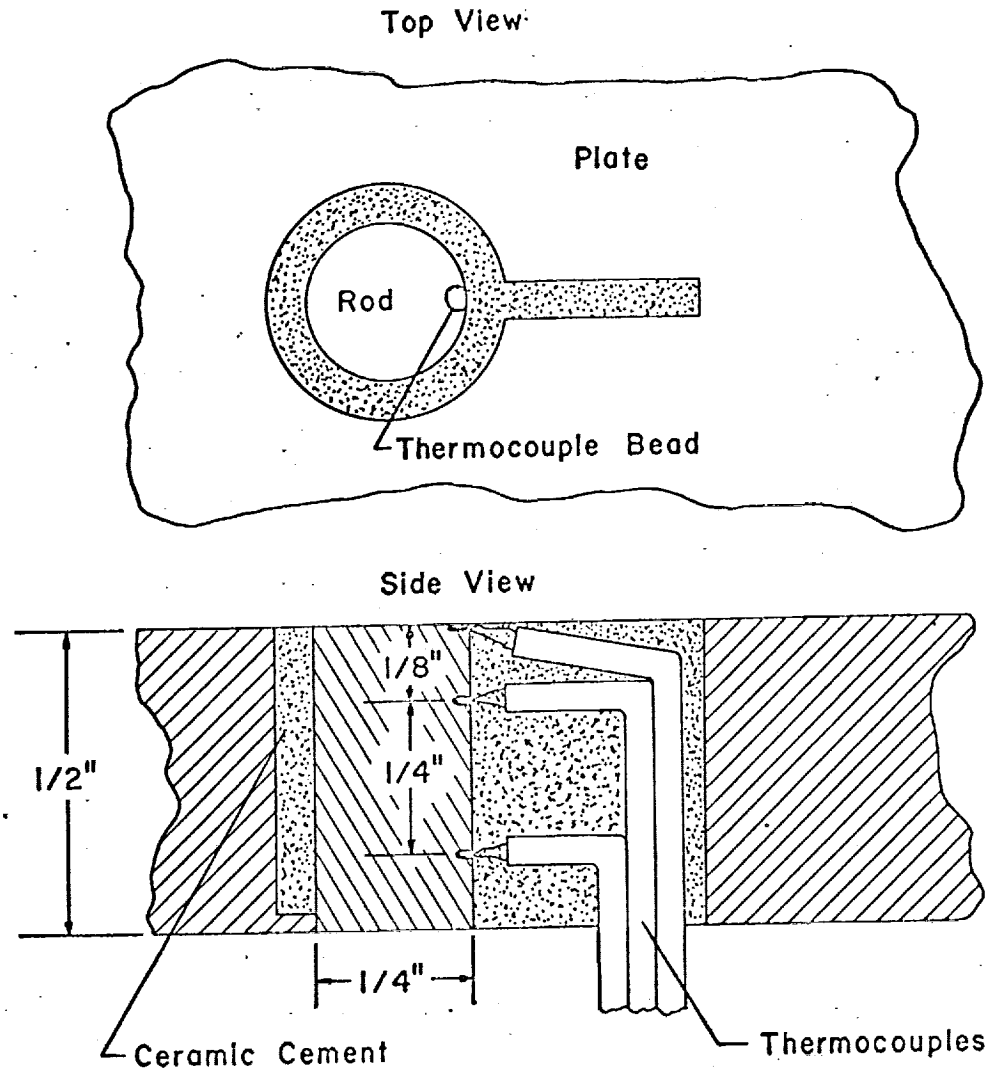

Figure 9

SCHEMATIC SKETCH OF HEAT FLUX PROBE

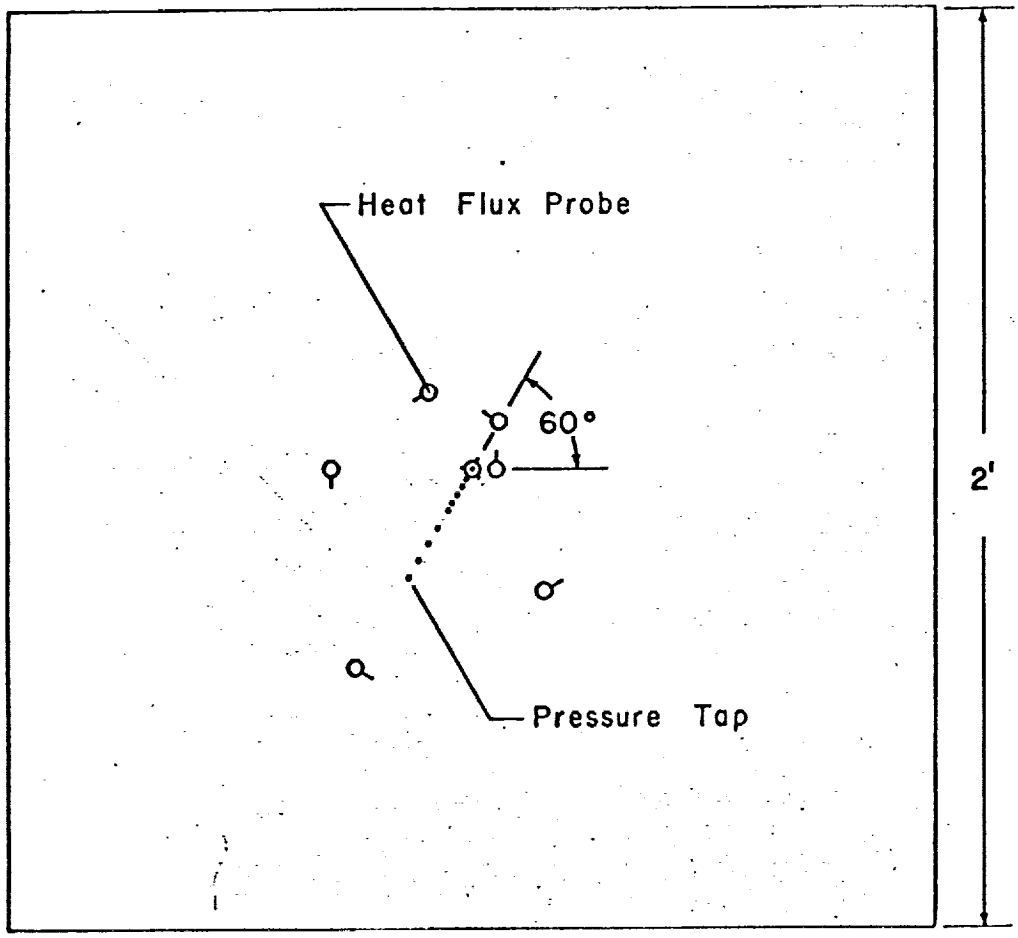

Figure 10

SCHEMATIC SKETCH OF FLAT PLATE

Table 1

The Locations of the Static Pressure Taps and the Heat Flux Probes.

Radial Positions of Static Pressure Taps (inches from stagnation point)	Radial Positions of Heat Flux Probes (inches from stagnation point)
0.000	0.00
0.312	0.60
0.562	1.34
0.812	2.31
1.062	3.68
1.312	3.68
1.812	6.00
2.312	
2.812	
3.312	

The plate was mounted in such a manner as to allow screw driven movement in any direction and easy levelling. The plate was aligned with the nozzle after steady-state conditions had been reached by using the transits.

4.2.3 The Stagnation Temperature and Total Head Probes

Stagnation temperature probes and total head probes were used in both the free jet and wall jet regions. Probe measurements were not made in the impingement region because of the difficulty of making such measurements in flow fields where the direction of flow is not known. Two total head probes and one stagnation temperature probe were used in the free jet, and one total head probe and one stagnation temperature probe were used in the wall jet. Estimates of the errors incurred in the flow measurements made with the probes are given in Appendix 9.7.

The stagnation temperature probe for the free jet was of standard, commercial design and consisted of a Chromel-Alumel thermocouple inside an Inconel sheath. Calibration curves for the recovery factor as a function of Mach Number and estimates of radiation and conduction errors were readily available (38), (39). A slight modification of the standard design was incorporated in the wall jet probe. Bending the sheath at a right angle and reducing the amount of sheath

extending past the thermocouple bead made possible the measurement of stagnation temperatures within 0.010 inches of the plate's surface. When the sheath of the probe touched the plate, the small bead of the thermocouple was 0.010 inches above the plate. Contact of the sheath and the wall was indicated by a current flow through an electrical circuit containing the plate and the probe. Schematic sketches of the stagnation temperature probes are shown in Figure 11.

Of the two free jet total head probes, one consisted merely of a short length of 0.025 inch diameter stainless steel hypodermic needle tubing attached by soldering to a larger piece of tubing which supported the probe. The other free jet total head probe was a miniature Kiel (40) probe. In this type of probe, the impact tube is located inside a small venturi. Total head pressures can be accurately measured when the probe is inclined at angles up to 40^{o} from the direction of flow. The Kiel probe was generally used in the fully developed jet, and the standard type of total head probe was used in the potential core and the transition region. The total head probe for the wall jet was similar to the one used in the potential core of the free jet. The only difference between the two was that the

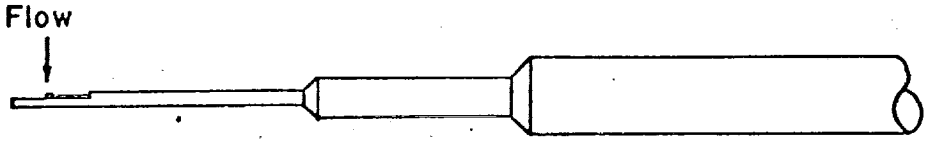

Free Jet Probe

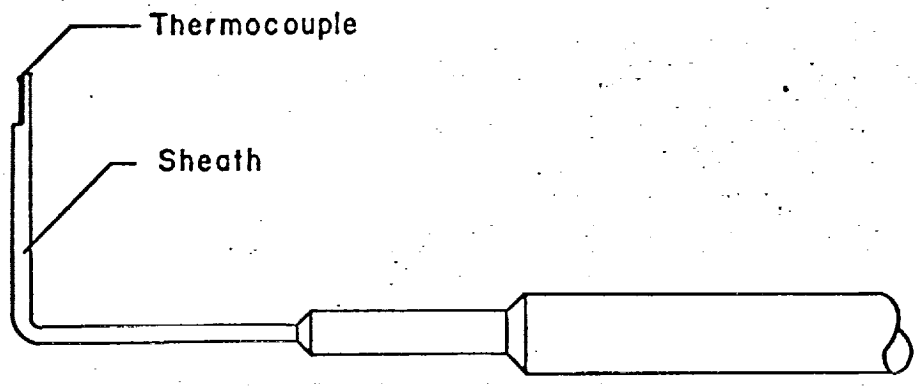

Wall Jet Probe

Figure 11

SCHEMATIC SKETCHES OF STAGNATION TEMPERATURE PROBES

hypodermic needle tubing for the wall jet probe was bent and shaped into a rectangular cross-section so that measurements could be made within 0.010 inches of the plate. This probe was also positioned at the wall using an electrical contact method. Schematic sketches of the total head probes are shown in Figure 12.

4.2.4 The Auxiliary Equipment

Various pieces of auxiliary equipment were used to indicate or record signals from the probes. The static pressures on the surface of the plate and the stagnation pressure in the nozzle were measured using manometers containing Meriam red oil (specific gravity of one) or mercury. These manometers were mounted on a common board for convenience. The pressures measured by the total head probes were converted into electrical signals by use of a variable reluctance type of pressure transducer. These signals were displayed on the digital dial of a transducer indicator box. Also, a probe positioning jig, constructed from three lathe drive mechanisms, was used to position the probes within 0.001 inches of the desired location. A picture of the probe positioning jig is shown in Figure 13.

The e.m.f.'s induced in the thermocouples of the heat flux probes were measured using a precision portable

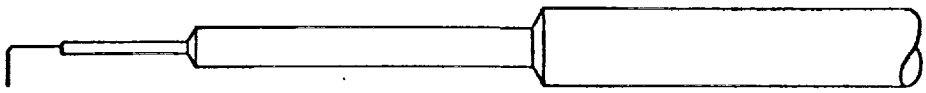

Standard Type Free Jet Probe

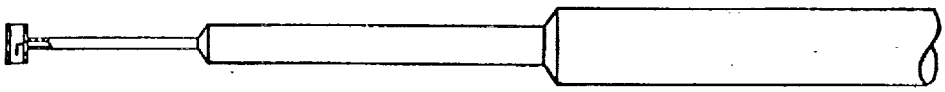

Kiel Type Free Jet Probe

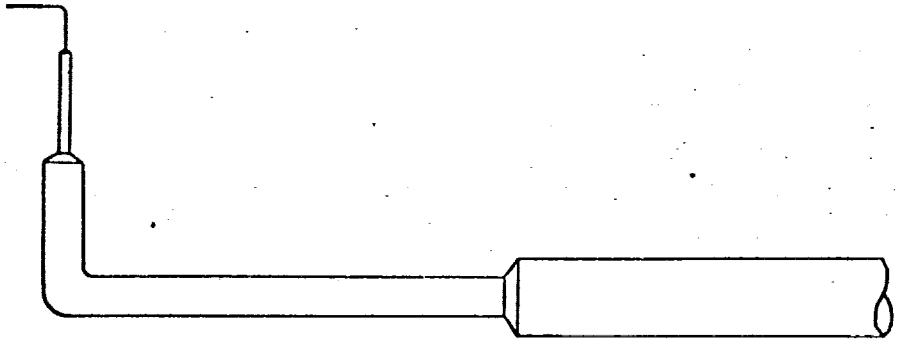

Wall Jet Probe

Figure 12

SCHEMATIC SKETCHES OF TOTAL HEAD PROBES

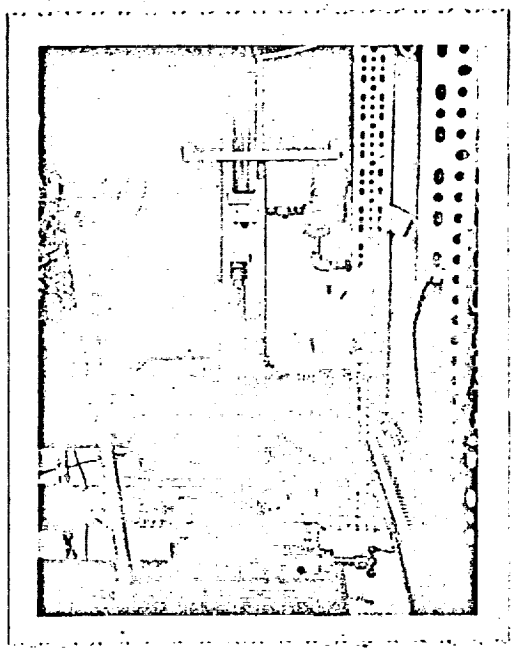

Figure 13

THE PROBE POSITIONING JIG

potentiometer. The stagnation temperature in the nozzle, the temperature of the air entering the heater, the ambient air temperature, and the temperatures of the stagnation temperature probes were all recorded on a 24 point recording potentiometer. A 24 point thermocouple switch was used in conjunction with a double pole switch so that any thermocouple e.m.f. could be either measured on the potentiometer or recorded.

The distance between the nozzle and the plate was measured optically with a cathetometer. The alignment of the nozzle and the alignment of the plate and the probes with the nozzle were performed optically using two transits.

4.3 EXPERIMENTAL PROCEDURE

The experimental variables were the Mach Number of the air flow at the nozzle exit, the stagnation temperature of the air in the nozzle, the distance between the nozzle and the plate, and the diameter of the nozzle. A listing of the experimental runs giving the conditions for each run is given in Table 2.

The sequence for a particular run was as follows. First the tank on the back of the plate was filled with water. The air flow rate was then set at the desired value by using the flow controller, and the power to the heater was turned

Table 2.

The Experimental Program

Run Number	(t_j/t_a)	M	t_j(F)	t_a(F)	v_{zj}(ft./sec.)	H(inches)	D(inches)
1	Preliminary run						
2	Preliminary run						
3	2.81	0.599	1037	73	1135	3.94	0.250
4	2.62	0.837	945	76	1538	3.94	0.250
5	2.68	0.755	983	78	1406	4.02	0.250
6	2.72	0.631	1011	80	1186	5.90	0.375
7	2.72	0.630	1024	85	1190	4.40	0.375
8	2.70	0.625	1015	86	1177	2.70	0.375
9	2.92	0.799	1134	88	1525	3.94	0.250
10	2.21	0.753	741	83	1279	3.94	0.250

on. A 5 to 8 hour period was then required during which the air flow at the nozzle exit and the thermocouples in the heat flux probes attained steady-state conditions. When temperatures did not vary more than $1^{o}F$ over a one-half hour period, it was assumed that the system was in steady-state operation.

Before any data were taken, the nozzle assembly was levelled by adjusting the levelling legs while the position of the assembly was checked using the transits. After the nozzle was levelled, the plate was levelled, and the center of the plate was positioned directly above the center of the nozzle. At this point, another check was made to insure that steady-state operation had indeed been reached.

The first data to be recorded were the static pressure distribution on the plate and the temperatures of the thermocouples in the heat flux probes. Next, stagnation temperature and total head pressure traverses were made in the wall jet region. The procedure was the same for both types of traverses. The probes were positioned on the jet axis by using the probe positioning jig and the transits. The probes were then moved to the desired radial position and "zeroed" at the wall using the electrical contact method. The probes

traversed the wall jet in a direction normal to the surface of the plate at three or four radial positions.

For the stagnation temperature and total head pressure traverses in the free jet region, the probes were positioned on the jet axis at the nozzle exit. The probes were then moved downstream along the jet axis for the traverse in the axial direction. Radial traverses were also made at several axial positions. Probe traverses in the radial direction were made across the entire width of the jet to check to assumed condition of angular symmetry. When all these data were taken, the power to the heater was turned off. Air flow was continued through the system until the air temperature at the outlet of the heater dropped to about 500°F in order to avoid damage to the heater.

4.4 EXPERIMENTAL DATA

The data obtained from the experimental runs were used to calculate velocity and temperature profiles in the free jet and wall jet regions and the static pressure, temperature, and heat flux distributions on the flat plate. The data reduction techniques and the computer program used are given in Appendix 9.8. Estimates of the errors in the experimental data are given in Appendix 9.7.

The reduced data from experimental run 5 is given here; reduced data from all the experimental runs are listed in tabular form in Appendix 9.9. The static pressure, temperature, and heat flux distribution on the flat plate are shown in Figures 14, 15, and 16 respectively. The variation of the axial component of velocity and the temperature with axial position in the free jet is shown in Figure 17. The variation of the axial component of velocity with radial position in the free jet is shown in Figure 18, and the variation of temperature with radial position in the free jet is shown in Figure 19. Velocity and temperature profiles in the wall jet are shown in Figures 20 and 21.

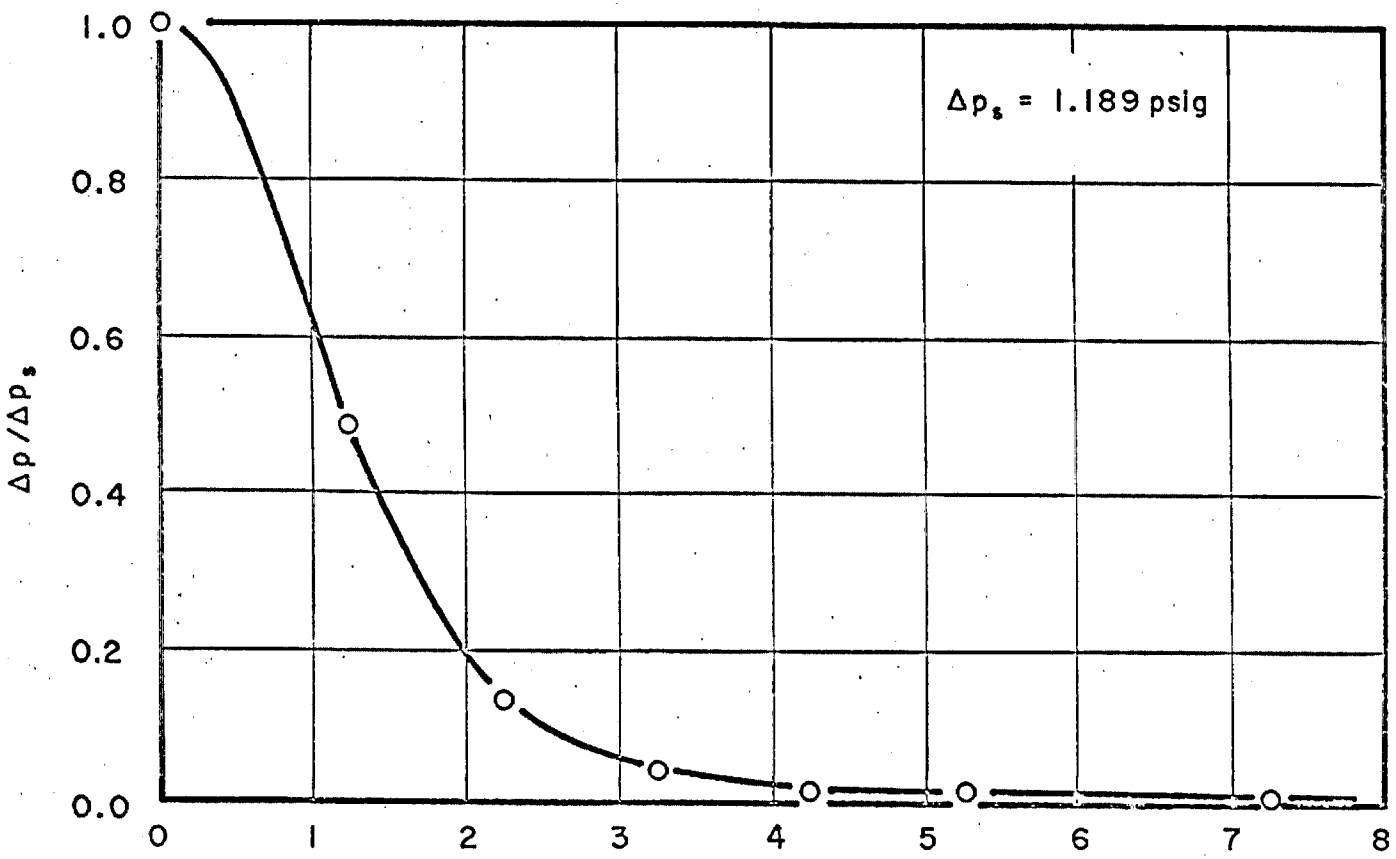

Figure 14

STATIC PRESSURE DISTRIBUTION ON PLATE, DATA FROM RUN 5

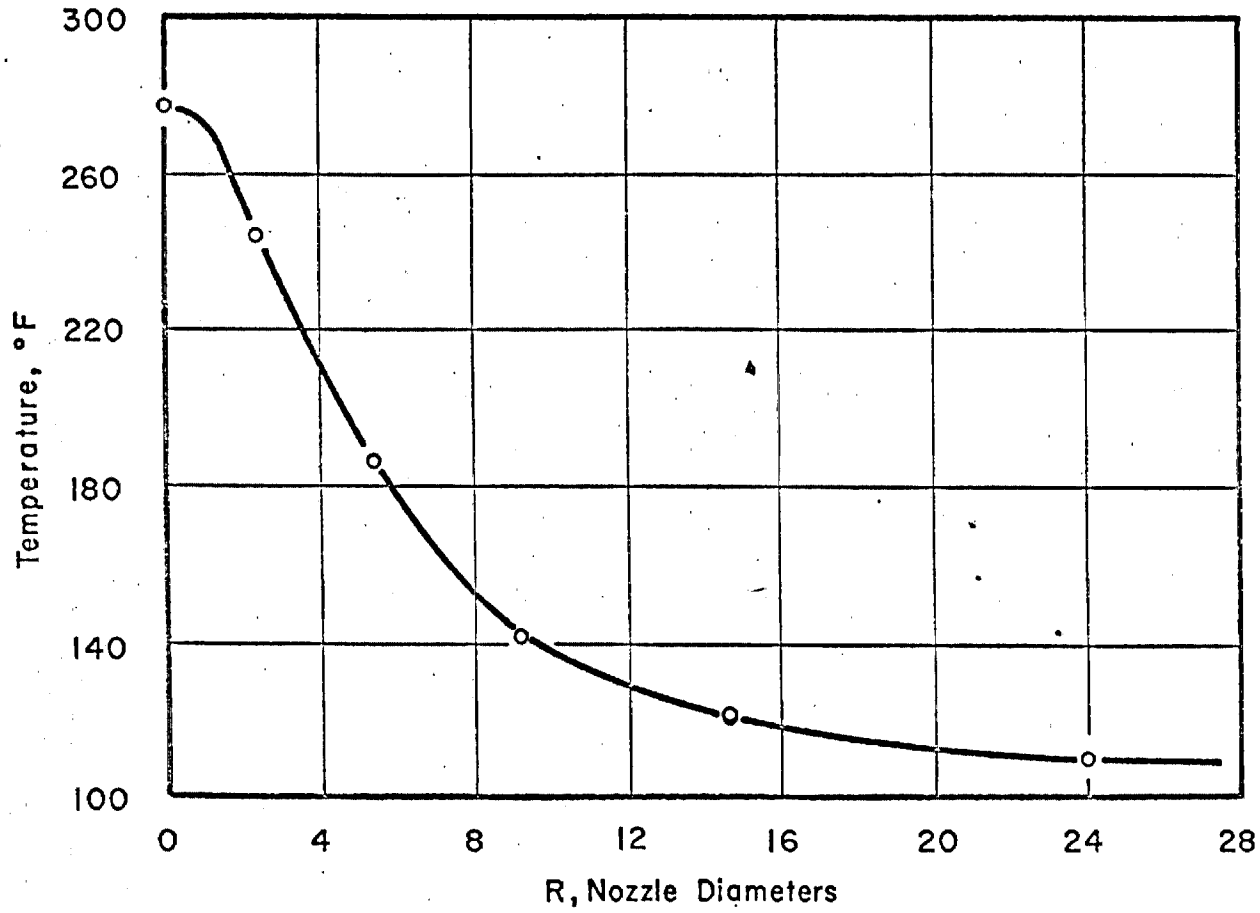

Figure 15

TEMPERATURE DISTRIBUTION ON SURFACE OF PLATE, DATA FROM RUN 5

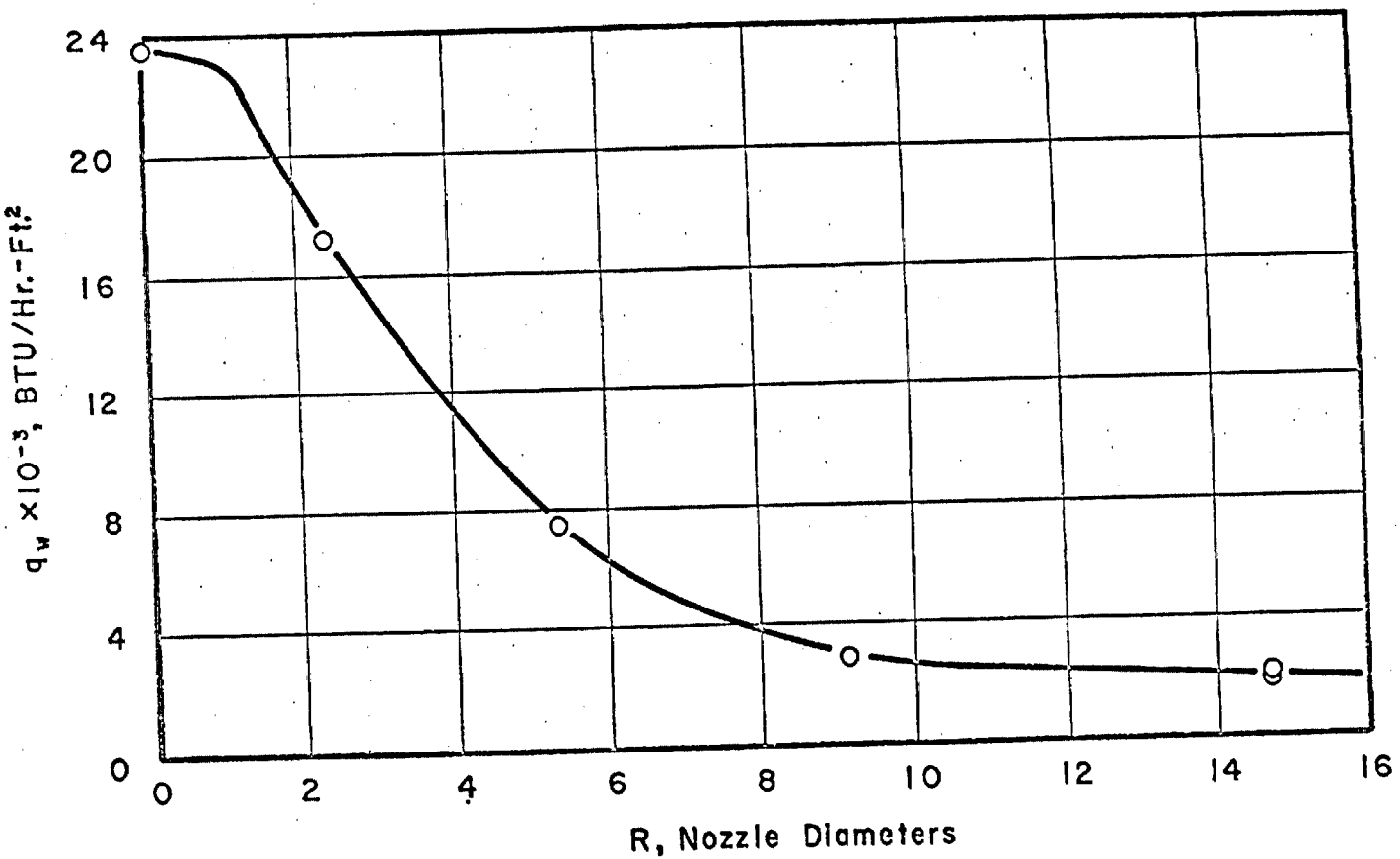

Figure 16

HEAT FLUX DISTRIBUTION, DATA FROM RUN 5

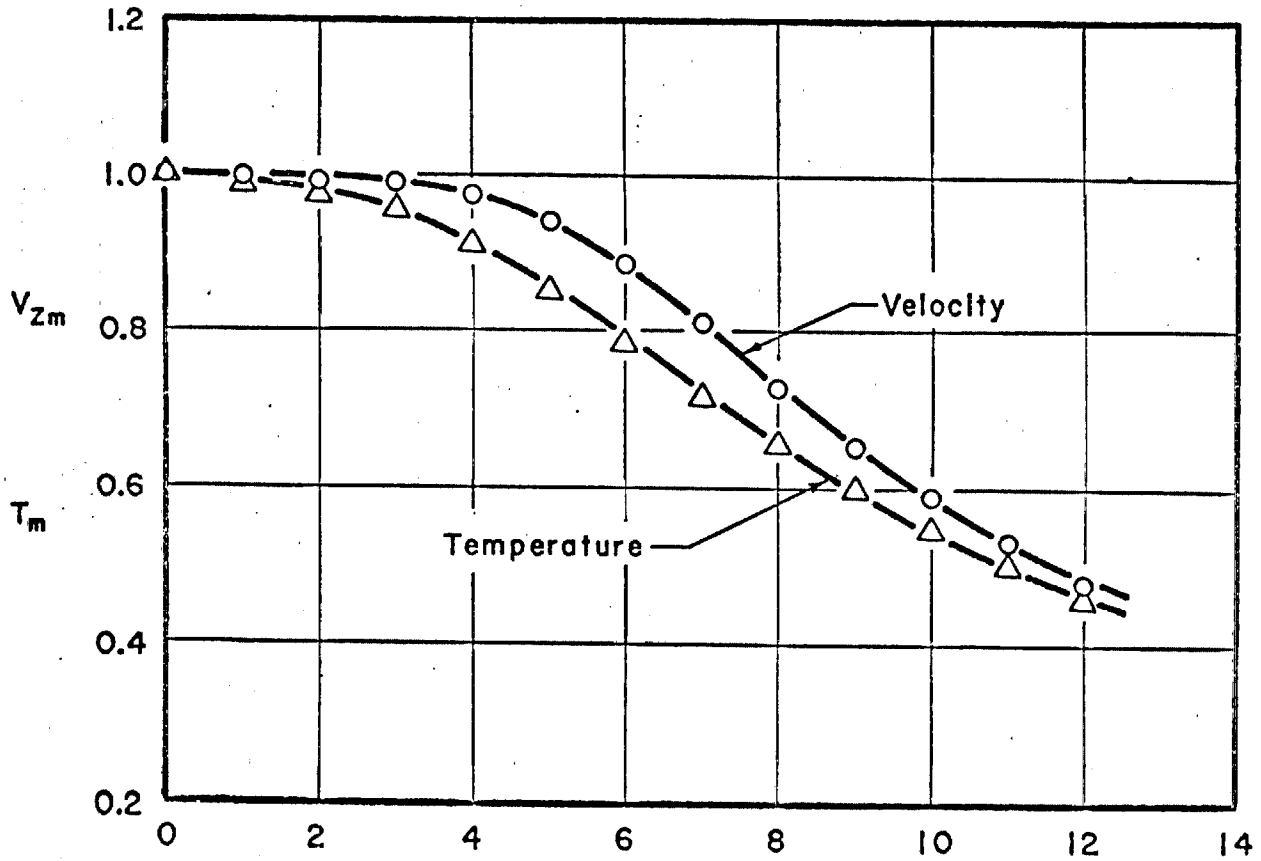

Figure 17

THE AXIAL DECAY OF AXIAL VELOCITY AND TEMPERATURE, DATA FROM RUN 5

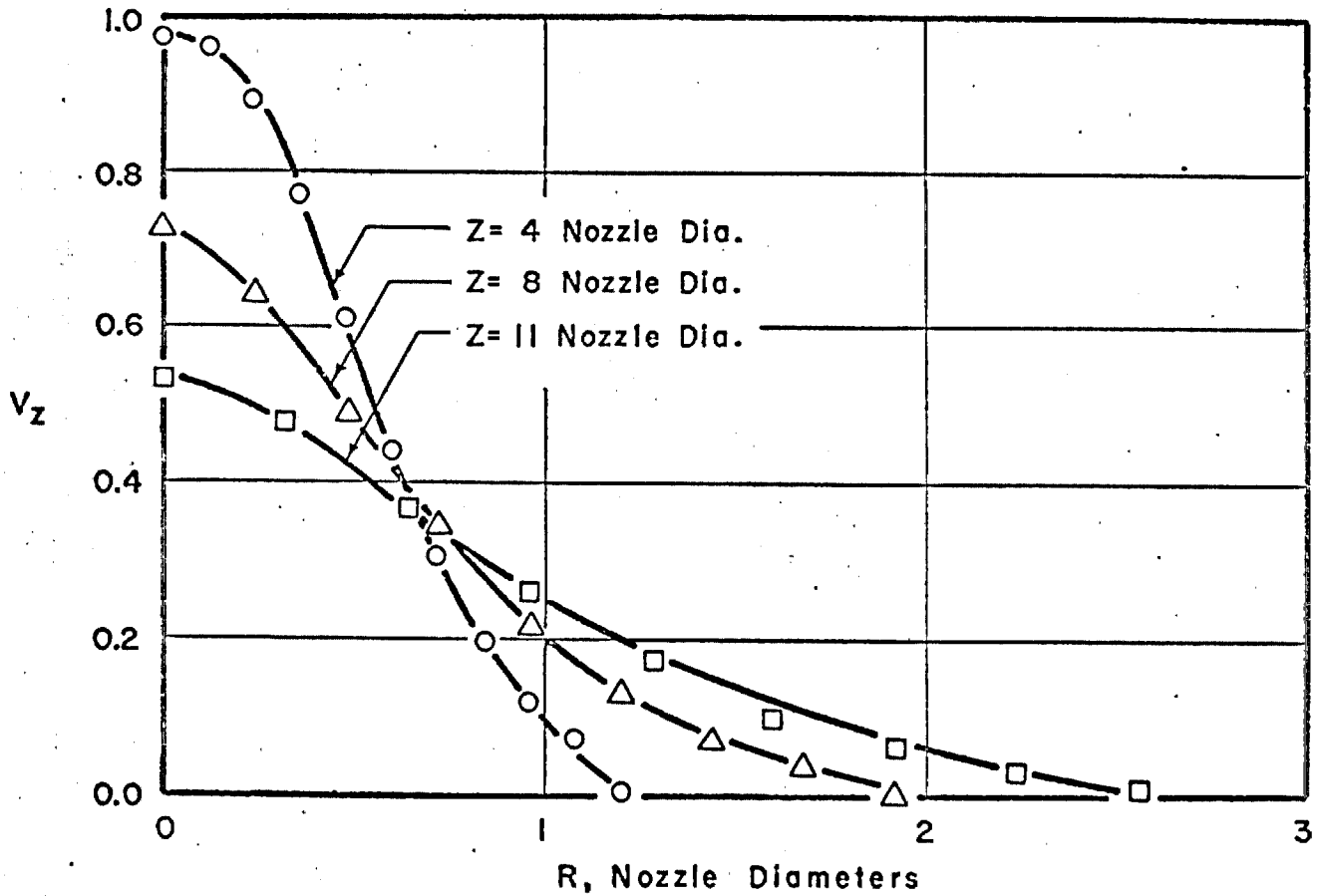

Figure 18

THE RADIAL DISTRIBUTION OF AXIAL VELOCITY, DATA FROM RUN 5

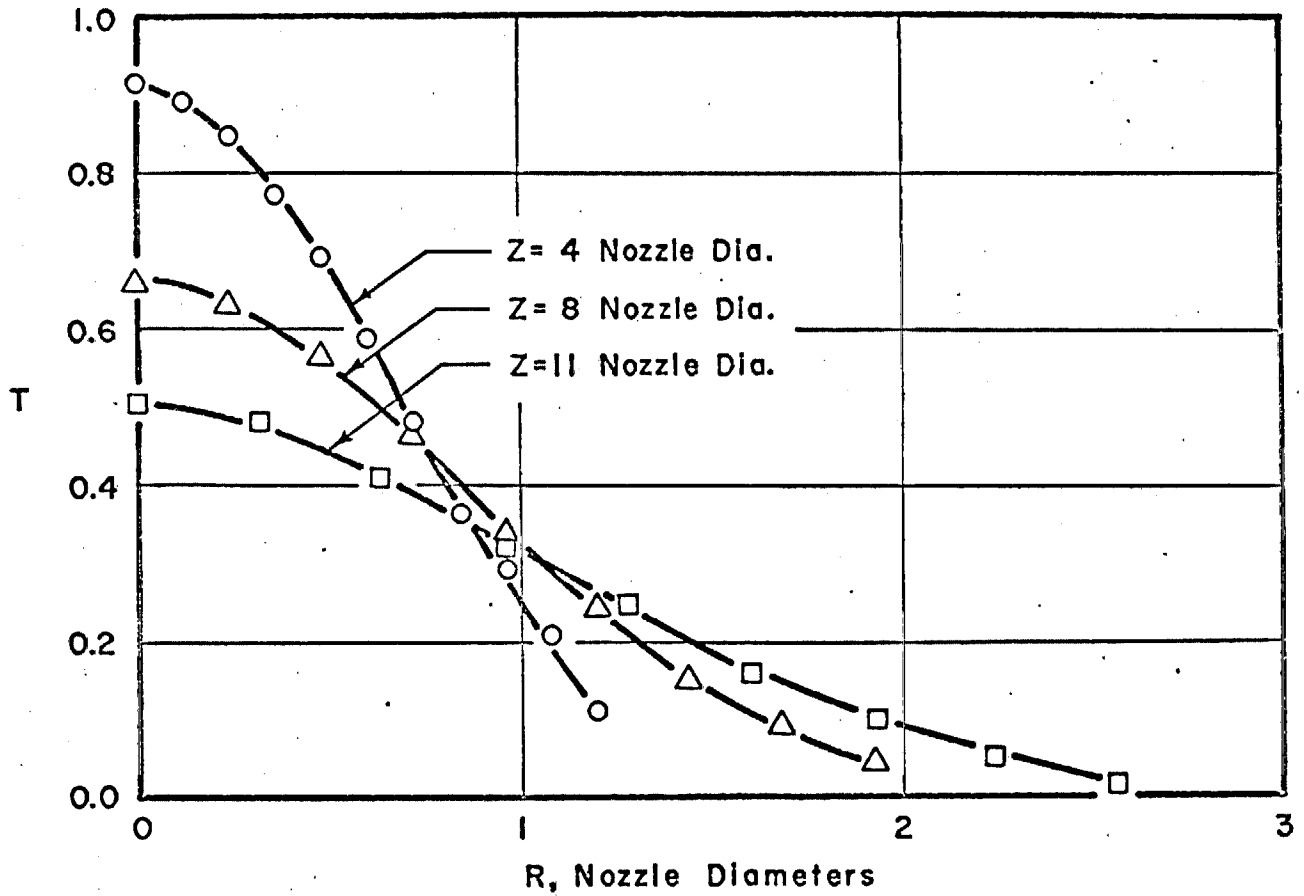

Figure 19

THE RADIAL DISTRIBUTION OF TEMPERATURE, DATA FROM RUN 5

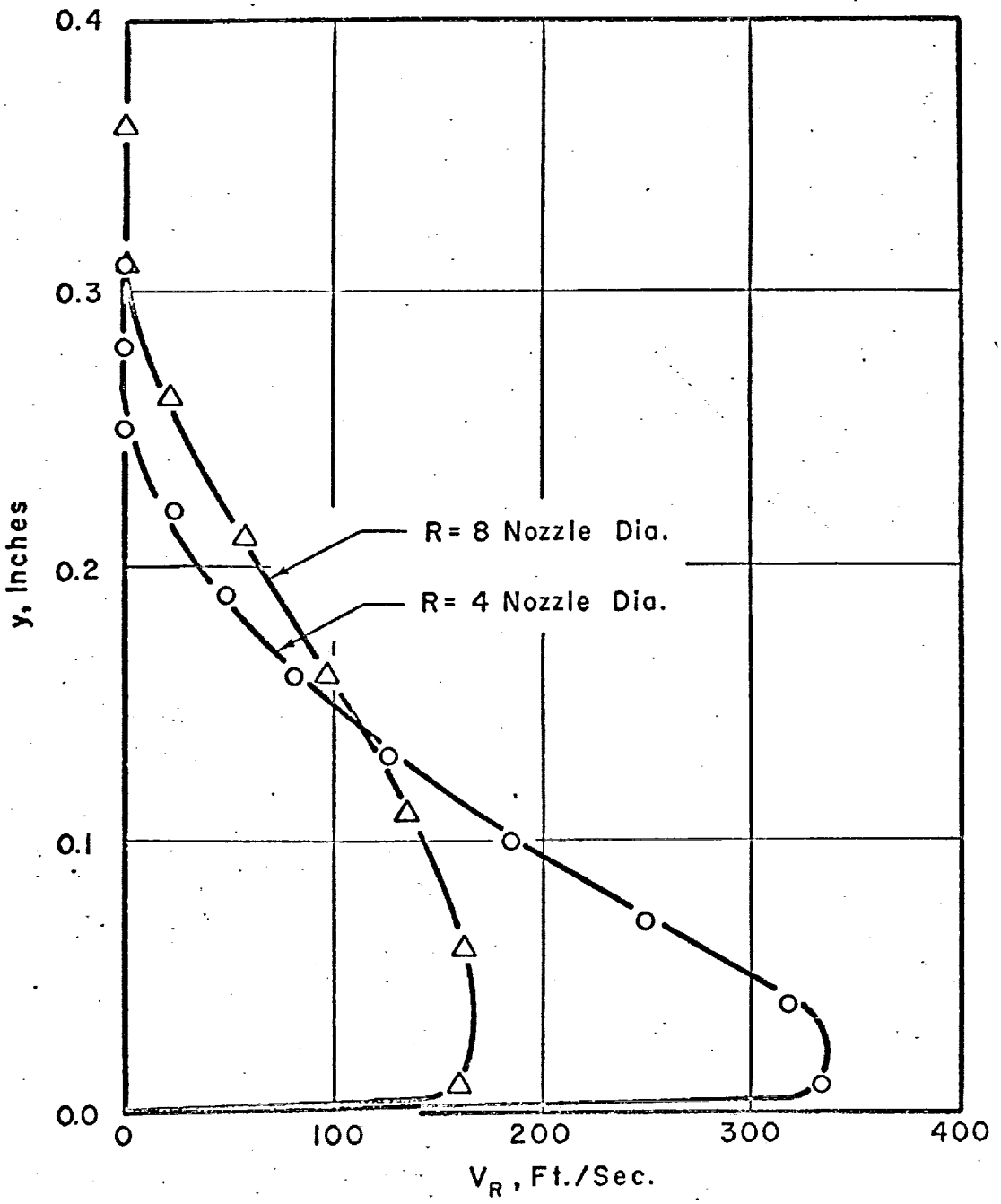

Figure 20

THE VARIATION OF VELOCITY
IN THE WALL JET, DATA FROM RUN 5

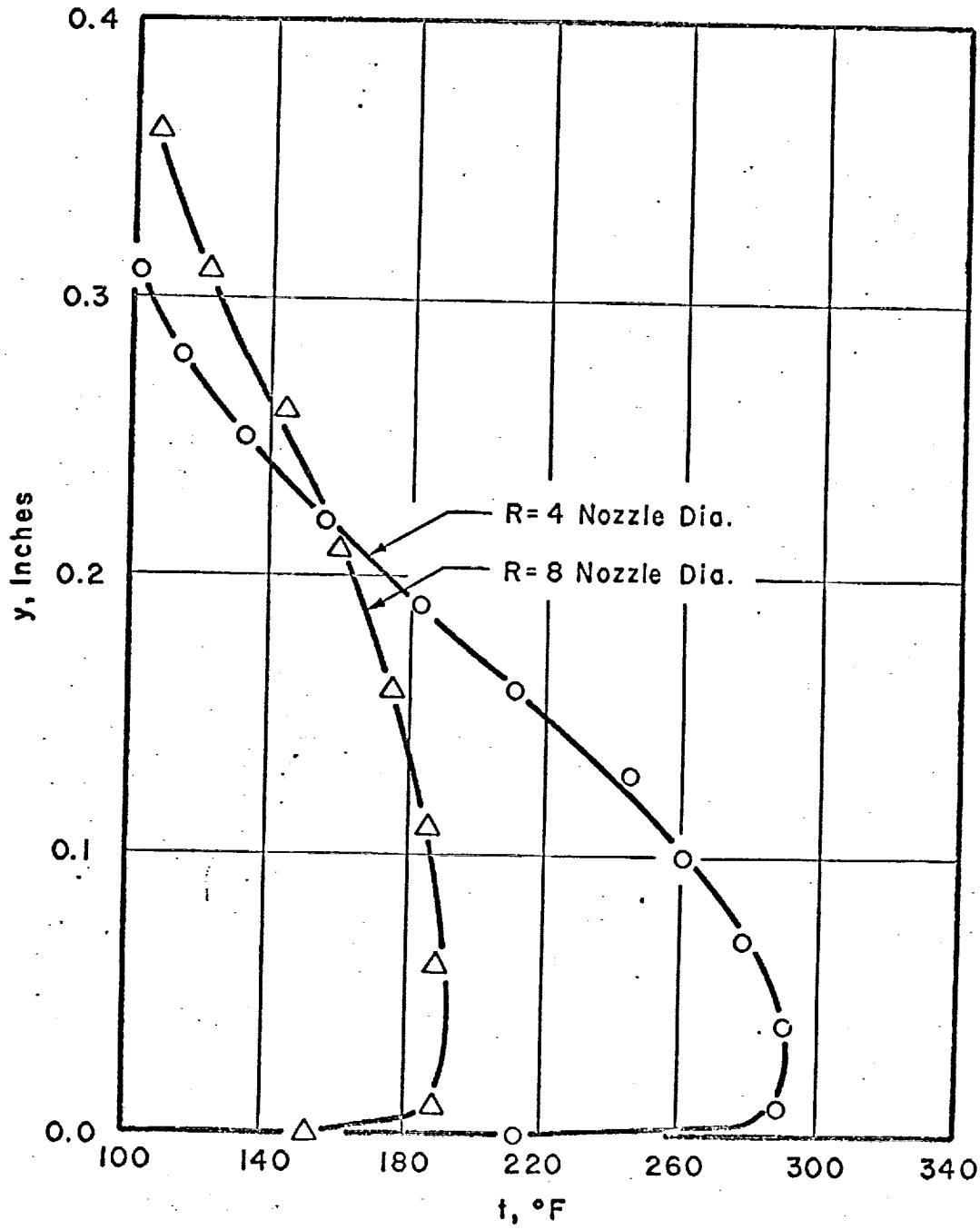

Figure 21

THE VARIATION OF TEMPERATURE IN THE WALL JET, DATA FROM RUN 5

5. RESULTS

5.1 THE FREE JET

The results of the numerical calculations are compared with the experimental data of Corrsin and Uberoi (2) in Figures 22 through 24. The jet Mach number and the jet temperature ratio (t_j/t_a) at which these data were taken were about 0.07 and 2.0 respectively. Figure 22 shows the results of the calculations compared with data for the axial decay of axial velocity and temperature. Calculated radial distributions of axial velocity and temperature at Z=15 are compared with the experimental data of Corrsin and Uberoi in Figures 23 and 24.

Calculated results are compared with experimental data from two experimental runs of the present investigation in Figures 25 through 33. A comparison of the calculated axial decay of axial velocity and temperature with data from one experimental run is shown in Figure 25. Radial distributions of axial velocity and temperature at Z=11 are compared with data from the same experimental run in Figures 26 and 27. Data for the axial decay of axial velocity and temperature from another experimental run are compared with the calculated results in Figure 28, and the data for the radial

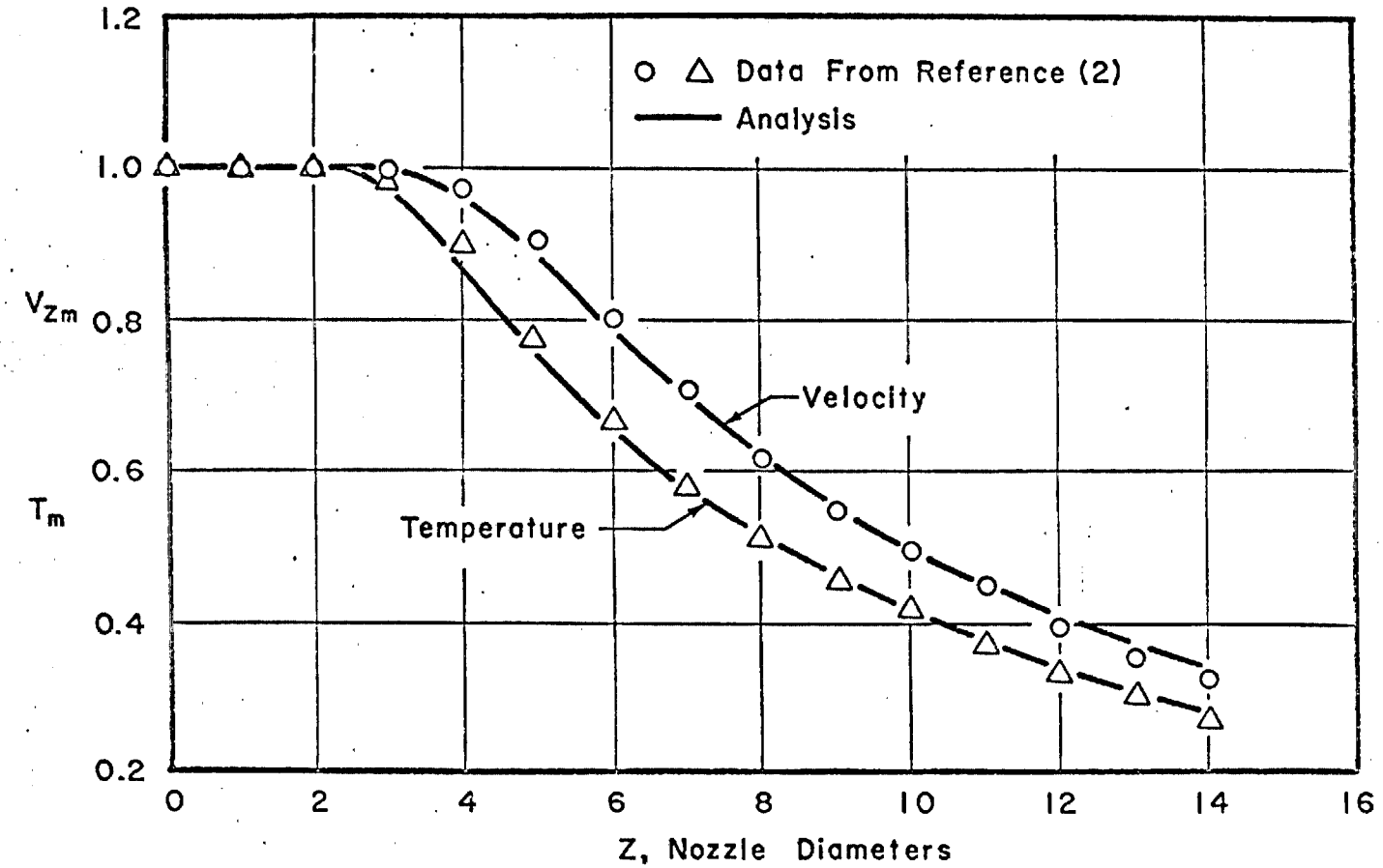

Figure 22

THE CALCULATED AND MEASURED AXIAL DECAY OF AXIAL VELOCITY AND TEMPERATURE

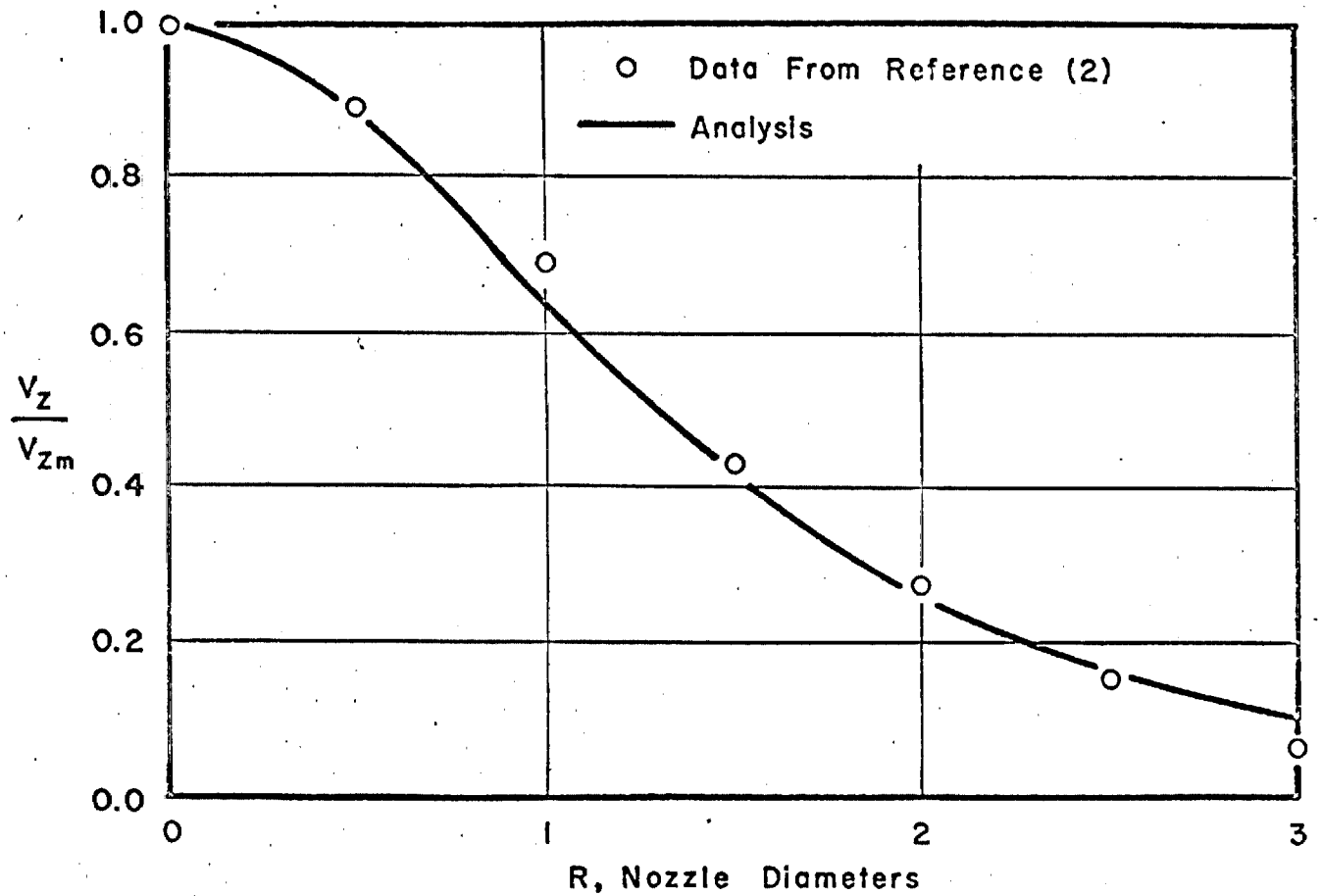

Figure 23

CALCULATED AND MEASURED RADIAL DISTRIBUTIONS OF AXIAL VELOCITY AT Z=15

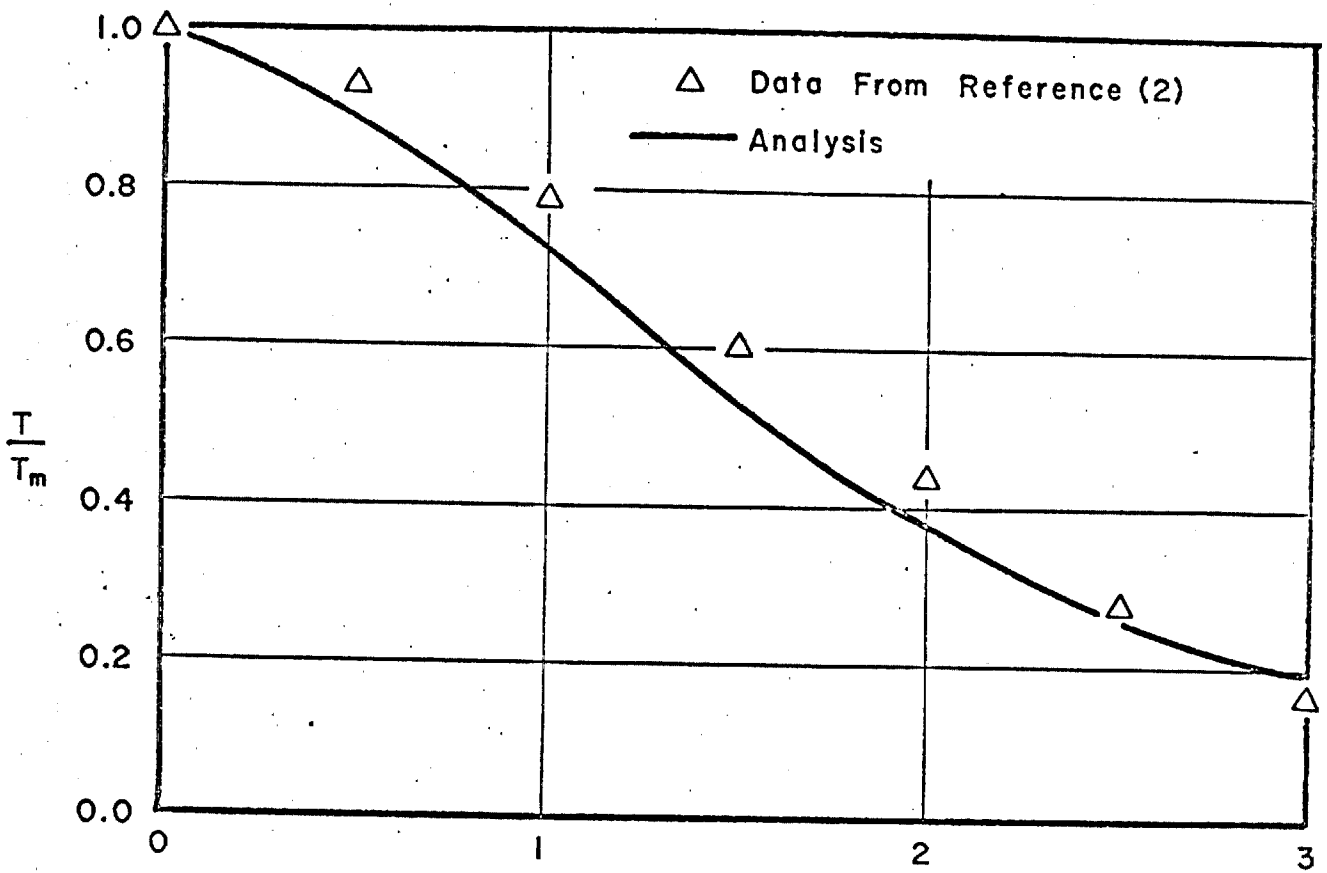

Figure 24
CALCULATED AND MEASURED RADIAL DISTRIBUTIONS OF TEMPERATURE AT Z=15

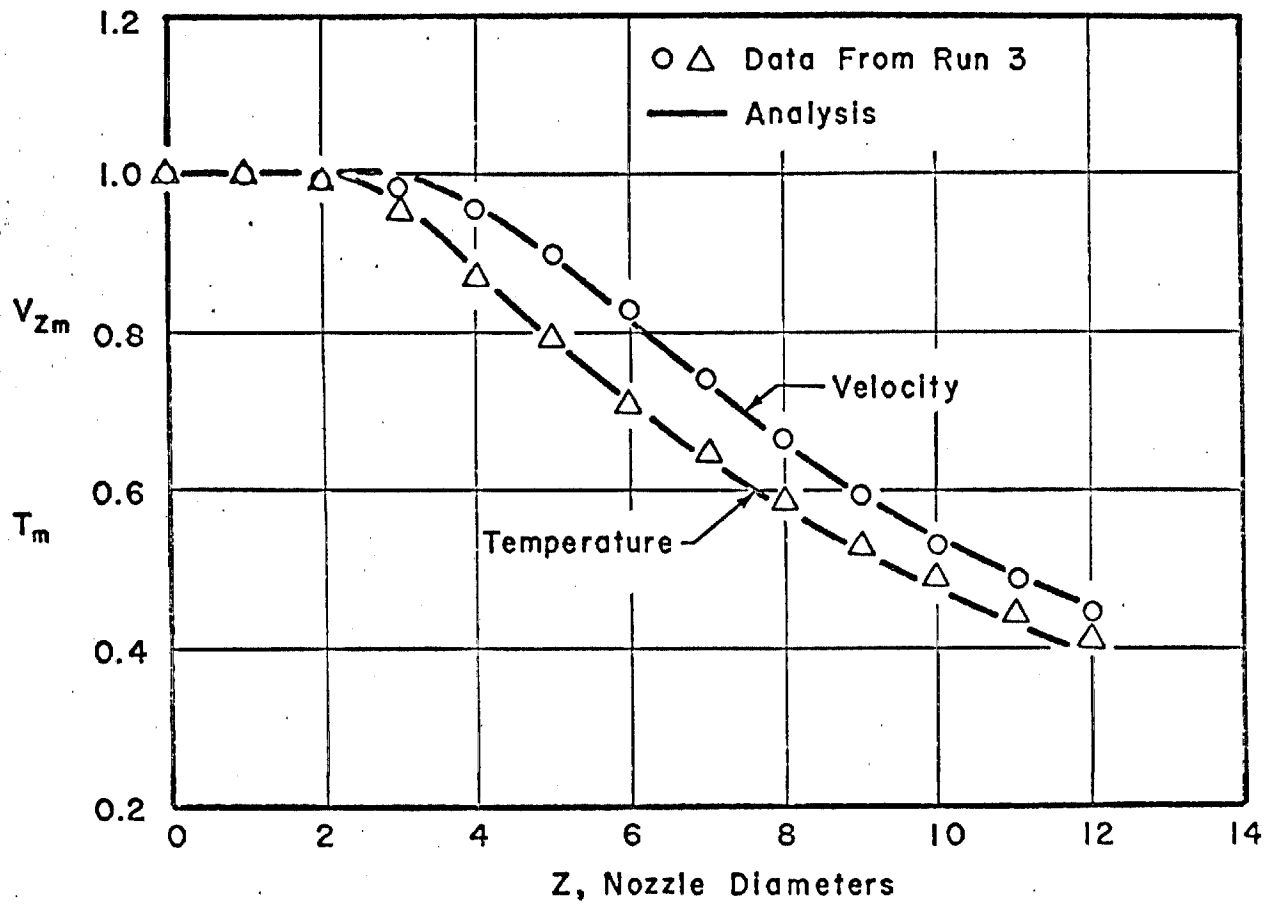

Figure 25
THE CALCULATED AND MEASURED AXIAL DECAY OF AXIAL VELOCITY AND TEMPERATURE

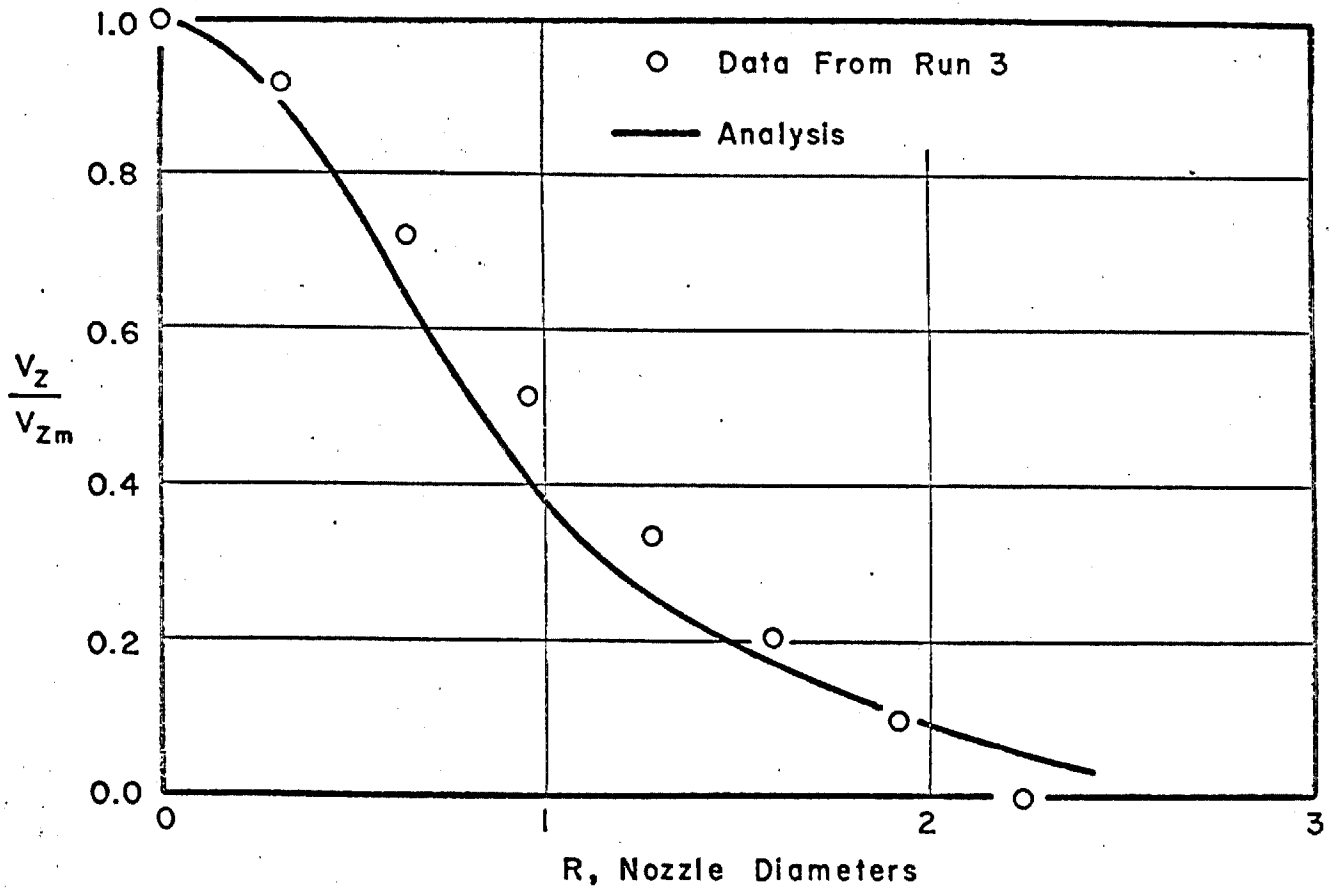

Figure 26

CALCULATED AND MEASURED RADIAL DISTRIBUTIONS OF AXIAL VELOCITY AT Z=11

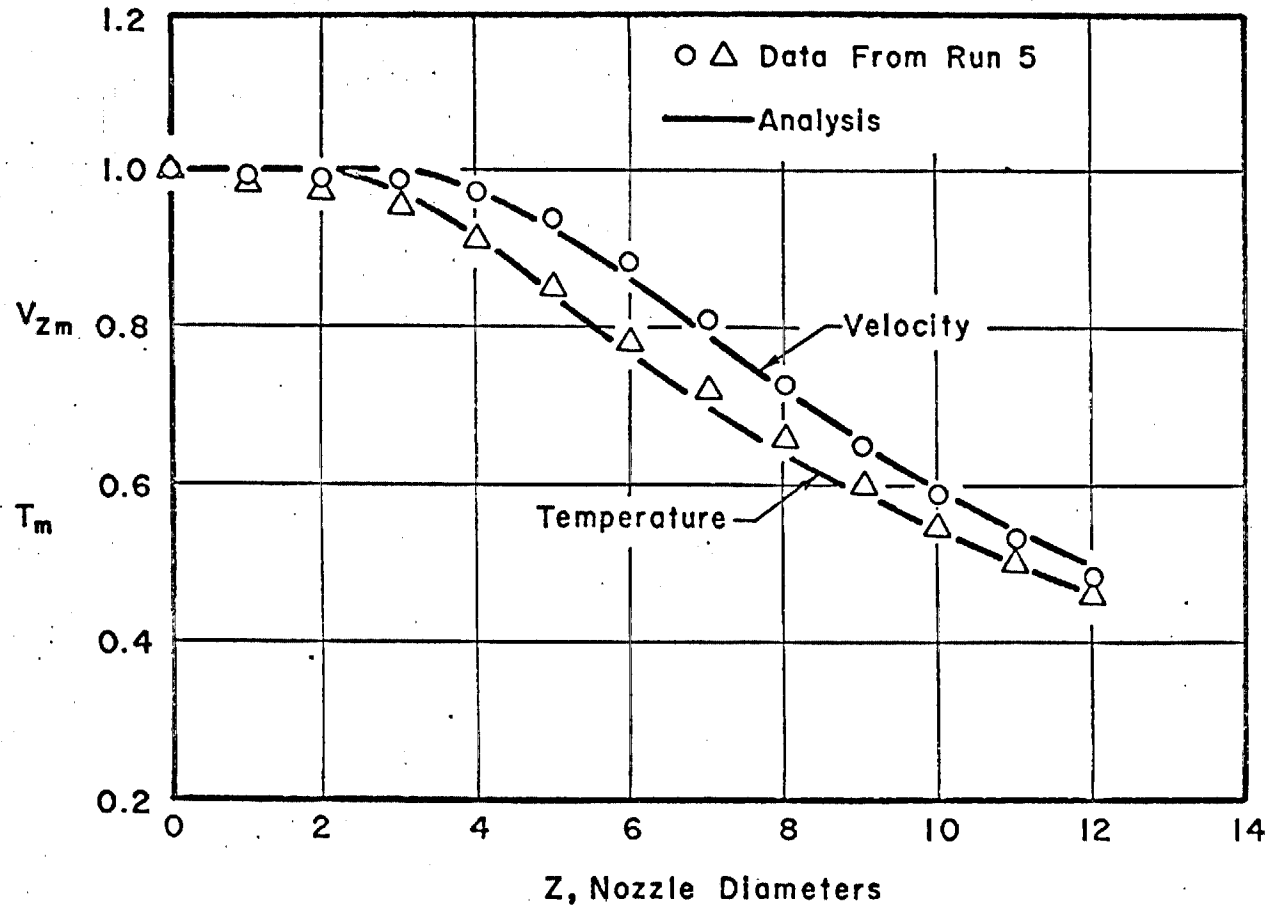

Figure 28
THE CALCULATED AND MEASURED AXIAL DECAY OF AXIAL VELOCITY AND TEMPERATURE

variation of axial velocity and temperature are compared with the calculated results at Z=4, which is at the end of the core region and the beginning of the transition region, and at Z=11, which is in the fully developed jet, in Figures 29 through 32.

Calculated results for the radial distribution of the radial velocity component are shown in Figure 33. There were no experimental measurements of radial velocity distributions available for comparison with the calculated results.

5.2 THE IMPINGEMENT REGION

The results of the numerical heat flux calculations are compared with experimental data from three experimental runs of the present investigation in Figures 34, 35, and 36. The dashed lines of the heat flux distribution curves represent the extension of impingement region calculations into the wall jet region.

Although no measurements were made of the velocity at the edge of the boundary layer or the boundary layer growth, calculated results for these quantities are shown, for one experimental run, in Figures 37 and 38 respectively.

Calculated values of the parameters of the static pressure distribution and stagnation point heat fluxes are compared with the measured values in Table 3.

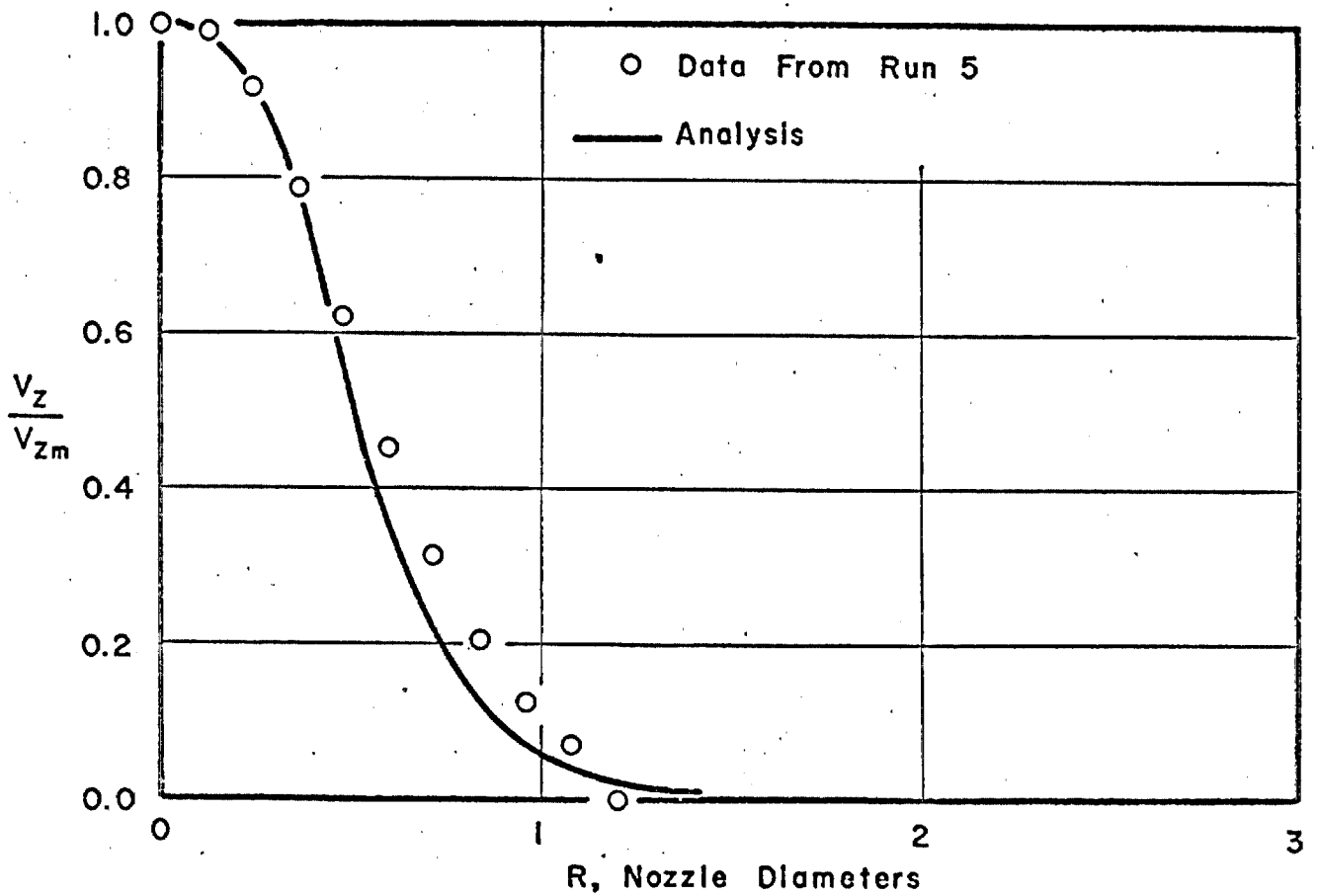

Figure 29

CALCULATED AND MEASURED RADIAL DISTRIBUTIONS OF AXIAL VELOCITY AT Z=4

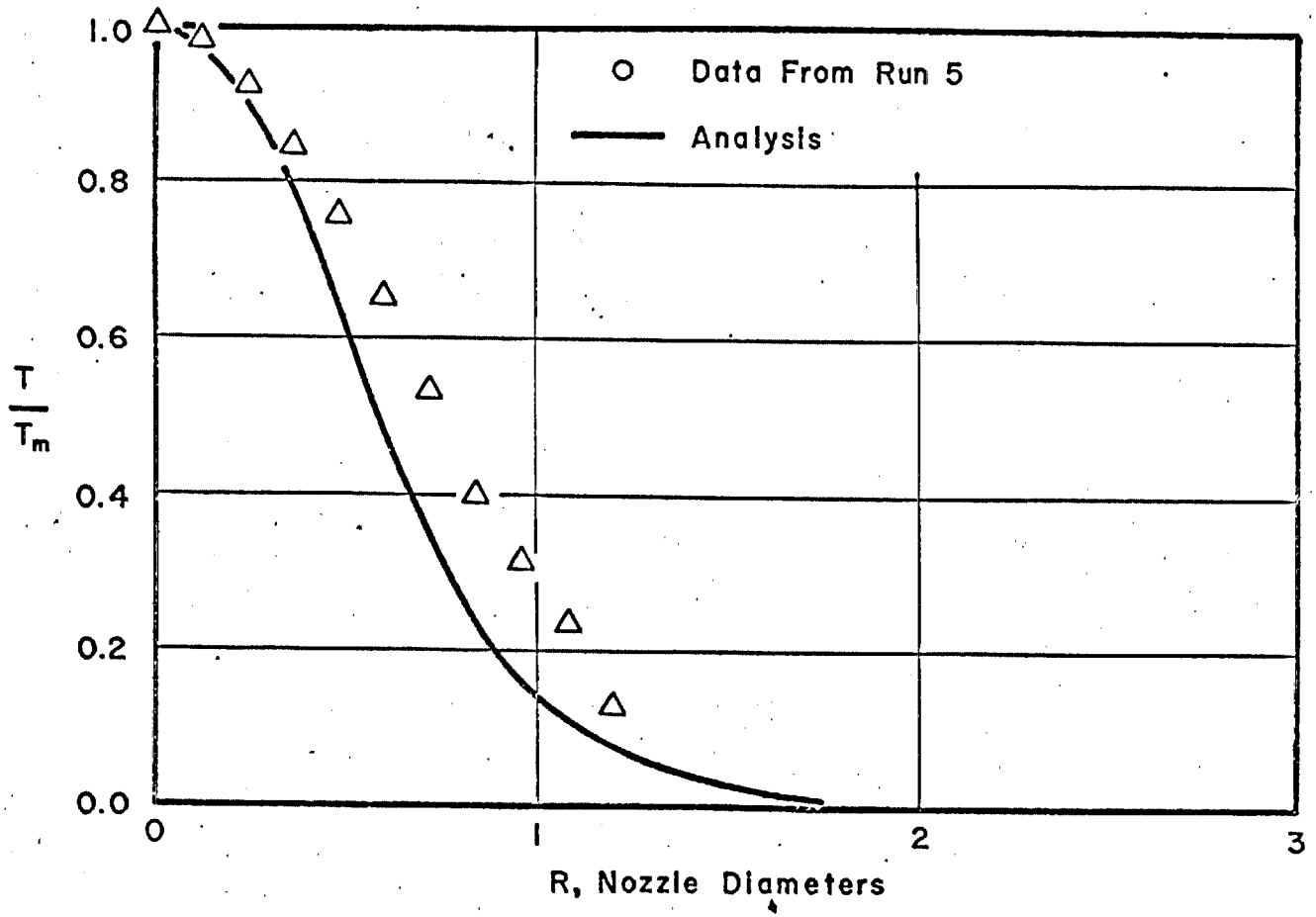

Figure 30

CALCULATED AND MEASURED RADIAL DISTRIBUTIONS OF TEMPERATURE AT Z = 4

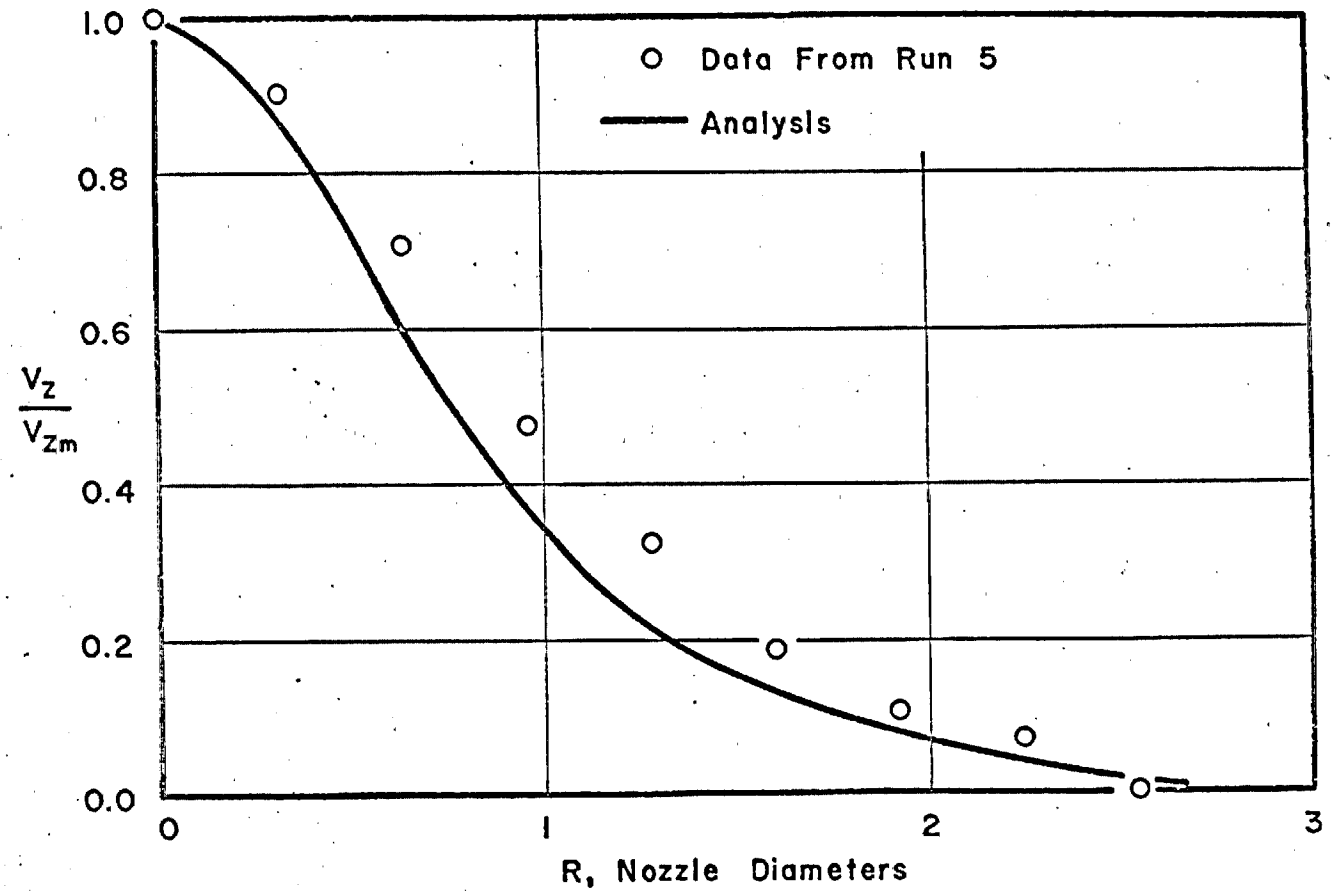

Figure 31

CALCULATED AND MEASURED RADIAL DISTRIBUTIONS OF AXIAL VELOCITY AT Z= 11

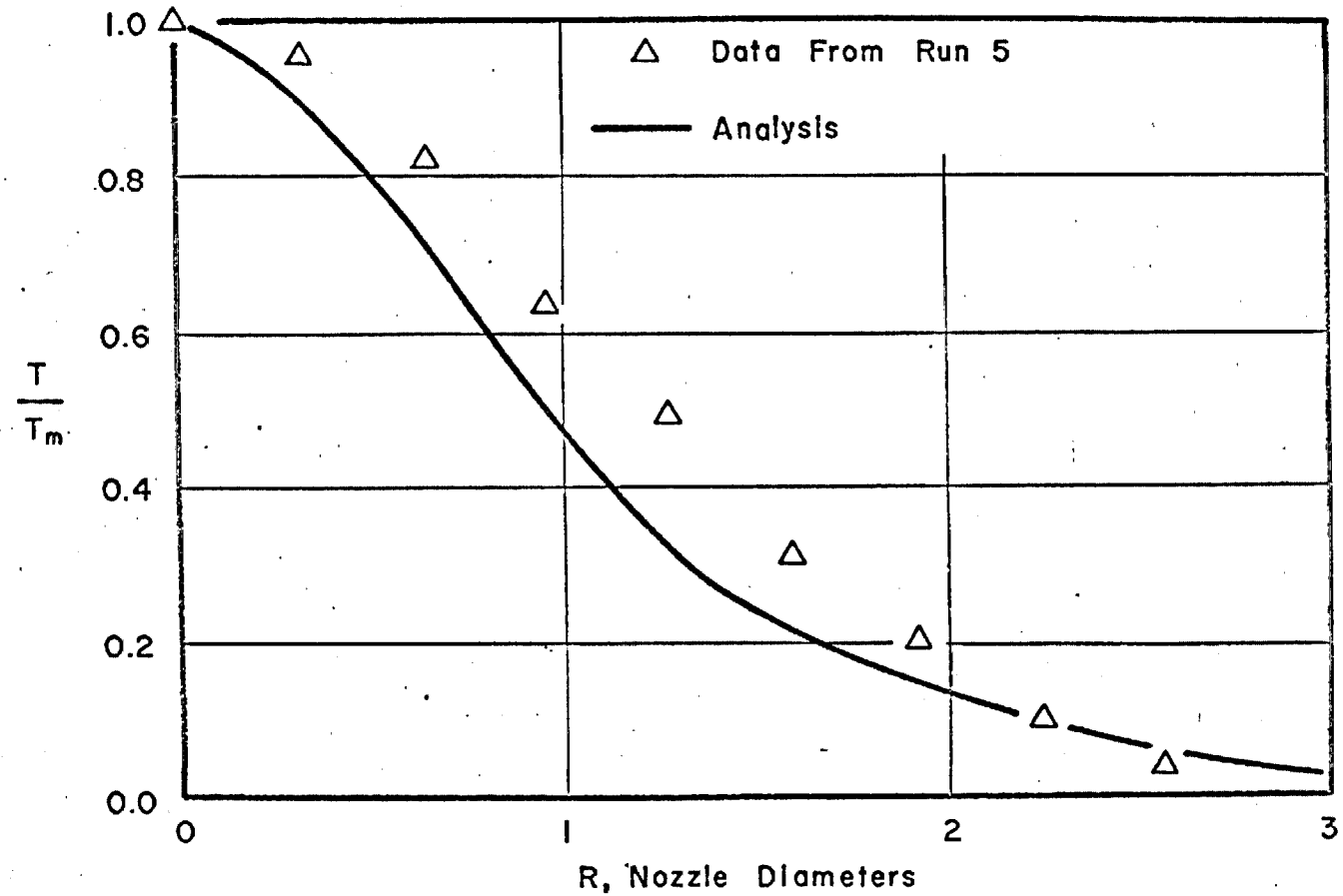

Figure 32

CALCULATED AND MEASURED RADIAL DISTRIBUTIONS OF TEMPERATURE AT Z=11

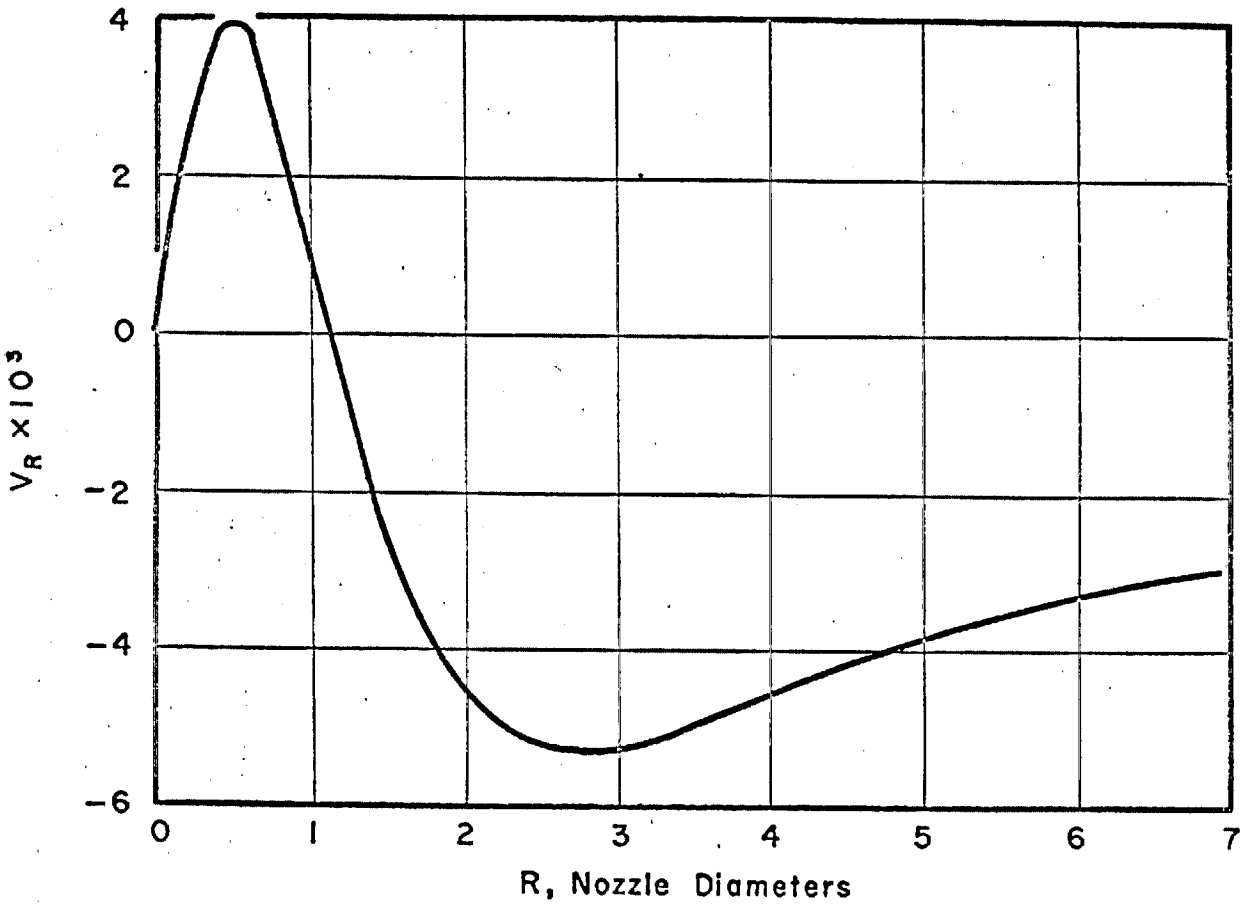

Figure 33

THE CALCULATED RADIAL DISTRIBUTION OF RADIAL VELOCITY AT Z = 11

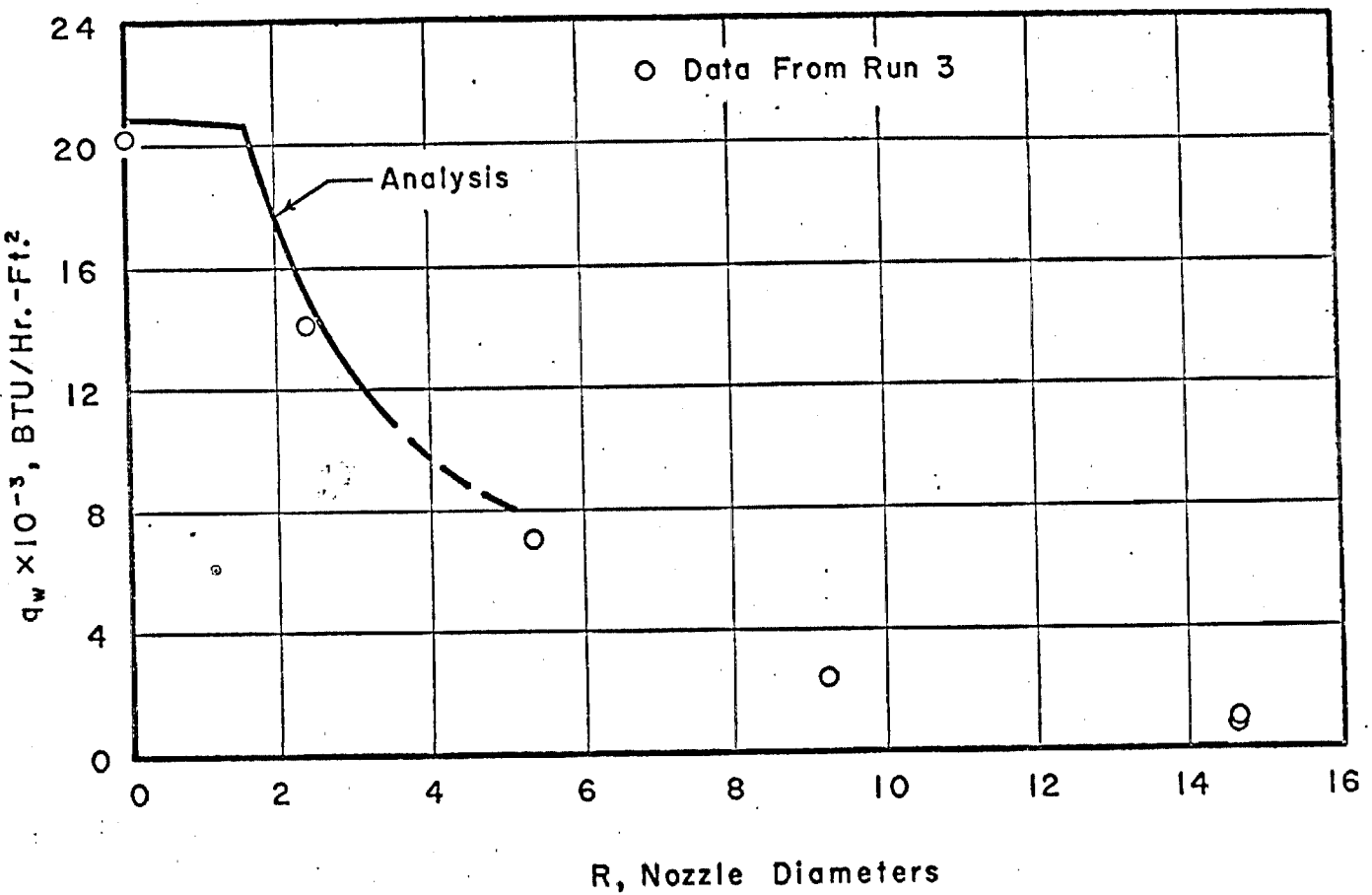

Figure 34

COMPARISON OF MEASURED AND CALCULATED HEAT FLUX DISTRIBUTIONS

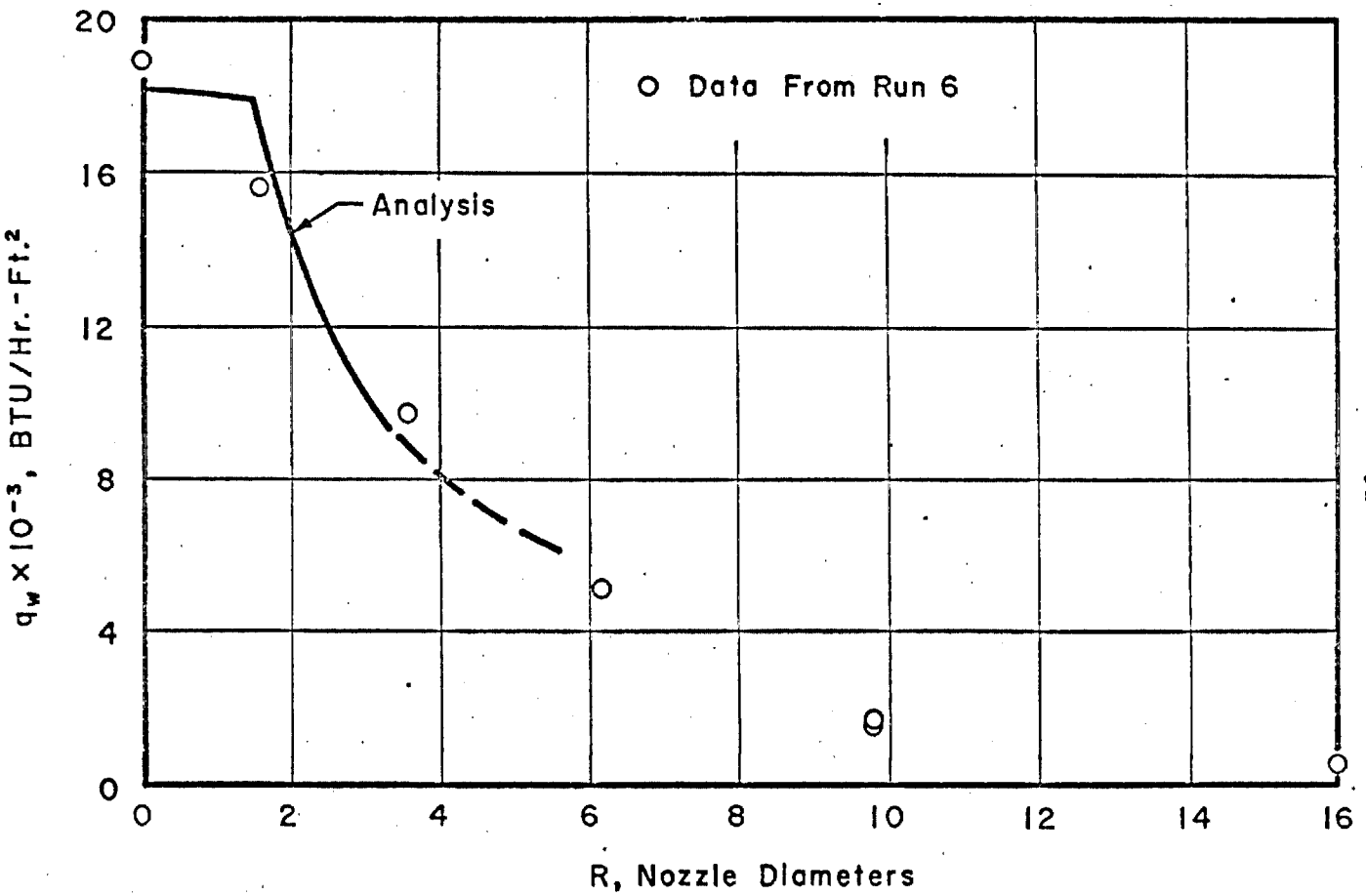

Figure 35

COMPARISON OF MEASURED AND CALCULATED HEAT FLUX DISTRIBUTIONS

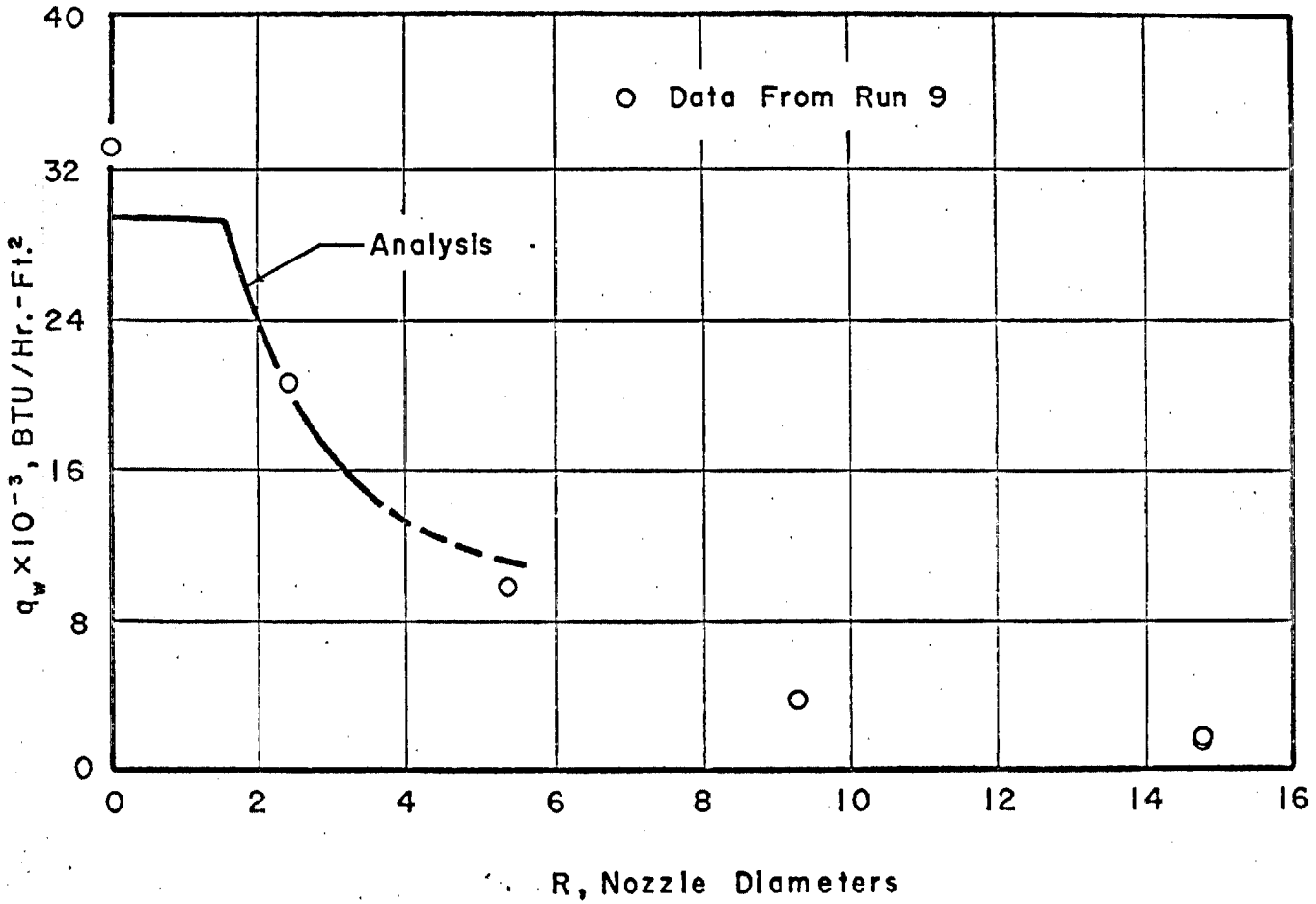

Figure 36

COMPARISON OF MEASURED AND CALCULATED HEAT FLUX DISTRIBUTIONS

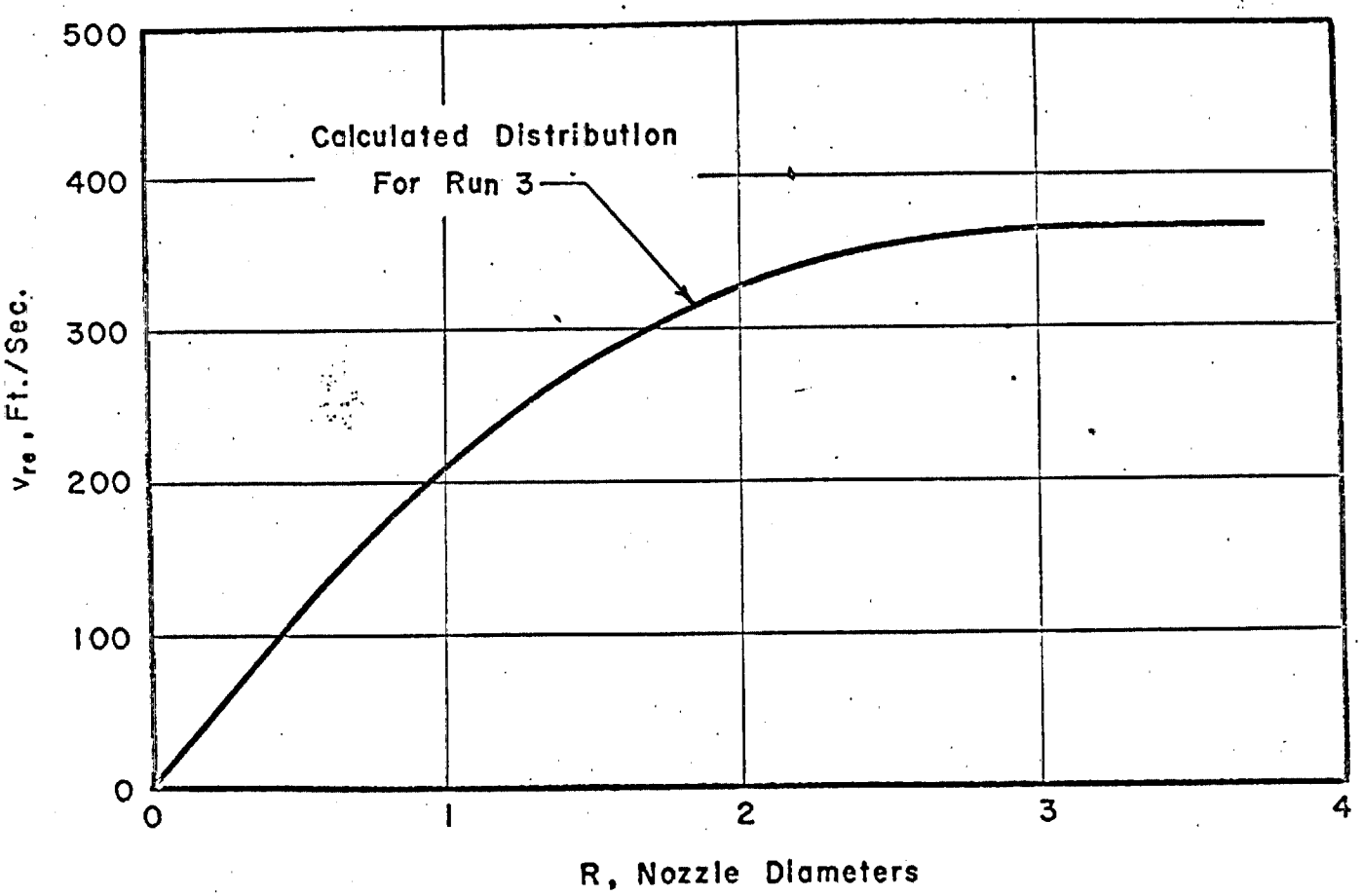

Figure 37

THE CALCULATED DISTRIBUTION OF THE VELOCITY AT THE EDGE OF THE IMPINGEMENT REGION BOUNDARY LAYER

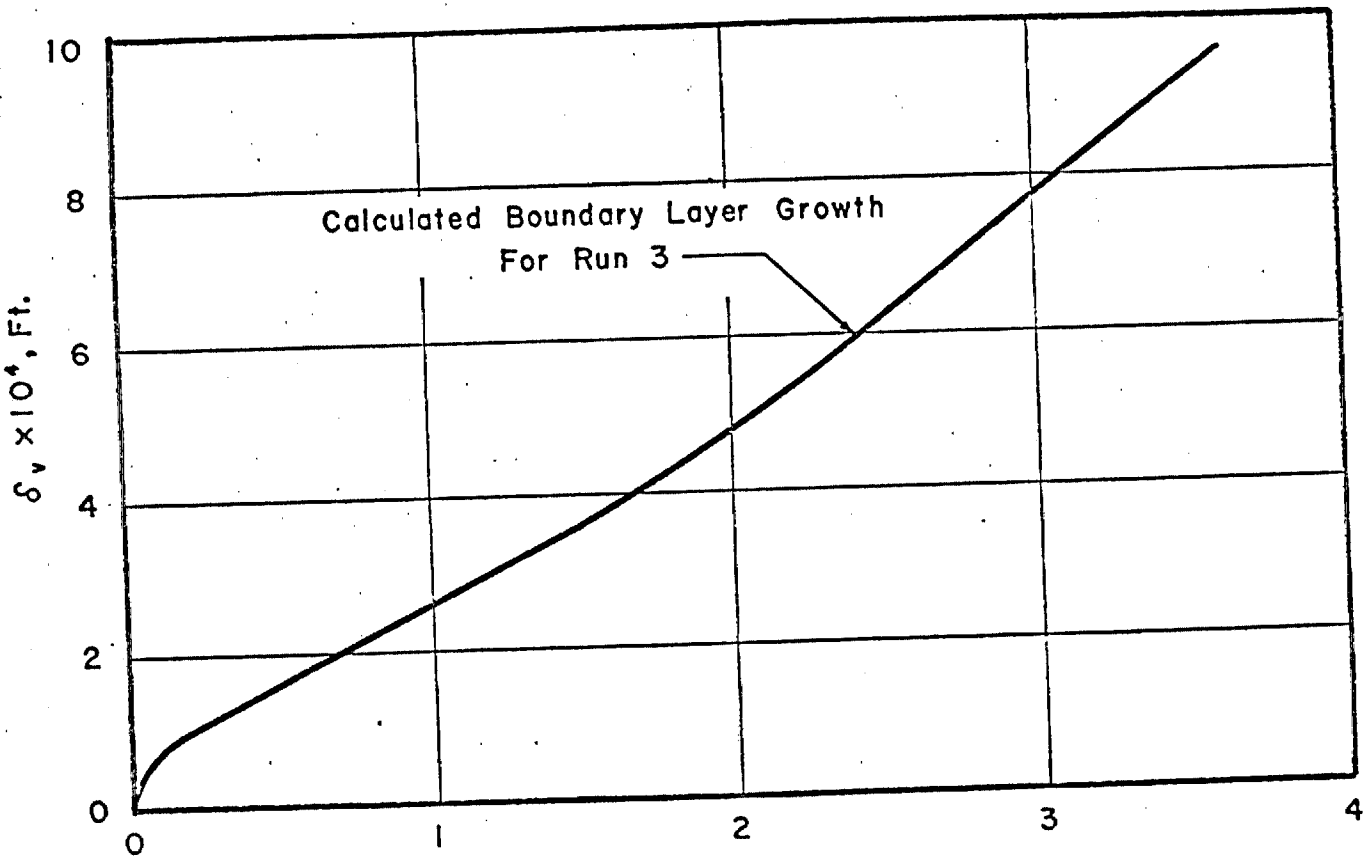

Figure 38

THE CALCULATED IMPINGEMENT REGION BOUNDARY LAYER GROWTH

Table 3

Comparison of Calculated Values of Parameters of the Static Pressure Distributions and Calculated Values of the Stagnation Point Heat Fluxes With Measured Values.

Run Number	p_s (psig)		r_5 (nozzle dia.)		q_{ws} (BTU/hr.-ft^2)	
	Calculated	Measured	Calculated	Measured	Calculated	Measured
3	0.781	0.752	1.33	1.26	20,911	20,214
4	1.626	1.552	1.29	1.22	27,573	24,472
5	1.480	1.189	1.22	1.22	26,319	23,623
6	0.930	0.872	1.28	1.18	18,104	18,919
7	1.606	1.557	0.98	0.92	28,298	41,992
8	3.029	3.487	0.70	0.64	42,015	77,578
9	1.564	1.351	1.22	1.30	29,355	32,576
10	1.611	1.385	1.16	1.17	20,712	20,419

6. DISCUSSION

6.1 THE FREE JET

It is evident that there is good general agreement between the calculated axial velocity and temperature profiles and the experimental results of this and previous investigations. There are some minor deviations between experiment and calculation, especially in the jet transition region. These are probably due to over-simplifications in the forms used for the eddy transfer coefficients.

The calculated radial distributions of velocities in the axial direction and temperatures consistently predict slightly lower velocities and temperatures over most of the distribution than are found experimentally. Much larger deviations occur, especially for high Mach number flows, if the viscous dissipation term of the energy equation (the last term of Equations (6) and (14)) is not included. At very large radial distances the calculated quantities become higher than the experimentally determined ones, but this deviation is very minor considering the accuracy of the data at positions far from the jet axis.

It is possible that there should be functions of radial position included in the transfer coefficient expressions in

order to improve the agreement between calculated radial distributions and experimental data. However, because of the magnitude of the deviations and the lack of knowledge of the turbulent shear structure of compressible free jets, it was not deemed justifiable to include such a modification at this time. The possibility that the differences in the results occur because the radial position chosen to represent an infinite radial distance in the numerical calculations was not large enough was investigated. Extensive calculations showed that this was not a factor.

The results demonstrate that the specification of only two initial properties suffices to provide the velocity and temperature characteristics of the compressible turbulent free jet. These are the jet Mach number (M) and the jet temperature ratio (t_j/t_a or P_a).

The effects of the jet temperature ratio and jet Mach number on the axial decay of velocity and temperature reported by Warren (7) have been corroborated. That is, for a given jet Mach number, an increase in the jet temperature ratio causes a more rapid decay of velocity and temperature; while for a given jet temperature, an increase in the jet Mach number causes a less rapid decay of the two quantities.

An advantage of the present calculational method is that calculated results for the radial distribution of the radial velocity component can also be obtained. The positive radial velocity near the jet axis is thought to be caused by the spread of the jet as it moves downstream, while the negative (inward) radial velocity at the larger radial distances is thought to be caused by the entrainment of ambient air. Experimental measurement of this velocity component will have to await the use of more sensitive techniques, such as hot-wire anemometry.

6.2 THE IMPINGEMENT REGION

The agreement between predicted and measured heat fluxes is good. In general, for experimental runs where the impingement region was located inside the fully developed region of the free jet flow, the per cent deviation between measured and calculated heat fluxes, based on the measured value, is never more than 13%. A check of the experimental method of measuring the heat fluxes showed that the experimental errors are 10% or less. Thus the deviations are of the same order of magnitude as the experimental errors. For the experimental runs where the impingement region was located within the transition region, the deviations are always negative and are as high as 46%, which is still

fairly good for this type of calculation in view of the assumptions which it was necessary to make.

These larger deviations are probably due to the much larger gradients of velocity, temperature, and pressure encountered when the impingement region is located within the transition region. Kemp, Rose and Detra (26) stated that "in regions of rapidly varying pressure there is evidence that the local similarity concept breaks down, and the theory underestimates the actual heat-transfer rate by up to 25 per cent." Also, in the impinging jet, and particularly when the impingement surface is located in the transition region, any turbulence of the flow near the stagnation point is greater than in a uniform impinging flow (18). This fact would also account for the lower value of the predicted heat flux at the stagnation point.

The heat flux measurements, themselves, do not definitely confirm the presence of a stagnation area in the heat flux distribution. Since the calculated heat fluxes do agree well with the measurements taken, and since other investigators have measured distributions showing the presence of stagnation areas (17), (15), the shape of the calculated heat flux distributions has some basis. Kezios (17), in fact, found that the heat flux at the outer edge of the

stagnation area was slightly higher than the heat flux at the stagnation point. This was probably caused by a uniform velocity profile entering the impingement region instead of a fully developed free jet flow. Such an effect was not indicated in the present study.

The radial position at which the impingement region heat flux solution becomes invalid is the radial position at which the impingement region ends and the wall jet region begins. This radial position, however, is very difficult to determine. Using the radial distance at which the gauge pressure is 0.1% of the gauge pressure at the stagnation point as the extent of the impingement region, this radial position is in the range of from 2.25 to 4.2 nozzle diameters for the various experimental runs of this investigation. Measurements of velocity and temperature variation in the wall jet, extrapolated toward the stagnation point in order to check the calculated velocity and temperature at the edge of the impingement region boundary layer, indicate that the extent of the impingement region is about 0.8 to 0.9 of that predicted from the pressure distributions. Whatever the exact extent of this region, it appears that the heat flux solution may be safely extrapolated a short dis-

tance into the wall jet region without introducing any larger errors.

Although no measurements were made of the velocity and temperature variation and boundary layer growth in the impingement region, measurements in the initial part of the wall jet flow indicate that the calculations give very reasonable values for these quantities. For example, extrapolating the impingement region boundary layer thickness solutions into initial part of the wall jet, the extrapolated values are within 10 to 15% of the measured boundary layer thicknesses. There is also qualitative agreement with the measured and calculated results of Tani and Komatsu (25).

The calculated values of the static pressure at the stagnation point and the "half-width" of the pressure distribution agree well with the measured values. In most cases the deviations between the calculated and measured values are around 10%, with the predicted values usually being higher than measured values.

7. CONCLUSIONS

7.1 THE FREE JET

A finite difference calculational technique has made possible a fairly simple yet very general solution of the boundary layer conservation equations for a compressible, turbulent, axially symmetric free jet. The generality of the present solution has eliminated the need for some of the simplifying assumptions that were required in previous investigations in order to obtain a solution. Modifications of eddy transfer coefficients given in the literature result in solutions which agree well with experimental data. However, the finite difference technique will be able to accommodate even more complex forms of eddy transfer coefficients when the accuracy of the available data justifies it. Another advantage of this calculational method is that distributions of the radial component of velocity are also obtained.

The jet Mach number and the jet temperature ratio are the only two initial jet properties which are necessary to obtain a good description of the compressible, turbulent free jet flow in terms of dimensionless variables. The axial velocity and temperature has been found to decay

faster when jet Mach numbers are decreased or jet temperature ratios are increased.

The experimental system which has been developed has been found to give reproducible data on the variation of velocity and temperature in a compressible, turbulent, axially symmetric free jet. An experimental program has been carried out to obtain free jet data at a variety of initial jet conditions where a lack of experimental data has existed, namely at high initial jet temperatures and high subsonic Mach numbers in order to evaluate the numerical solution. The free jet study provided the necessary starting point for the study of the impingement region.

7.2 THE IMPINGEMENT REGION

The adaptation of the stagnation area heat transfer theory developed for uniform impinging flows by Kemp, Rose and Detra (26) to impinging jets flows has been shown to give calculated heat flux distributions in the stagnation area which agree well with experimental data. Also, a solution of the integral momentum equation for the impingement region boundary layer has made possible the calculation of the heat flux distributions for the remainder of the impingement region, and the calculational technique may even be used to extrapolate these heat flux distributions into

the initial part of the wall jet flow. An attempt was made to keep the number of assumptions to a minimum and to provide some justification for the assumptions which it was necessary to make in developing the solution. The end result -- the agreement between the calculated and experimental quantities is also an important test of the assumptions which were made.

The method of solution which is presented here should be valid for any type of impinging flow with any wall temperature distribution which can be treated by the theory of Kemp, Rose and Detra (26) and whose dimensionless impingement region pressure distribution can be correlated by some equation, except possibly where turbulence effects are fairly large near the stagnation point, dissociation effects are large, or the Prandtl number differs greatly from unity.

Reproducible data on the variation of static pressure and heat flux in the impingement region have been obtained. The data were obtained for high temperature impinging jet flows with a variable plate surface temperature. These data have filled a gap which has existed in available experimental results.

8. ACKNOWLEDGEMENTS

The author wishes to acknowledge support received from NASA Multi-Disciplinary Research Grant NSG-58 to Washington University for the initiation of the work reported above and from NSF Grant No. 22296 to Washington University Computational Facilities which made possible the extensive computations required for this study. He would also like to acknowledge the assistance of Mr. Fred Epstein of the Industrial Engineering and Equipment Company of St. Louis in the design, fabrication, and testing of the air heater.

9. APPENDICES

APPENDIX 9.1

Nomenclature

English Letters

a = constant in Equation (54).

A_t = constant in dimensionless free jet energy equation, defined by Equation (15).

A_v = constant in dimensionless free jet momentum equation, defined by Equation (13).

b = constant in Equation (54).

c = constant in Equation (54).

C_p = heat capacity at constant pressure.

C_1 = constant in stagnation area heat flux equation.

D = diameter of the free jet nozzle.

$f_t(Z)$ = function defining the axial dependence of the eddy thermal conductivity in the free jet, defined by Equation (11).

$f_v(Z)$ = function defining the axial dependence of the eddy momentum transfer coefficient in the free jet, defined by Equation (10).

$F(M)$ = function defining the Mach number dependence of the eddy momentum transfer coefficient and the eddy thermal conductivity in the free jet, defined by Equation (10).

g_c = gravitational conversion factor.

h = enthalpy.

H = nozzle to plate distance.

I = number of last line of the free jet finite difference network in the z-direction.

J = number of the last point of the free jet finite difference network in the r-direction.

k = thermal conductivity.

l = height of the differential fluid element used in the derivation of the impingement region integral momentum boundary layer equation.

M = initial jet Mach number.

n = constant in exponent of the impingement region power profile for velocity.

N_{Ec} = Eckert number.

N_{Pr} = Prandtl number.

N_{Re} = Reynolds number.

p = absolute pressure.

q = heat flux.

Q = variable defined by Equation (50).

r = radial coordinate.

R = dimensionless radial coordinate, r/D.

t = temperature.

T = dimensionless temperature, $(t-t_a)/(t_j-t_a)$.

v_r = radial velocity.

V_r = dimensionless free jet radial velocity, v_r/v_{zj}.

W = variable defined by Equation (53).

v_z = free jet axial velocity.

V_z = dimensionless free jet axial velocity, v_z/v_{zj}.

y = impingement region coordinate normal to plate.

z = free jet axial coordinate.

Z = dimensionless free jet axial coordinate, z/D.

Greek Letters

$\beta(r)$ = variable in stagnation area heat flux equation, defined by Equation (40).

γ = heat capacity ratio.

δ = boundary layer thickness.

Δp = gauge pressure.

ΔR = free jet finite difference step size in radial direction.

ΔZ = free jet finite difference step size in axial direction.

ϵ_v = eddy kinematic viscosity.

$\eta(r)$ = variable in stagnation area heat flux solution, defined by Equation (41).

κ = eddy thermal conductivity.

μ = viscosity.

ν = kinematic viscosity.

ξ = impingement region dimensionless radial coordinate, defined by Equation (23).

π = 3.14159-----.

ρ = density.

P = dimensionless free jet density, p/p_j.

τ = shear stress.

τ_{rz} = shear stress exerted in the z-direction on a fluid surface of constant r.

Subscripts

a - denotes ambient conditions.

c - referring to outer edge of stagnation area.

ct - referring to potential core for temperature.

cv - referring to potential core for velocity.

e - denotes conditions at the edge of the impingement region boundary layer.

i - denotes the radial extent of the potential core for velocity.

j - denotes initial jet properties.

m - denotes center-line properties.

r,R - denotes radial component.

s - denotes stagnation point conditions.

t - referring to energy equation.

v - referring to momentum equation.

w - denotes conditions at the wall.

z,Z - denotes axial component.

½ - referring to the free jet radial position where $v_z/v_{zm}=0.5$.

5 - referring to the impingement region radial position where $\Delta p/\Delta p_s=0.5$.

Superscripts

o - denotes stagnation conditions of the uniform flow in the solution of Kemp, Rose, and Detra (26).

(t) - referring to turbulent flow.

$'$ - denotes fluctuating component of turbulent flow variable.

Other

$\overline{(\,)}$ - denotes time averaged component of turbulent flow variable.

APPENDIX 9.2

The Derivation of the Boundary Layer Equations for a Compressible, Axially Symmetric, Turbulent Free Jet

The general equations for the conservation of mass, momentum and energy (41) are as follows:

Continuity:

$$\frac{1}{r}\frac{\partial}{\partial r}(\rho r v_r) + \frac{\partial}{\partial z}(\rho v_z) = 0 \qquad \text{(A-1)}$$

Momentum, r-direction:

$$\rho v_r \frac{\partial v_r}{\partial r} + \rho v_z \frac{\partial v_r}{\partial z} = \frac{4}{3}\frac{\mu}{r}\frac{\partial v_r}{\partial r} + \frac{4}{3}\mu\frac{\partial^2 v_r}{\partial r^2} - \frac{4}{3}\frac{\mu}{r^2}v_r + \frac{1}{3}\mu\frac{\partial^2 v_z}{\partial r \partial z} + \mu\frac{\partial^2 v_r}{\partial z^2} \qquad \text{(A-2)}$$

Momentum, Z-direction:

$$\rho v_r \frac{\partial v_z}{\partial r} + \rho v_z \frac{\partial v_z}{\partial z} = \frac{\mu}{r}\frac{\partial v_z}{\partial r} + \mu\frac{\partial^2 v_z}{\partial r^2} + \frac{1}{3}\frac{\mu}{r}\frac{\partial v_r}{\partial z} + \mu\frac{\partial^2 v_r}{\partial r \partial z} + \frac{4}{3}\mu\frac{\partial^2 v_z}{\partial z^2} - \frac{2}{3}\mu\frac{\partial^2 v_z}{\partial r \partial z} \qquad \text{(A-3)}$$

Energy:

$$\rho v_r C_p \frac{\partial t}{\partial r} + \rho v_z C_p \frac{\partial t}{\partial z} = \frac{k}{r}\frac{\partial t}{\partial r} + k\frac{\partial^2 t}{\partial r^2}$$

$$+ k\frac{\partial^2 t}{\partial z^2} + \frac{4}{3}\mu\left(\frac{\partial v_r}{\partial r}\right)^2 + \frac{4}{3}\mu\left(\frac{v_r}{r}\right)^2$$

$$- \frac{4}{3}\mu\frac{v_r}{r}\left(\frac{\partial v_r}{\partial r}\right) + \frac{4}{3}\mu\left(\frac{\partial v_z}{\partial z}\right)^2 - \frac{4}{3}\mu\frac{\partial v_r}{\partial r}\frac{\partial v_z}{\partial z}$$

$$- \frac{4}{3}\mu\frac{v_r}{r}\frac{\partial v_z}{\partial z} + \mu\left(\frac{\partial v_z}{\partial r}\right)^2 + 2\mu\frac{\partial v_z}{\partial r}\frac{\partial v_r}{\partial z}$$

$$+ \mu\left(\frac{\partial v_r}{\partial z}\right)^2 \qquad \text{(A-4)}$$

Pressure gradients and buoyancy terms are neglected for subsonic free jets (1), and the heat capacity, viscosity and thermal conductivity are assumed constant.

9.2.1 Boundary Layer Assumptions

In order to apply the boundary layer assumptions, the equations must be put into a dimensionless form by making the following substitutions.

$$R = \frac{r}{D} \qquad \text{(A-5)}$$

$$Z = \frac{z}{D} \qquad \text{(A-6)}$$

$$V_R = \frac{v_r}{v_{zj}} \qquad \text{(A-7)}$$

$$V_Z = \frac{v_z}{v_{zj}} \qquad \text{(A-8)}$$

$$P = \frac{\rho}{\rho_j} \tag{A-9}$$

$$T = \frac{t - t_a}{t_j - t_a} \tag{A-10}$$

Thus the dimensionless equations become

Continuity:

$$\frac{1}{R}\frac{\partial}{\partial R}(PRV_R) + \frac{\partial}{\partial Z}(PV_Z) = 0 \tag{A-11}$$

Momentum, r-direction:

$$PV_R\frac{\partial V_R}{\partial R} + PV_Z\frac{\partial V_R}{\partial Z} = \frac{4}{3}\frac{1}{N_{Re}}\frac{1}{R}\frac{\partial V_R}{\partial R} + \frac{4}{3}\frac{1}{N_{Re}}\frac{\partial^2 V_R}{\partial R^2} - \frac{4}{3}\frac{1}{N_{Re}}\frac{V_R}{R^2} + \frac{1}{3}\frac{1}{N_{Re}}\frac{\partial^2 V_Z}{\partial Z \partial R} + \frac{1}{N_{Re}}\left(\frac{\partial^2 V_R}{\partial Z^2}\right) \tag{A-12}$$

Momentum, Z-direction:

$$PV_R\frac{\partial V_Z}{\partial R} + PV_Z\frac{\partial V_Z}{\partial Z} = \frac{1}{N_{Re}}\frac{1}{R}\frac{\partial V_Z}{\partial R} + \frac{1}{N_{Re}}\frac{\partial^2 V_Z}{\partial R^2} + \frac{1}{3}\frac{1}{N_{Re}}\frac{1}{R}\frac{\partial V_R}{\partial Z} + \frac{1}{N_{Re}}\frac{\partial^2 V_R}{\partial R \partial Z} + \frac{4}{3}\frac{1}{N_{Re}}\frac{\partial^2 V_Z}{\partial Z^2} - \frac{2}{3}\frac{1}{N_{Re}}\frac{\partial^2 V_Z}{\partial R \partial Z} \tag{A-13}$$

Energy:

$$PV_R\frac{\partial T}{\partial R}+PV_Z\frac{\partial T}{\partial Z}=\frac{1}{N_{Re}N_{Pr}}\frac{1}{R}\frac{\partial T}{\partial R}+\frac{1}{N_{Re}N_{Pr}}\frac{\partial^2 T}{\partial R^2}$$
$$+\frac{1}{N_{Re}N_{Pr}}\frac{\partial^2 T}{\partial Z^2}+\frac{4}{3}\frac{N_{Ec}}{N_{Re}}\left(\frac{\partial V_R}{\partial R}\right)^2$$
$$+\frac{4}{3}\frac{N_{Ec}}{N_{Re}}\left(\frac{V_R}{R}\right)^2+\frac{4}{3}\frac{N_{Ec}}{N_{Re}}\left(\frac{\partial V_Z}{\partial Z}\right)^2$$
$$-\frac{4}{3}\frac{N_{Ec}}{N_{Re}}\left(\frac{V_R}{R}\right)\left(\frac{\partial V_R}{\partial R}\right)-\frac{4}{3}\frac{N_{Ec}}{N_{Re}}\left(\frac{\partial V_R}{\partial R}\right)\left(\frac{\partial V_Z}{\partial Z}\right)$$
$$-\frac{4}{3}\frac{N_{Ec}}{N_{Re}}\left(\frac{V_R}{R}\right)\left(\frac{\partial V_Z}{\partial Z}\right)+\frac{N_{Ec}}{N_{Re}}\left(\frac{\partial V_Z}{\partial R}\right)^2$$
$$+2\frac{N_{Ec}}{N_{Re}}\left(\frac{\partial V_Z}{\partial R}\right)\left(\frac{\partial V_R}{\partial Z}\right)+\frac{N_{Ec}}{N_{Re}}\left(\frac{\partial V_R}{\partial Z}\right)^2 \qquad \text{(A-14)}$$

where

$$N_{Re}=\frac{D v_{zj}\rho_i}{\mu} \qquad \text{(A-15)}$$

$$N_{Pr}=\frac{\mu C_p}{k} \qquad \text{(A-16)}$$

$$N_{Ec}=\frac{v_{zj}^2}{C_p(t_j-t_a)} \qquad \text{(A-17)}$$

Making the standard boundary layer assumptions that the thickness of the boundary layer is very small compared to the length and that the velocity along the boundary layer is much larger than the velocity across the boundary layer, the following order of magnitude approximations can be postulated.

$$R = [1] \tag{A-18}$$

$$Z = \left[\frac{1}{\delta}\right] \tag{A-19}$$

$$V_R = [\delta] \tag{A-20}$$

$$V_Z = [1] \tag{A-21}$$

$$P = [1] \tag{A-22}$$

$$T = [1] \tag{A-23}$$

where δ = boundary layer thickness

$$\delta \ll 1$$

Also, by physical reasoning, it may be deduced (5) that

$$N_{Re} = \left[\frac{1}{\delta^2}\right] \tag{A-24}$$

$$N_{Pr} = [1] \tag{A-25}$$

$$N_{Ec} = [1] \tag{A-26}$$

Making these order of magnitude approximations in the boundary layer equations, the entire r-direction momentum equation and certain terms of the z-direction momentum energy equation are extremely small and can be neglected. Thus the laminar boundary layer equations become

Continuity:

$$\frac{1}{R}\frac{\partial}{\partial R}(PRV_R)+\frac{\partial}{\partial Z}(PV_z)=0 \qquad \text{(A-27)}$$

Momentum:

$$PV_R\frac{\partial V_z}{\partial R}+PV_z\frac{\partial V_z}{\partial Z}=\frac{\mu}{\rho_j v_{zj} D}\frac{1}{R}\frac{\partial}{\partial R}\left(R\frac{\partial V_z}{\partial R}\right) \qquad \text{(A-28)}$$

Energy:

$$PV_R\frac{\partial T}{\partial R}+PV_z\frac{\partial T}{\partial Z}=\frac{k}{\rho_j v_{zj} DC_P}\frac{1}{R}\frac{\partial}{\partial R}\left(R\frac{\partial T}{\partial R}\right)$$

$$+\frac{\mu v_{zj}}{\rho_j DC_P(t_j-t_a)}\left(\frac{\partial V_z}{\partial R}\right)^2 \qquad \text{(A-29)}$$

9.2.2 Time-Smoothing for Turbulent Flow

Writing Equations (A-27) through (A-29) in the dimensional form, they become

$$\frac{1}{r}\frac{\partial}{\partial r}(\rho r v_r)+\frac{\partial}{\partial z}(\rho v_z)=0 \qquad \text{(A-30)}$$

$$\rho v_r\frac{\partial v_z}{\partial r}+\rho v_z\frac{\partial v_z}{\partial z}=\frac{\mu}{r}\frac{\partial}{\partial r}\left(r\frac{\partial v_z}{\partial r}\right) \qquad \text{(A-31)}$$

$$\rho v_r C_P\frac{\partial t}{\partial r}+\rho v_z C_P\frac{\partial t}{\partial z}=k\frac{1}{r}\frac{\partial}{\partial r}\left(r\frac{\partial t}{\partial r}\right)+\mu\left(\frac{\partial v_z}{\partial r}\right)^2 \qquad \text{(A-32)}$$

Expanding the continuity equation, Equation (A-30), we have

$$\frac{\partial}{\partial z}(\rho v_z)+\frac{\partial}{\partial r}(\rho v_r)+\frac{\rho v_r}{r}=0 \qquad \text{(A-33)}$$

Now, writing (ρv_z) and (ρv_r) as the sum of a mean and a fluctuating component.

$$(\rho v_z) = (\overline{\rho v_z}) + (\rho v_z)' \qquad \text{(A-34)}$$

$$(\rho v_r) = (\overline{\rho v_r}) + (\rho v_r)' \qquad \text{(A-35)}$$

Note that average values are obtained by averaging over a time period which is long enough to obtain a mean value but short enough to show the transient behavior.

Substituting Equations (A-34) and (A-35) into Equation (A-33) and "time-smoothing" by averaging over this time period, the "time-smoothed" continuity equation is

$$\frac{\partial}{\partial z}(\overline{\rho v_z}) + \frac{\partial}{\partial r}(\overline{\rho v_r}) + \frac{(\overline{\rho v_r})}{r} = 0 \qquad \text{(A-36)}$$

since $\overline{(\ )'} = 0$

and $\overline{\frac{\partial(\ )}{\partial[\ ]}} = \frac{\partial(\ )}{\partial[\ ]}$

The momentum equation, Equation (A-31), written in a different form, becomes

$$\rho v_z \frac{\partial v_z}{\partial z} + \rho v_r \frac{\partial v_z}{\partial r} = \frac{\mu}{r}\frac{\partial}{\partial r}\left(r \frac{\partial v_z}{\partial r}\right) = -\frac{1}{r}\frac{\partial}{\partial r}(r\tau_{rz}) \qquad \text{(A-37)}$$

Multiplying the continuity equation, Equation (A-30), by v_z and then adding it to Equation (A-37), we have

$$\frac{\partial}{\partial z}\left[(\rho v_z) v_z\right] + \frac{\partial}{\partial r}\left[(\rho v_r) v_z\right] + \frac{(\rho v_r) v_z}{r}$$

$$= -\frac{\partial \tau_{rz}}{\partial r} - \frac{\tau_{rz}}{r} \qquad \text{(A-38)}$$

Again, the variables will be defined as the sum of a mean and a fluctuating component.

$$v_z = \overline{v_z} + v_z' \qquad \text{(A-39)}$$

$$\tau_{rz} = \overline{\tau_{rz}} + \tau_{rz}' \qquad \text{(A-40)}$$

Substituting Equations (A-34), (A-35), (A-39), and (A-40) into Equation (A-38) and time averaging, we have

$$\frac{\partial}{\partial z}\left[\overline{(\rho v_z)}\,\overline{v_z} + \overline{(\rho v_z)' v_z'}\right] + \frac{\partial}{\partial r}\left[\overline{(\rho v_r)}\,\overline{v_z} + \overline{(\rho v_r)' v_z'}\right]$$

$$+ \frac{1}{r}\left[\overline{(\rho v_r)}\,\overline{v_z} + \overline{(\rho v_r)' v_z'}\right] = -\frac{\partial \overline{\tau}_{rz}}{\partial r} - \frac{\overline{\tau}_{rz}}{r} \qquad \text{(A-41)}$$

Multiplying the "time-smoothed" continuity equation, Equation (A-36), by $\overline{v_z}$ and subtracting it from Equation (A-41), we have

$$\overline{(\rho v_z)}\frac{\partial \overline{v_z}}{\partial z} + \overline{(\rho v_r)}\frac{\partial \overline{v_z}}{\partial r} = -\frac{1}{r}\frac{\partial}{\partial r}(r\overline{\tau}_{rz})$$

$$-\frac{1}{r}\frac{\partial}{\partial r}\left[r\overline{(\rho v_r)' v_z'}\right] - \frac{\partial}{\partial z}\left[\overline{(\rho v_z)' v_z'}\right] \qquad \text{(A-42)}$$

The boundary layer assumptions applied to this equation show that

$$\frac{1}{r}\frac{\partial}{\partial r}\left[\overline{r(\rho v_r)' v_z'}\right] \gg \frac{\partial}{\partial z}\left[\overline{(\rho v_z)' v_z'}\right] \tag{A-43}$$

Therefore the "time-smoothed" momentum equation becomes

$$\overline{(\rho v_z)}\frac{\partial \overline{v_z}}{\partial z} + \overline{(\rho v_r)}\frac{\partial \overline{v_z}}{\partial r} = -\frac{1}{r}\frac{\partial}{\partial r}(r\overline{\tau}_{rz}) - \frac{1}{r}\frac{\partial}{\partial r}\left\{r\left[\overline{(\rho v_r)' v_z'}\right]\right\} \tag{A-44}$$

Adopting the usual notation, we can define the turbulent shear stress or Reynolds' stress, and then use Boussinesq's definition of eddy kinematic viscosity to get

$$\left[\overline{(\rho v_r)' v_z'}\right] = \tau_{rz}^{(t)} = -\overline{\rho}\epsilon_v \frac{\partial \overline{v_z}}{\partial r} \tag{A-45}$$

Therefore, the "time-smoothed" momentum equation becomes

$$\overline{(\rho v_z)}\frac{\partial \overline{v_z}}{\partial z} + \overline{(\rho v_r)}\frac{\partial \overline{v_z}}{\partial r} = -\frac{1}{r}\frac{\partial}{\partial r}\left[\overline{\tau}_{rz} + \tau_{rz}^{(t)}\right] = \frac{1}{r}\frac{\partial}{\partial r}\left[r(\mu + \overline{\rho}\epsilon_v)\frac{\partial \overline{v_z}}{\partial r}\right] \tag{A-46}$$

The energy equation, Equation (A-32), written in a slightly different form becomes

$$\rho v_r C_p \frac{\partial t}{\partial r} + \rho v_z C_p \frac{\partial t}{\partial z} = -\frac{1}{r}\frac{\partial}{\partial r}(rq_r) - \tau_{rz}\frac{\partial v_z}{\partial r} \tag{A-47}$$

Multiplying the continuity equation, Equation (A-30), by and adding it to Equation (A-47), we have

$$C_p \frac{\partial}{\partial z}\left[(\rho v_z)t\right] + C_p \frac{\partial}{\partial r}\left[(\rho v_r)t\right] + \frac{C_p(\rho v_r)t}{r}$$

$$= -\frac{1}{r}\frac{\partial}{\partial r}(rq_r) - \tau_{rz}\frac{\partial v_z}{\partial r} \qquad \text{(A-48)}$$

The momentum equation, Equation (A-31), multiplied by v_z is

$$\rho v_z^2 \frac{\partial v_z}{\partial z} + \rho v_r v_z \frac{\partial v_z}{\partial r} = -v_z \frac{\partial \tau_{rz}}{\partial r} - \frac{v_z \tau_{rz}}{r} \qquad \text{(A-49)}$$

The first two terms of Equation (A-49) may be expanded to give

$$\rho v_z^2 \frac{\partial v_z}{\partial z} = \frac{1}{2}\frac{\partial}{\partial z}(\rho v_z^3) - \frac{1}{2} v_z^2 \frac{\partial(\rho v_z)}{\partial z} \qquad \text{(A-50)}$$

$$\rho v_r v_z \frac{\partial v_z}{\partial r} = \frac{1}{2}\frac{\partial}{\partial r}(\rho v_r v_z^2) - \frac{1}{2} v_z^2 \frac{\partial(\rho v_r)}{\partial r} \qquad \text{(A-51)}$$

Substituting Equations (A-50) and (A-51) into Equation (A-49), we have

$$\frac{1}{2}\frac{\partial}{\partial z}(\rho v_z^3) - \frac{1}{2} v_z^2 \frac{\partial(\rho v_r)}{\partial z} + \frac{1}{2}\frac{\partial}{\partial r}(\rho v_r v_z^2)$$

$$-\frac{1}{2} v_z^2 \frac{\partial(\rho v_r)}{\partial r} = v_z \frac{\partial \tau_{rz}}{\partial r} - \frac{v_z \tau_{rz}}{r} \qquad \text{(A-52)}$$

Multiplying the continuity equation, Equation (A-30), by $\frac{1}{2} v_z^2$ and adding it to Equation (A-52), we have

$$\frac{1}{2}\frac{\partial}{\partial z}(\rho v_z^3)+\frac{1}{2}\frac{\partial}{\partial r}(\rho v_r v_z^2)+\frac{1}{2}\frac{\rho v_r v_z^2}{r}$$

$$=-v_z\frac{\partial \tau_{rz}}{\partial r}-\frac{v_z\tau_{rz}}{r} \qquad \text{(A-53)}$$

The addition of Equation (A-53) to Equation (A-48) gives

$$C_p\frac{\partial}{\partial z}\left[(\rho v_z)t\right]+C_p\frac{\partial}{\partial r}\left[(\rho v_r)t\right]+\frac{C_p(\rho v_r)t}{r}$$

$$+\frac{1}{2}\frac{\partial}{\partial z}(\rho v_z^3)+\frac{1}{2}\frac{\partial}{\partial r}(\rho v_r v_z^2)+\frac{1}{2}\frac{\rho v_r v_z^2}{r}$$

$$=-\frac{1}{r}\frac{\partial}{\partial r}(rq_r)-\frac{\partial}{\partial r}(v_z\tau_{rz})-\frac{v_z\tau_{rz}}{r} \qquad \text{(A-54)}$$

Again the variables will be defined as the sum of a mean and a fluctuating component.

$$q_r=\overline{q_r}+q_r' \qquad \text{(A-55)}$$

Substituting Equations (A-34), (A-35), (A-39), (A-40), and (A-55) into Equation (A-54) and time averaging, we have

$$C_p\frac{\partial}{\partial z}\left[\overline{(\rho v_z)}\,\bar{t}+\overline{(\rho v_z)'t'}\right]+C_p\frac{\partial}{\partial r}\left[\overline{(\rho v_r)}\,\bar{t}+\overline{(\rho v_r)'t'}\right]$$

$$+\frac{C_p}{r}\left[\overline{(\rho v_r)}\,\bar{t}+\overline{(\rho v_r)'t'}\right]+\frac{1}{2}\frac{\partial}{\partial z}\left[\overline{(\rho v_z)}\,\overline{v_z^2}+\overline{(\rho v_z)}\,\overline{v_z'^2}\right.$$

$$+ 2\overline{(\rho v_z)' v_z'}\,\bar{v}_z + \overline{(\rho v_z)' v_z'^2}\Big] + \frac{1}{2}\frac{\partial}{\partial r}\Big[\overline{(\rho v_r)}\,\bar{v}_z^2$$

$$+ \overline{(\rho v_r)}\,\overline{v_z'^2} + 2\,\overline{(\rho v_r)' v_z'}\,\bar{v}_z + \overline{(\rho v_r)' v_z'^2}\Big]$$

$$+ \frac{1}{2r}\Big[\overline{(\rho v_r)}\,\bar{v}_z^2 + \overline{(\rho v_r)}\,\overline{v_z'^2} + 2\,\overline{(\rho v_r)' v_z'}\,\bar{v}_z$$

$$+ \overline{(\rho v_r)' v_z'^2}\Big] = -\frac{1}{r}\frac{\partial}{\partial r}(r\bar{q}_r) - \frac{\partial}{\partial r}(\bar{v}_z\bar{\tau}_{rz} + \overline{v_z'\tau_{rz}'})$$

$$- \frac{1}{r}(\bar{v}_z\bar{\tau}_{rz} + \overline{v_z'\tau_{rz}'}) \qquad \text{(A-56)}$$

This equation will now be converted to the standard form by using the "time-smoothed" continuity and momentum equations. First, the "time-smoothed" momentum equation, Equation (A-44), is multiplied by $\bar{v}_z$ to give

$$\overline{(\rho v_z)}\,\bar{v}_z\frac{\partial \bar{v}_z}{\partial z} + \overline{(\rho v_r)}\,\bar{v}_z\frac{\partial \bar{v}_z}{\partial r} = -\bar{v}_z\frac{\partial \bar{\tau}_{rz}}{\partial r} - \frac{\bar{v}_z\bar{\tau}_{rz}}{r}$$

$$- \frac{\bar{v}_z}{r}\frac{\partial}{\partial r}\Big\{r\Big[\overline{(\rho v_r)' v_z'}\Big]\Big\} \qquad \text{(A-57)}$$

Expanding the first two terms of Equation (A-57), we have

$$\overline{(\rho v_z)}\,\bar{v}_z\frac{\partial \bar{v}_z}{\partial z} = \frac{1}{2}\frac{\partial}{\partial z}\Big[\overline{(\rho v_z)}\,\bar{v}_z^2\Big] - \frac{1}{2}\bar{v}_z^2\frac{\partial(\overline{\rho v_z})}{\partial z} \qquad \text{(A-58)}$$

$$\overline{(\rho v_r)}\,\bar{v}_z\frac{\partial \bar{v}_z}{\partial r} = \frac{1}{2}\frac{\partial}{\partial r}\Big[\overline{(\rho v_r)}\,\bar{v}_z^2\Big] - \frac{1}{2}\bar{v}_z^2\frac{\partial(\overline{\rho v_r})}{\partial r} \qquad \text{(A-59)}$$

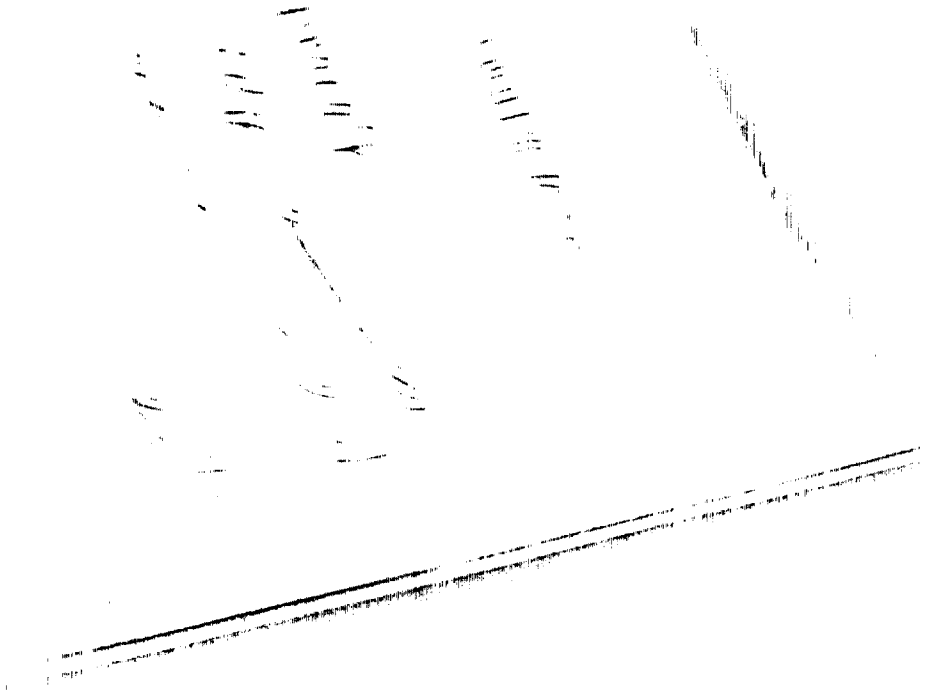

Substituting Equations (A-58) and (A-59) into Equation (A-57), we have

$$\frac{1}{2}\frac{\partial}{\partial z}\left[(\overline{\rho v_z})\,\overline{v_z}^2\right]-\frac{1}{2}\overline{v_z}^2\frac{\partial(\overline{\rho v_z})}{\partial z}+\frac{1}{2}\frac{\partial}{\partial r}\left[(\overline{\rho v_r})\,\overline{v_z}^2\right]$$

$$-\frac{1}{2}\overline{v_z}^2\frac{\partial(\overline{\rho v_r})}{\partial r}=-\overline{v_z}\frac{\partial\overline{\tau_{rz}}}{\partial r}-\frac{\overline{v_z}\,\overline{\tau_{rz}}}{r}-\frac{\overline{v_z}}{r}\frac{\partial}{\partial r}\left\{r\left[\overline{(\rho v_r)'v_z'}\right]\right\} \qquad \text{(A-60)}$$

Next, the "time-smoothed" continuity equation, Equation (A-36), is multiplied by $\frac{1}{2}\overline{v_z}^2$ to give

$$\frac{1}{2}\overline{v_z}^2\frac{\partial(\overline{\rho v_z})}{\partial z}+\frac{1}{2}\overline{v_z}^2\frac{\partial(\overline{\rho v_r})}{\partial r}+\frac{1}{2}\frac{(\overline{\rho v_r})\overline{v_z}^2}{r}=0 \qquad \text{(A-61)}$$

Adding Equations (A-60) and (A-61), we have

$$\frac{1}{2}\frac{\partial}{\partial z}\left[(\overline{\rho v_z})\overline{v_z}^2\right]+\frac{1}{2}\frac{\partial}{\partial r}\left[(\overline{\rho v_r})\overline{v_z}^2\right]+\frac{1}{2}\frac{(\overline{\rho v_r})\overline{v_z}^2}{r}$$

$$=-\overline{v_z}\frac{\partial\overline{\tau_{rz}}}{\partial r}-\frac{\overline{v_z}\,\overline{\tau_{rz}}}{r}-\frac{\overline{v_z}}{r}\frac{\partial}{\partial r}\left\{r\left[\overline{(\rho v_r)'v_z'}\right]\right\} \qquad \text{(A-62)}$$

Now, subtracting Equation (A-62) from Equation (A-56), we have

$$C_p\frac{\partial}{\partial z}\left[(\overline{\rho v_z})\bar{T}\right]+C_p\frac{\partial}{\partial z}\left[\overline{(\rho v_z)'T'}\right]+C_p\frac{\partial}{\partial r}\left[(\overline{\rho v_r})\bar{T}\right]$$

$$+C_p\frac{\partial}{\partial r}\left[\overline{(\rho v_r)'T'}\right]+\frac{C_p}{r}\left[(\overline{\rho v_r})\bar{T}\right]+\frac{C_p}{r}\left[\overline{(\rho v_r)'T'}\right]$$

$$+\frac{1}{2}\frac{\partial}{\partial z}\left[(\overline{\rho v_z})\overline{v_z'^2}+2\,\overline{(\rho v_z)'v_z'}\,\overline{v_z}+\overline{(\rho v_z)'v_z'^2}\right]$$

$$+\frac{1}{2}\frac{\partial}{\partial r}\left[(\overline{\rho v_r})\overline{v_z'^2} + 2\,\overline{(\rho v_r)'v_z'}\,\overline{v_z} + \overline{(\rho v_r)'v_z'^2}\right]$$

$$+\frac{1}{2r}\left[(\overline{\rho v_r})\overline{v_z'^2} + 2\,\overline{(\rho v_r)'v_z'}\,\overline{v_z} + \overline{(\rho v_r)'v_z'^2}\right]$$

$$=-\frac{1}{r}\frac{\partial}{\partial r}(r\bar{q}_r) - \bar{\tau}_{rz}\frac{\partial \bar{v}_z}{\partial r} - \frac{\partial}{\partial r}\left[\overline{v_z'\tau_{rz}'}\right] - \frac{\overline{v_z'\tau_{rz}'}}{r}$$

$$+\frac{\bar{v}_z}{r}\frac{\partial}{\partial r}\left\{r\left[\overline{(\rho v_r)'v_z'}\right]\right\} \qquad \text{(A-63)}$$

The turbulent flow continuity equation, Equation (A-36), multiplied by $C_p\bar{T}$ gives

$$C_p\bar{T}\frac{\partial}{\partial z}(\overline{\rho v_z}) + C_p\bar{T}\frac{\partial}{\partial r}(\overline{\rho v_r}) + \frac{C_p\bar{T}(\overline{\rho v_r})}{r} = 0 \qquad \text{(A-64)}$$

Subtracting Equation (A-64) from Equation (A-63) and rearranging, we have

$$(\overline{\rho v_z})C_p\frac{\partial \bar{T}}{\partial z} + (\overline{\rho v_r})C_p\frac{\partial \bar{T}}{\partial r} = -C_p\frac{\partial}{\partial z}\left[\overline{(\rho v_z)'t'}\right]$$

$$-C_p\frac{\partial}{\partial r}\left[\overline{(\rho v_r)'t'}\right] - \frac{C_p}{r}\left[\overline{(\rho v_r)'t'}\right] - \frac{1}{2}\frac{\partial}{\partial z}\left[(\overline{\rho v_z})\overline{v_z'^2}\right]$$

$$-\frac{\partial}{\partial z}\left[\overline{(\rho v_z)'v_z'}\,\overline{v_z}\right] - \frac{1}{2}\frac{\partial}{\partial z}\left[\overline{(\rho v_z)'v_z'^2}\right] - \frac{1}{2}\frac{\partial}{\partial r}\left[(\overline{\rho v_r})\overline{v_z'^2}\right]$$

$$-\frac{\partial}{\partial r}\left[\overline{(\rho v_r)'v_z'}\,\overline{v_z}\right] - \frac{1}{2}\frac{\partial}{\partial r}\left[\overline{(\rho v_r)'v_z'^2}\right] - \frac{1}{2r}\left[(\overline{\rho v_r})\overline{v_z'^2}\right]$$

$$-\frac{1}{r}\left[\overline{(\rho v_r)' v_z'}\,\bar{v}_z\right] - \frac{1}{2r}\left[\overline{(\rho v_r)' v_z'^2}\right] - \frac{1}{r}\frac{\partial}{\partial r}(r\bar{q}_r)$$

$$-\bar{\tau}_{rz}\frac{\partial \bar{v}_z}{\partial r} - \frac{\partial}{\partial r}\left[\overline{v_z'\tau_{rz}'}\right] - \frac{\overline{v_z'\tau_{rz}'}}{r}$$

$$+\frac{\bar{v}_z}{r}\frac{\partial}{\partial r}\left\{r\left[\overline{(\rho v_r)' v_z'}\right]\right\} \qquad \text{(A-65)}$$

By applying the boundary layer assumptions, the following approximations can be made.

$$C_p\frac{\partial}{\partial r}\left[\overline{(\rho v_r)' t'}\right] \gg C_p\frac{\partial}{\partial z}\left[\overline{(\rho v_z)' t'}\right] \qquad \text{(A-66)}$$

$$\frac{\partial}{\partial r}\left[\overline{(\rho v_r)' v_z'}\,\bar{v}_z\right] \gg \frac{1}{2}\frac{\partial}{\partial z}\left[(\overline{\rho v_z})\overline{v_z'^2}\right]$$

$$+\frac{1}{2}\frac{\partial}{\partial r}\left[(\overline{\rho v_r})\overline{v_z'^2}\right] \qquad \text{(A-67)}$$

$$\bar{\tau}_{rz}\frac{\partial \bar{v}_z}{\partial r} \gg \frac{\partial}{\partial r}\left[\overline{v_z'\tau_{rz}'}\right] + \frac{\overline{v_z'\tau_{rz}'}}{r} \qquad \text{(A-68)}$$

Also, all triple correlations are extremely small compared to the other terms.

Using these approximations, Equation (A-65) becomes

$$(\overline{\rho v_z})C_p\frac{\partial \bar{t}}{\partial z} + (\overline{\rho v_r})C_p\frac{\partial \bar{t}}{\partial r} = -C_p\frac{\partial}{\partial r}\left[\overline{(\rho v_r)' t'}\right]$$

$$-\frac{C_p}{r}\left[\overline{(\rho v_r)' t'}\right] - \frac{\partial}{\partial r}\left[\overline{(\rho v_r)' v_z'}\,\bar{v}_z\right] - \frac{1}{r}\left[\overline{(\rho v_r)' v_z'}\,\bar{v}_z\right]$$

$$-\frac{1}{r}\frac{\partial}{\partial r}(r\bar{q}_r) - \bar{\tau}_{rz}\frac{\partial \bar{v}_z}{\partial r} + \frac{\bar{v}_z}{r}\frac{\partial}{\partial r}\left\{r\left[\overline{(\rho v_r)' v_z'}\right]\right\} \qquad \text{(A-69)}$$

However, it may be noted that

$$\frac{1}{r}\frac{\partial}{\partial r}\left[r\,\overline{(\rho v_r)'v_z'}\,\overline{v_z}\right] = \frac{\overline{v_z}}{r}\frac{\partial}{\partial r}\left\{r\left[\overline{(\rho v_r)'v_z'}\right]\right\} + \left[\overline{(\rho v_r)'v_z'}\right]\frac{\partial \overline{v_z}}{\partial r} \qquad \text{(A-70)}$$

Substituting Equation (A-70) into Equation (A-69), we have

$$(\overline{\rho v_z})C_p\frac{\partial \overline{t}}{\partial z} + (\overline{\rho v_r})C_p\frac{\partial \overline{t}}{\partial r} = -\frac{C_p}{r}\frac{\partial}{\partial r}\left[r\,\overline{(\rho v_r)'t'}\right] - \frac{1}{r}\frac{\partial}{\partial r}(r\overline{q_r}) - \overline{\tau_{rz}}\frac{\partial \overline{v_z}}{\partial r} - \left[\overline{(\rho v_r)'v_z'}\right]\frac{\partial \overline{v_z}}{\partial r} \qquad \text{(A-71)}$$

Now, a turbulent heat flux and an eddy thermal conductivity is defined.

$$C_p\left[\overline{(\rho v_r)'t'}\right] = q_r^{(t)} = -\kappa\frac{\partial \overline{t}}{\partial r} \qquad \text{(A-72)}$$

Substituting Equations (A-72) and (A-45) into Equation (A-71), we have

$$(\overline{\rho v_z})C_p\frac{\partial \overline{t}}{\partial z} + (\overline{\rho v_r})C_p\frac{\partial \overline{t}}{\partial r} = -\frac{1}{r}\frac{\partial}{\partial r}\left[r(\overline{q_r} + q_r^{(t)})\right] - (\overline{\tau_{rz}} + \tau_{rz}^{(t)})\frac{\partial \overline{v_z}}{\partial r}$$

$$= \frac{1}{r}\frac{\partial}{\partial r}\left[r(\kappa + k)\frac{\partial \overline{t}}{\partial r}\right] + \left[(\mu + \rho\epsilon_v)\left(\frac{\partial \overline{v_z}}{\partial r}\right)^2\right] \qquad \text{(A-73)}$$

Finally, dropping the bars above the "time-smoothed" variables and neglecting the laminar momentum and heat fluxes in comparison to the turbulent fluxes, the turbulent conservation equations become

$$\frac{\partial}{\partial z}(\rho v_z) + \frac{1}{r}\frac{\partial}{\partial r}(r\rho v_r) = 0 \qquad \text{(A-74)}$$

$$\rho v_z \frac{\partial v_z}{\partial z} + \rho v_r \frac{\partial v_z}{\partial r} = \frac{1}{r}\frac{\partial}{\partial r}\left[r(\rho\epsilon_v)\frac{\partial v_z}{\partial r}\right] \qquad \text{(A-75)}$$

$$\rho v_z C_p \frac{\partial t}{\partial z} + \rho v_r C_p \frac{\partial t}{\partial r} = \frac{1}{r}\frac{\partial}{\partial r}\left[r k \frac{\partial t}{\partial r}\right] + (\rho\epsilon_v)\left(\frac{\partial v_z}{\partial r}\right)^2 \qquad \text{(A-76)}$$

APPENDIX 9.3

The Free Jet Calculational Technique

9.3.1 Description of the Calculations

The object of this calculational technique, which was implemented by the computer program listed in section 9.3.3 of this Appendix, was to obtain the velocity and temperature variation in the free jet region. The only input data for these computer calculations which were changed when calculating results for the various experimental runs, were the initial jet velocity -- v_{zj} , the initial jet temperature -- t_j, the ambient temperature -- t_a, and the value of F(M) at the initial jet Mach number.

The step sizes can be left unchanged for most free jet calculations. Hwang and Fan (14) derived a condition for the maximum step size ratio which should be used in order to reduce truncation errors. This condition is

$$\frac{P V_z \Delta R^2}{12 A_v \Delta Z} \ll \frac{1}{2} \qquad \text{(A-77)}$$

In the present work, the step sizes were varied within the finite difference network. The condition imposed on the choices of either the ΔR's or ΔZ's was that the largest step size should be an integral multiple of both the smallest and the intermediate step sizes.

In the calculations, for a line of the finite difference network at $Z+\Delta Z$, the axial position was first checked to see which of the step sizes is to be used for that line. Then, values of velocities, temperatures, and densities, for the first iteration were assumed to be the values of these variables at the previous line, or at Z. At this point, the eddy transfer coefficients, which are a function of axial position, were calculated. The simultaneous equations for the temperatures at the points along the line at $Z+\Delta Z$ were solved with Thomas' method (12), and these temperatures were used in the solution of the simultaneous equations for the axial velocities along the same line. Then, both of these newly calculated quantities were used in the finite difference form of the continuity equation to calculate the radial velocities.

This completed an iteration. Reaching this point, Wegstein's (13) procedure for accelerating convergence was applied. This consisted of merely replacing the velocities and temperatures just calculated with a weighted average of the newly calculated values and those from the previous iteration. The iterative process was then checked for convergence. Convergence was considered to have taken place when the velocities and temperatures of two successive

iterations were the same within 0.25 per cent of their values at the jet nozzle. Three to seven iterations were usually required to obtain a converged solution for one line of the network. Calculations were then made for the next line and this procedure was carried downstream until a prescribed limiting axial distance was reached.

The output from the computer calculations consisted of the radial distribution of axial velocity, radial velocity, temperature, and density at each nozzle diameter of axial distance. All of these variables were printed out in the dimensionless form.

9.3.2 Computer Program Nomenclature

Indices

N=1,2,3···, J--number of points along a line of the finite difference network

Nonsubscripted Variables

AT--the absolute temperature.

CONST--the value of F(M) for that particular computation.

CP--the heat capacity.

CPC--the value of $f_t(Z)$ and $f_v(Z)$ in the core regions of the free jet,

DELR--the ΔR at the line of calculation.

DELR1, DELR2, DELR3--the smallest, the intermediate size, and the largest R-direction step sizes.

DELZ1, DELZ2, DELZ3--the smallest, the intermediate size, and the largest Z-direction step sizes.

DIFF-the difference between temperatures of two successive iterations.

ERROR--the difference between axial velocities of two successive iterations.

FT--$f_t(Z)$ in the free jet analysis.

FVZ--$f_v(Z)$ in the free jet analysis.

II, IS, IT--the numbers of the last lines of the smallest, the intermediate size, and the largest step sizes respectively plus one.

INCR--the iteration counter.

J--the number of points along the line being calculated.

JI, JS, JT--the number of points in the regions of the smallest, the intermediate size, and the largest step sizes respectively.

KNOZ--the number of the point whose radial position is equal to that of nozzle wall.

LIMIT--the number of the lines of constant Z for which calculations are made.

POS--an index to determine when Z reaches an integral number of nozzle diameters in order to print the calculated results.

PRK-- A_t in the free jet analysis.

PRNO--the turbulent Prandtl number.

R--the radial coordinate.

REYK-- A_v in the free jet analysis.

SET--another index which, when matched by POS, indicates that the calculated results should be printed.

TA--the ambient temperature.

THETA--the dimensionless temperature at the previous line.

TO--the initial jet temperature.

TOL--the tolerance for convergence of the iterative process.

UO--the initial jet velocity.

Z--the axial coordinate.

ZPOTC-- Z_{ct} in the free jet analysis.

ZTPC-- Z_{cv} in the free jet analysis.

Subscripted Variables

A(N), B(N), C(N), D(N)--constants of the systems of algebraic equations to be solved, written in matrix form.

OLDRO(N)---the densities at points along the previous line.

OLDVR(N)---the radial velocities at points along the previous line.

OLDVZ(N)---the axial velocities at points along the previous line.

RO(N)---the densities along the line being calculated.

T(N)--the temperatures along the line being calculated.

TEST(N)---the temperatures or velocities of the previous iteration along the line being calculated.

VR(N)---the radial velocities along the line being calculated.

VZ(N)---the axial velocities along the line being calculated.

9.3.3 Computer Program Listing

```
C     THIS PROGRAM SOLVES THE FREE JET PROBLEM BY USING
C     AN ABBOTT-TYPE FINITE DIFFERENCE SOLUTION OF THE
C     CONSERVATIONS EQUATIONS.
C     INPUT DATA
C     TC-JET EXIT TEMPERATURE,DEG. R
C     TA-AMBIENT TEMPERATURE,DEG. R
C     UC-JET EXIT VELOCITY,FT./SEC.
C     DELZ1-FIRST Z-DIRECTION FINITE DIFFERENCE STEP SIZE
C     DELZ2-SECOND Z-DIRECTION FINITE DIFFERENCE STEP SIZE
C     DELZ3-THIRD Z-DIRECTION FINITE DIFFERENCE STEP SIZE
C     DELR1-FIRST R-DIRECTION FINITE DIFFERENCE STEP SIZE
C     DELR2-SECOND R-DIRECTION FINITE DIFFERENCE STEP SIZE
C     DELR3-THIRD R-DIRECTION FINITE DIFFERENCE STEP SIZE
C     PRNC-TURBULENT PRANDTL NUMBER
C     TCL-TOLERANCE FOR ITERATIVE CONVERGENCE
C     II-NUMBER OF LINES OF THE FIRST Z-DIRECTION STEP
C     SIZE PLUS ONE.
C     IS-NUMBER OF LINES OF THE SECOND Z-DIRECTION STEP
C     SIZE PLUS ONE.
C     IT-NUMBER OF LINES OF THE THIRD Z-DIRECTION STEP
C     SIZE PLUS ONE.
C     JI-NUMBER OF LINES OF FIRST R-DIRECTION STEP SIZE
C     JS-NUMBER OF LINES OF SECOND R-DIRECTION STEP SIZE
C     JT-NUMBER OF LINES OF THIRD R-DIRECTION STEP SIZE
C     KNOZ-Z-DIRECTION LINE NUMBER OF NOZZLE
C     LIMIT-LIMITING NUMBER OF ITERATIONS
      DIMENSION OLDVZ(501),OLDVR(501),OLDRO(501),VZ(501),VR(
     X501),T(501),
     1RO(501),A(501),B(501),C(501),D(501),TEST(501)
 1002 READ (1,100) TO,TA,UO,DELZ1,DELZ2,DELZ3,DELR1,DELR2,DE
     XLR3,PRNO,TCL
  100 FORMAT (8F10.0)
      READ (1,200) II,IS,IT,JI,JS,JT,KNOZ,LIMIT
  200 FORMAT (8I5)
      READ (1,300) CONST,CPC
  300 FORMAT (2F10.0)
      PAR=0.333
      J=JI
      KAPPA=DELR2/DELR1
      NU=DELR3/DELR2
      PKAP=DELZ2/DELZ1
      OMEGA=DELZ3/DELZ1
      KNOZ1=KNOZ-1
      DO 1 N=1,KNOZ1
      OLDVZ(N)=1.0
      OLDVR(N)=0.0
    1 OLDRO(N)=1.0
      DO 2 N=KNOZ,J
```

```
      OLDVZ(N)=0.0
      OLDVR(N)=0.0
    2 OLDRO(N)=TO/TA
      DO 8 N=1,J
      VZ(N)=OLDVZ(N)
      VR(N)=OLDVR(N)
    8 RO(N)=OLDRO(N)
      POS=1.0
      M=2
 2001 IF (II-M) 1003,2003,3003
 1003 IF (IS-M) 4003,5003,6003
 4003 IF (IT-M) 2000,2000,7003
 3003 ZP1=M-1
      Z=ZP1*DELZ1
      DELZ=DELZ1
      DELR=DELR1
      J=JI
      POS=POS+1.0
      SET=1.0/DELZ1+1.0
      GO TO 1001
 2003 DO 13 N=1,JI,KAPPA
      NEW=(N-1)/KAPPA+1
      OLDVZ(NEW)=OLDVZ(N)
      OLDVR(NEW)=OLDVR(N)
   13 OLDRO(NEW)=OLDRO(N)
      DO 14 N=NEW,JS
      OLDVZ(N)=0.0
      NM=N-1
      RP=N
      RPM=N-1
      OLDVR(N)=OLDVR(NM)*RPM/RP
   14 OLDRO(N)=TO/TA
 6003 ZP1=(II-2)
      ZP2=M-II+1
      Z=ZP1*DELZ1+ZP2*DELZ2
      DELZ=DELZ2
      DELR=DELR2
      J=JS
      POS=POS+PKAP
      GO TO 1001
 5003 DO 15 N=1,JS,NU
      NEW=(N-1)/NU+1
      OLDVZ(NEW)=OLDVZ(N)
      OLDVR(NEW)=OLDVR(N)
   15 OLDRO(NEW)=OLDRO(N)
      DO 16 N=NEW,JT
      OLDVZ(N)=0.0
      NM=N-1
      RP=N
      RPM=N-1
      OLDVR(N)=OLDVR(NM)*RPM/RP
```

```
   16 CLDRO(N)=TO/TA
 7003 ZP2=IS-II
      ZP3=M-IS+1
      Z=ZP1*DELZ1+ZP2*DELZ2+ZP3*DELZ3
      DELZ=DELZ3
      DELR=DELR3
      J=JT
      POS=POS+OMEGA
 1001 INCR=0.0
      J1=J-1
      J2=J-2
      ZPOTC=4.73/((TO/TA)**0.5)
      IF (Z-ZPOTC) 1004,1004,2004
 1004 FVZ=CPC
      GO TO 3004
 2004 FVZ=1.0
 3004 REYK=CONST*((TO/TA)**0.5)*OLDRO(1)*FVZ
      ZTPC=3.43/((TO/TA)**0.5)
      IF (Z-ZTPC) 1005,1005,2005
 1005 FT=CPC*PRNO
      GO TO 3005
 2005 FT=1.0
 3005 PRK=(CONST*((TO/TA)**0.5)*OLDRO(1)*FT)/PRNO
      C1=REYK/(DELR*DELR)
      CC1=PRK/(DELR*DELR)
 3001 WRITE (2,50)
   50 FORMAT (120HO                    VZ(N)                    VR(N)
     1  T(N)                RO(N)     M     N                  Z
     X           R
     2)
      VZ(J)=0.0
      T(J)=0.0
      RO(J)=TO/TA
 8001 A(1)=RO(1)*VZ(1)/DELZ+4.0*CC1
      B(1)=-4.0*CC1
      D(1)=RO(1)*VZ(1)*(1.0/OLDRO(1)-TA/TO)/((1.0-TA/TO)*DEL
     XZ)
      DO 18 N=2,J1
      RP=N-1
      R=RP*DELR
      CC2=PRK/(2.0*R*DELR)
      CC3=RO(N)*VR(N)/(2.0*DELR)
      CC4=RO(N)*VZ(N)/DELZ
      NP=N+1
      NM=N-1
      C(N)=CC2-CC3-CC1
      A(N)=CC4+2.0*CC1
      B(N)=CC3-CC2-CC1
      AT=(1.0/RO(N))*TO
      CP=171.5+0.02629*AT-0.00000396*AT*AT
      THETA = (1.0/OLDRO(N)-TA/TO)/(1.0-TA/TO)
```

```
   18 D(N)=CC4*THETA+U0*U0/(32.2*CP*(T0-TA))*REYK*(VZ(NP)*VZ
     X(NP)-2.0*VZ(
     1NP)*VZ(NM)+VZ(NM)*VZ(NM))/(4.0*DELR*DELR)
      DO 22 N=1,J
   22 TEST(N)=T(N)
      D(1)=D(1)/A(1)
      DO 19 N=2,J1
      N1=N-1
      B(N1)=B(N1)/A(N1)
      A(N)=A(N)-C(N)*B(N1)
   19 D(N)=(D(N)-C(N)*D(N1))/A(N)
      T(J1)=D(J1)
      RC(J1)=1.0/(T(J1)*(1.0-TA/T0)+TA/T0)
      DO 20 N=1,J2
      NN=J2-N+1
      NN1=NN+1
   20 T(NN)=D(NN)-B(NN)*T(NN1)
      DO 66 N=1,J
      T(N)=PAR*TEST(N)+(1.0-PAR)*T(N)
   66 RC(N)=1.0/(T(N)*(1.0-TA/T0)+TA/T0)
      DO 23 N=1,J
      DIFF=ABSF(TEST(N)-T(N))
      IF(DIFF-TOL) 23,23,9001
   23 CONTINUE
      ERR1=0.0
      GO TO 24
 9001 ERR1=1.0
   24 A(1)=RO(1)*VZ(1)/DELZ+4.0*C1
      B(1)=-4.0*C1
      D(1)=RC(1)*VZ(1)*OLDVZ(1)/DELZ
      DO 3 N=2,J1
      RP=N-1
      R=RP*DELR
      C2=REYK/(2.0*R*DELR)
      C3=RO(N)*VR(N)/(2.0*DELR)
      C4=RO(N)*VZ(N)/DELZ
      C(N)=C2-C3-C1
      A(N)=C4+2.0*C1
      B(N)=C3-C2-C1
    3 D(N)=C4*OLDVZ(N)
      DO 17 N=1,J
   17 TEST(N)=VZ(N)
      D(1)=D(1)/A(I)
      DO 4 N=2,J1
      N1=N-1
      B(N1)=B(N1)/A(N1)
      A(N)=A(N)-C(N)*B(N1)
    4 D(N)=(D(N)-C(N)*D(N1))/A(N)
      VZ(J1)=D(J1)
      DO 5 N=1,J2
      NN=J2-N+1
```

```
      NN1=NN+1
    5 VZ(NN)=D(NN)-B(NN)*VZ(NN1)
      DO 666 N=1,J
  666 VZ(N)=PAR*TEST(N)+(1.0-PAR)*VZ(N)
      DO 6 N=2,J
      N1=N-1
      RP=N1
      R=RP*DELR
      CE1=1.0/((2.0*RO(N))/DELR-RO(N1)/DELR+RO(N)/R)
      CE2=RO(N)*(OLDVZ(N)-VZ(N))/DELZ
      CE3=VZ(N)*(OLDRO(N)-RO(N))/DELZ
      CE4=RO(N)*VR(N1)/DELR
    6 VR(N)=CE1*(CE2+CE3+CE4)
      DO 10 N=1,J1
      ERROR=ABSF(TEST(N)-VZ(N))
      IF (ERROR-TOL) 10,10,5001
   10 CONTINUE
      IF (ERR1) 26,26,5001
   26 CONTINUE
      IF (POS-SET) 4001,3002,2000
 3002 PCS=1.0
      DO 7 N=1,J
      RP=N-1
      R=RP*DELR
      WRITE (2,150) VZ(N),VR(N),T(N),RO(N),M,N,Z,R
  150 FORMAT (4F20.8,2I5,2F15.8)
    7 CONTINUE
 4001 DO 9 N=1,J
      OLDVZ(N)=VZ(N)
      OLDVR(N)=VR(N)
    9 OLDRO(N)=RO(N)
      WRITE (2,999) INCR
  999 FORMAT (I5)
      M=M+1
      GO TO 2001
 5001 INCR=INCR+1
      IF (INCR-LIMIT) 6001,6001,7001
 6001 IF(SENSE SWITCH 1) 7001,1009
 1009 GO TO 8001
 7001 DO 12 N=1,J
      RP=N-1
      R=RP*DELR
      WRITE (2,250) VZ(N),VR(N),T(N),RO(N),M,N,Z,R
  250 FORMAT (4F20.8,2I5,2F15.8)
      WRITE (2,99) TEST(N)
   99 FORMAT (F20.8)
   12 CONTINUE
      WRITE (2,9999) INCR
 9999 FORMAT (I5)
      GO TO 2000
 2000 CONTINUE
```

```
      IF(1.0) 3000,3000,1002
3000  CONTINUE
      END
```

APPENDIX 9.4

The Calculational Technique for the Stagnation Area Heat Flux Distribution and the Static Pressure Districution on the Flat Plate

9.4.1 Description of the Calculations

The object of the calculational procedure, which was implemented by the two computer programs listed in section 9.4.3 of the Appendix, was to obtain the static pressure distribution on the plate and the stagnation area heat flux distribution. The first program was used to compute the static pressure distribution and the stagnation point heat flux. The second program was used to compute the stagnation area heat flux.

The input to the first computer program included the nozzle to plate distance, the nozzle diameter, the jet exit velocity, the jet exit temperature, the temperature of the plate at the stagnation point, the ambient temperature, and the barometric pressure. Also, velocities temperatures, and densities on the center-line of the free jet as determined by the free jet solution were read in as input.

To begin a particular calculation, the total velocity head of the free jet flow was calculated at several axial

positions, and these calculated values were fitted with a least squares polynomial. The gauge static pressure on the plate at the stagnation point was taken as being equal to the total velocity head at an axial position corresponding to the nozzle to plate distance. Then, the "half-width" of the pressure distribution, r_s , was calculated using Equation (26).

At this point, another least squares procedure was used to obtain a second order polynomial for the stagnation temperature on the center-line of the free jet as a function of axial position. This second order polynomial was used to determine h^* for use in the stagnation point heat flux calculation. Calculating $\left(\frac{dv_{re}}{dr}\right)_s$ with Equation (34) and noting that $\beta(r)$ is 0.5 at the stagnation point (26), q_w at the stagnation point was calculated by using Equation (39).

The input to the second computer program included the barometric pressure, the static gauge pressure at the stagnation point, the "half-width" of the pressure distribution, and the stagnation point heat flux calculated by the first computer program. The measured plate surface temperatures and their axial positions were also input data to the program.

To begin the computations, a least squares procedure was used to obtain a third order polynomial for the surface temperature of the plate as a function of the radial position. Next, v_{re} was calculated from Equation (38) at a number of radial positions, and Equation (41) was numerically integrated by using Simpson's Rule (29) to give $\eta(r)$. Then $\frac{dv_{re}}{dr}$ was determined by Equation (42). These intermediate results were used in Equation (45) to obtain $\beta(r)$ which, in turn, was used in Equation (39) to calculate q_w for the stagnation area. Thus, two relatively simple computer programs were used to calculate the static pressure distribution on the plate and the stagnation area heat flux distribution.

9.4.2 Computer Program Nomenclature

Program 1

Indices

N=1,2,3---,NF--Number of points for least squares data fits.

Nonsubscripted Variables

AP--the ambient or barometric pressure.

DO--the nozzle diameter.

DVRMS--$(\frac{dv_{rf}}{dr})$s in the impingement region analysis.

GMUWS--the viscosity of air at the temperature of the plate at the stagnation point.

INDEX--the number of the experimental run.

HCRAT--the heat capacity ratio.

HNTOP--the nozzle to plate distance.

HS--$\dot{h}$ in the impingement region analysis.

HWS--the enthalpy of air at the temperature of the plate at the stagnation point.

NF--the total number of points for the least squares data fits.

PAR1 ⟶ PAR 6--the constants in the least squares polynomials.

PR--the laminar Prandtl number.

WSC--the calculated stagnation point heat flux.

QSM--the measured stagnation point heat flux.

ROMS--the density at the edge of the impingement region boundary layer.

R5--the "half-width" of the pressure distribution on the plate.

STS--temperature at the edge of the impingement region boundary layer.

TO--the initial jet temperature.

TS--the stagnation temperature corresponding to $\dot{h}$.

TWS--the plate temperature at the stagnation point.

TVHPS--the gauge static pressure on the plate at the stagnation point.

UO--the initial jet velocity.

Subscripted Variables

RO(N)--densities at the free jet axis.

VZ(N)--axial velocities at the free jet axis.

T(N)--temperatures at the free jet axis.

Z(N)--axial positions in the free jet.

Program 2

Indices

N=1,2,3----,NF--number of points of least squares data fit.

N-1,2,3,---,NI--number of points for numerical integration procedure.

Nonscripted Variables

AP--the ambient or barometric pressure.

C1, C2, C3--constants of the polynomial for stagnation temperatures on the center-line of the free jet as a function of axial position.

DELR--the step size for the numerical integration of $\eta(r)$.

DO--the nozzle diameter.

HNTOP--the nozzle to plate distance.

INDEX--the number of the experimental run.

NI--the number of points for the numerical integration.

NF--the total number of points for the least squares data fit.

PAR1⟶PAR4--the constants in the least squares polynomial.

QC--the calculated heat flux at some radial position in the stagnation area.

QSC--the calculated heat flux at the stagnation point.

ROW--the density of air at the surface temperature of the plate.

ROMS--the density at the edge of the impingement region boundary layer.

R5--the "half-width" of the pressure distribution on the plate.

STS--the temperature at the edge of the impingement region boundary layer.

TVHPS--the static pressure on the plate at the stagnation point.

TW--the surface temperature of the plate.

VRM-- v_{r_e} in the impingement region analysis.

Subscripted Variables

BETA(N)--the values of $\beta(r)$.

R(N)--radial positions of the numerical integration.

TP(N)--measured plate surface temperatures.

ZETA(N)--the values of $\eta(r)$.

9.4.3 Computer Program Listings

PROGRAM 1

```
C     CALCULATION OF THE STAGNATION POINT HEAT FLUXES AND
C     THE STATIC PRESSURE AT THE STAGNATION POINT FROM THE
C     RESULTS OF THE FREE JET SOLUTION AND CERTAIN GIVEN
C     CONDITIONS.
C     INPUT DATA
C     HNTOP-NOZZLE TO PLATE DISTANCE,INCHES
C     DO-NOZZLE DIAMETER,INCHES
C     UO-VELOCITY AT NOZZLE EXIT,FT./SEC.
C     TO-TEMPERATURE AT NOZZLE EXIT,DEG. F
C     TWS-WALL TEMPERATURE AT STAGNATION POINT,DEG. F
C     QSM-MEASURED STAGNATION POINT HEAT
C     FLUX, BTU/HR.-SQ. FT.
C     AP-AMBIENT PRESSURE,PSIA
C     NF- NUMBER OF POINTS FOR LEAST-SQUARE FITS
C     INDEX-NUMBER OF EXPERIMENTAL RUN
C     VZ(N)-VELOCITY AT FREE JET AXIS,DIMENSIONLESS
C     RO(N)-DENSITY AT FREE JET AXIS,DIMENSIONLESS
C     T(N)-TEMPERATURE AT FREE JET AXIS,DIMENSIONLESS
C     Z(N)-AXIAL DISTANCE FROM JET NOZZLE,DIMENSIONLESS
      DIMENSION VZ(40),RO(40),T(40),X(40),Y(40),A(3),B(3),C(
     X3),D(3),BA(3
     1),CA(3),DA(3),TDEGR(40),SSNX2(40),ST(40),TVHP(40),Z(40
     X),V(40),V2(4
     20)
   87 READ (1,99) HNTOP,DO,UO,TO,TWS,TA,QSM,AP
   99 FORMAT (8F10.0)
      READ (1,333) NF,INDEX
  333 FORMAT (2I5)
      READ (1,100) (VZ(N),RO(N),T(N),Z(N),N=1,NF)
  100 FORMAT (4F10.0)
      TC=TO+460.0
      TA=TA+460.0
      TWS=TWS+460.0
      ROO=530.0*0.0808/TO
      HNTOP=HNTOP/DO
      DO 1 N=1,NF
      TVHP(N)=ROO*UO*UO*RO(N)*VZ(N)*VZ(N)/64.4
      Y(N)=TVHP(N)
    1 X(N)=Z(N)
      N=NF
      DO 4 J=1,3
      A(J)=0.0
      B(J)=0.0
      C(J)=0.0
      D(J)=0.0
```

```
      DO 5 I=1,N
      A(J)=A(J)+(X(I)**(J-1))
      B(J)=B(J)+(X(I)**J)
      C(J)=C(J)+(X(I)**(J+1))
    5 D(J)=D(J)+((X(I)**(J-1))*Y(I))
      IF (A(J)) 4,86,4
    4 CONTINUE
      A(1)=N
      D(1)=0.0
      DO 42 I=1,N
   42 D(1)=D(1)+Y(I)
      DO 6 J=2,3
      BA(J)=(B(J)/A(J))-(B(1)/A(1))
      IF (BA(J)) 7,86,7
    7 CA(J)=(C(J)/A(J))-(C(1)/A(1))
    6 DA(J)=(D(J)/A(J))-(D(1)/A(1))
      CB=(CA(3)/BA(3))/(CA(2)/BA(2))
      DB=(DA(3)/BA(3))-(DA(2)/BA(2))
      PAR3=DB/CB
      PAR2=(DA(3)-CA(3)*PAR3)/BA(3)
      PAR1=(D(3)-C(3)*PAR3-B(3)*PAR2)/A(3)
      DO 28 J=1,N
      V(J)=PAR1+PAR2*X(J)+PAR3*X(J)*X(J)
   28 V2(J)=V(J)*V(J)
      SUMV=0.0
      SUMV2=0.0
      DO 29 J=1,N
      SUMV=SUMV+V(J)
   29 SUMV2=SUMV2+V2(J)
      WRITE (2,94) INDEX
   94 FORMAT (43H1 THIS CALCULATION IS FOR EXPERIMENTAL RUN
     XI2)
      WRITE (2,999)
  999 FORMAT (74HO PARAMETERS FOR FIT OF TOTAL VELOCITY HEAD
     X PRESSURE VE
     1RSUS AXIAL POSITION)
      WRITE (2,95) PAR1,PAR2,PAR3,SUMV,SUMV2
   95 FORMAT (6HOPAR1=E18.8/6HOPAR2=E18.8/6HOPAR3=E18.8/6HOS
     XUMV=E18.8/7H
     1OSUMV2=E17.8//)
      TVHPS=PAR1+PAR2*HNTOP+PAR3*HNTOP*HNTOP
      TVHPS=TVHPS/144.0
      RCWS=530.0*0.0808*(TVHPS+AP)/(TWS*14.7)
      R5X2=1.388*RCO*UO*UO/(8.0*32.2*TVHPS*144.0)
      R5=(R5X2**0.5)
      R5FT=R5*CO/12.0
      DO 2 N=1,NF
      TDEGR(N)=T(N)*(TO-TA)+TA
      SSNX2(N)=VZ(N)*VZ(N)/(2402.96*TDEGR(N))
      HCRAT=1.430-0.0000513*TDEGR(N)
      Z2=(HCRAT-1.0)/2.0
```

```
      ST(N)=TDEGR(N)*(1.0+Z2*SSNX2(N))
      Y(N)=ST(N)
    2 X(N)=Z(N)
      N=NF
      DO 14 J=1,3
      A(J)=0.0
      B(J)=0.0
      C(J)=0.0
      D(J)=0.0
      DO 15 I=1,N
      A(J)=A(J)+(X(I)**(J-1))
      B(J)=B(J)+(X(I)**J)
      C(J)=C(J)+(X(I)**(J+1))
   15 D(J)=D(J)+((X(I)**(J-1))*Y(I))
      IF (A(J)) 14,86,14
   14 CONTINUE
      A(1)=N
      D(1)=0.0
      DO 142 I=1,N
  142 D(1)=D(1)+Y(I)
      DO 16 J=2,3
      BA(J)=(B(J)/A(J))-(B(1)/A(1))
      IF (BA(J)) 17,86,17
   17 CA(J)=(C(J)/A(J))-(C(1)/A(1))
   16 DA(J)=(D(J)/A(J))-(D(1)/A(1))
      CB=(CA(3)/BA(3))/(CA(2)/BA(2))
      DB=(DA(3)/BA(3))-(DA(2)/BA(2))
      PAR6=DB/CB
      PAR5=(DA(3)-CA(3)*PAR6)/BA(3)
      PAR4=(D(3)-C(3)*PAR6-B(3)*PAR5)/A(3)
      DO 25 J=1,N
      V(J)=PAR4+PAR5*X(J)*PAR6*X(J)*X(J)
   25 V2(J)=V(J)*V(J)
      SUMV=0.0
      SUMV2=0.0
      DO 26 J=1,N
      SUMV=SUMV+V(J)
   26 SUMV2=SUMV2+V2(J)
      WRITE (2,998)
  998 FORMAT (69HO PARAMETERS FOR FIT OF STAGNATION TEMPERAT
     XURES VERSUS
     1AXIAL POSITION)
      WRITE (2,96) PAR4,PAR5,PAR6,SUMV,SUMV2
   96 FORMAT (6HOPAR4=E18.8/6HOPAR5=E18.8/6HOPAR6=E18.8/6HOS
     XUMV=E18.8/7H
     1OSUMV2=E17.8//)
      ZI=HNTOP-3.16*R5
      TS=PAR4+PAR5*ZI+PAR6*ZI*ZI
      STS=PAR4+PAR5*HNTOP+PAR6*HNTOP*HNTOP
      ROMS=0.0808*(TVHPS+AP)*530.0/(STS*14.7)
      DVSX2=1.388*TVHPS*144.0*32.2/(ROMS*R5FT*R5FT)
```

```
      DVRMS=CVSX2**0.5
      HS=(0.2388+0.00002*TS)*TS
      HWS=(0.2388+C.00002*TWS)*TWS
      GMUWS=0.00C017*((TWS/715.0)**0.5)
      PR=0.73
      QSC=0.728*((TWS/TS)**0.219)*((ROWS*GMUWS*DVRMS)**0.5)*
     X(HS-HWS)*360
     10.0/PR
      DEV=(QSC-QSM)*100.0/QSM
      TS=TS-460.0
      WRITE (2,97)
   97 FCRMAT (100H0      TVHPS,LBF/SQ. IN.          R5,
     XN.D.          TS,D
     1EG. F      QSC,BTU/HR.-SQ. FT.       DEV,PERCENT)
      WRITE (2,98) TVHPS,R5,TS,QSC,DEV
   98 FCRMAT (5F20.8)
      IF (1.) 86,86,87
   86 CCNTINUE
      END
```

PROGRAM 2

```
C     CALCULATION CF THE STAGNATION AREA HEAT FLUX
C     DISTRIBUTICN.
C     INPUT DATA
C     INDEX-NUMBER OF EXPERIMENTAL RUN
C     NF-NUMBER OF WALL TEMPERATURES FOR LEAST-SQUARES FIT
C     NI-NUMBER OF POINTS ALONG THE WALL FOR
C     THE NUMERICAL INTEGRATION.
C     AP AMBIENT PRESSURE,PSIA
C     TVHPS-PLATE STAGNATION PRESSURE,PSIG
C     DELR-RADIAL INCREMENT FOR THE NUMERICAL
C     INTEGRATION, NOZZLE DIAMETERS.
C     R5-HALF-WIDTH OF THE PRESSURE
C     DISTRIBUTION, NOZZLE DIAMETERS.
C     QSC-CALCULATED STAGNATION HEAT FLUX,BTU/HR.-SQ. FT.
C     C1,C2,C3-PARAMETERS OF LEAST-SQUARE FIT OF STAGNATION
C     TEMPERATURES(DEG. R) VERSUS DISTANCE FROM
C     NCZZLE(NCZZLE DIAMETERS.
C     HNTOP-NOZZLE TO PLATE DISTANCE,INCHES
C     DC-NOZZLE DIAMETER,INCHES
C     START-BEGINNING VALUE FOR LEAST-SQUARE FIT EVALUATION
C     H-INCREMENT FOR LEAST-SQUARE FIT EVALUATION
C     FINAL-FINAL VALUE FOR LEAST-SQUARE FIT EVALUATION
C     TP-WALL TEMPERATURE,DEGREES F.
C     R-RADIAL POSITION,NOZZLE DIAMETERS
      DIMENSION TP(20),R(80),BOI(100),DZETA(100),ZETA(100),B
     XETA(100),X(1
     10C),Y(100),A(5),B(5),C(5),D(5),F(5),BA(5),CA(5),DA(5),
     XFA(5),CB(5),
```

```
      2DB(5),FB(5),DC(5),FC(5),V(100),V2(100),DYDX(100),D2YDX
      X(100),VRM(10
      30)
  200 READ (1,1200) INDEX,NF,NI,AP,TVHPS,DELR,R5,QSC
 1200 FORMAT (3I5,5F10.0)
      READ (1,900) C1,C2,C3,HNTOP,DO
  900 FORMAT (5F10.0)
      HNTOP=HNTOP/DO
      WRITE (2,94) INDEX
   94 FORMAT (43H1 THIS CALCULATION IS FOR EXPERIMENTAL RUN
     XI2)
      READ (1,1444) START,H,FINAL
 1444 FORMAT (3F10.0)
      READ (1,1201) (TP(N),R(N),N=1,NF)
 1201 FORMAT (2F10.0)
      DO 1202 N=1,NF
      TP(N)=TP(N)+460.0
      Y(N)=TP(N)
 1202 X(N)=R(N)
      N=NF
      WRITE (2,300)
  300 FORMAT (70HO PARAMETERS FOR FIT OF WALL TEMPERATURE(DE
     XG. R) VERSUS
     1 DISTANCE(N.D.))
      WRITE (2,33)
   33 FORMAT(81HO             X                    Y
     X        DY/DX
     1                D2Y/DX2     //)
      DO 4 J=1,4
      A(J)=0.0
      B(J)=0.0
      C(J)=0.0
      D(J)=0.0
      F(J)=0.0
      DO 5 I=1,N
      A(J)=A(J)+(X(I)**(J-1))
      B(J)=B(J)+(X(I)**J)
      C(J)=C(J)+(X(I)**(J+1))
      D(J)=D(J)+(X(I)**(J+2))
    5 F(J)=F(J)+(Y(I)*(X(I)**(J-1)))
      IF(A(J)) 4,90,4
    4 CONTINUE
      A(1)=N
      F(1)=0.0
      DO 42 I=1,N
   42 F(1)=F(1)+Y(I)
      DO 6 J=2,4
      BA(J)=(B(J)/A(J))-(B(1)/A(1))
      IF(BA(J)) 7,90,7
    7 CA(J)=(C(J)/A(J))-(C(1)/A(1))
      DA(J)=(D(J)/A(J))-(D(1)/A(1))
```

```
    6 FA(J)=(F(J)/A(J))-(F(1)/A(1))
      DO 8 J=3,4
      CB(J)=(CA(J)/BA(J))-(CA(2)/BA(2))
      IF(CB(J)) 9,90,9
    9 DB(J)=(DA(J)/BA(J))-(DA(2)/BA(2))
    8 FB(J)=(FA(J)/BA(J))-(FA(2)/BA(2))
      J=4
      DC(J)=(DB(J)/CB(J))-(DB(3)/CB(3))
      IF(C(J)) 10,90,10
   10 FC(J)=(FB(J)/CB(J))-(FB(3)/CB(3))
      PAR4=FC(4)/DC(4)
      PAR3=(FB(4)-DB(4)*PAR4)/CB(4)
      PAR2=(FA(4)-DA(4)*PAR4-CA(4)*PAR3)/BA(4)
      PAR1=(F(4)-D(4)*PAR4-C(4)*PAR3-B(4)*PAR2)/A(4)
      DO 15 J=1,N
      V(J)=PAR1+PAR2*X(J)+PAR3*X(J)*X(J)+PAR4*(X(J)**3)-Y(J)
   15 V2(J)=V(J)*V(J)
      SUMV=0.0
      SUMV2=0.0
      DO 16 J=1,N
      SUMV=SUMV+V(J)
   16 SUMV2=SUMV2+V2(J)
      X(1)=START
      I=1
   27 Y(I)=PAR1+PAR2*X(I)+PAR3*X(I)*X(I)+PAR4*(X(I)**3)
      DYDX(I)=PAR2+2.0*PAR3*X(I)+3.0*PAR4*X(I)*X(I)
      D2YDX(I)=2.0*PAR3+6.0*PAR4*X(I)
      I=I+1
      X(I)=X(I-1)+H
      IF(X(I)-FINAL)27,27,28
   28 L=((FINAL-START)/H)+1.0
      IF(L)90,52,52
   52 CONTINUE
      WRITE (2,98) (X(I),Y(I),DYDX(I),D2YDX(I),I=1,L)
   98 FORMAT(1H 4E20.8)
      WRITE (2,99) PAR1,PAR2,PAR3,PAR4,SUMV,SUMV2
   99 FORMAT(6HOPAR1=E18.8/6HOPAR2=E18.8/6HOPAR3=E18.8/6HOPA
     XR4=E18.8/6HO
     1SUMV=E18.8/7HOSUMV2=E17.8//)
      WRITE (2,1000)
 1000 FORMAT (119HO   N              R,N.D.          TW,
     XDEG. F       VRM,
     1FT./SEC.                ZETA              BETA  QC,BTU/
     XHR.-SQ. FT.)
      STS=C1+C2*HNTOP+C3*HNTOP*HNTOP
      TVHPS=TVHPS*144.0
      AP=AP*144.0
      VRMK=2.0*32.2*TVHPS
      DO 1203 N=1,NI
      RP=N-1
      R(N)=RP*DELR
```

```
      EPT=-0.694*R(N)*R(N)/(R5*R5)
      PPT=EXPF(EPT)
      TW=PAR1+PAR2*R(N)+PAR3*R(N)*R(N)+PAR4*R(N)*R(N)*R(N)
      ROW=0.0808*(PPT*TVHPS+AP)*530.0/(TW*14.7*144.0)
      ROWS=0.0808*(PPT*TVHPS+AP)*530.0/(STS*14.7*144.0)
      VISW=0.000017*((TW/715.0)**0.5)
      VRMX2=VRMK*(1.0-PPT)/ROWS
      VRM(N)=VRMX2**0.5
 1203 BOI(N)=ROW*VISW*R(N)*R(N)*VRM(N)
      ZETA(1)=0.0
      DO 1204 N=3,NI,2
      N1=N-1
      N2=N-2
      DZETA(N)=(DELR/3.0)*(BOI(N2)+4.0*BOI(N1)+BOI(N))
      ZETA(N)=ZETA(N2)+DZETA(N)
      EPT=-0.694*R(N)*R(N)/(R5*R5)
      PPT=EXPF(EPT)
      BT=1.0-PPT
      TW=PAR1+PAR2*R(N)+PAR3*R(N)*R(N)+PAR4*R(N)*R(N)*R(N)
      ROW=0.0808*(PPT*TVHPS+AP)*530.0/(TW*14.7*144.0)
      ROWS=0.0808*(PPT*TVHPS+AP)*530.0/(STS*14.7*144.0)
      VISW=0.000017*((TW/715.0)**0.5)
      BTT3P=BT**1.5
      VRMCT=((VRMK/ROWS)**0.5)
      BETA(N)=(1.388*PPT*ZETA(N))/(BTT3P*R(N)*R5*R5*ROW*VISW
     X*VRMCT)
      QRAT=0.703*(1.0+0.096*(BETA(N)**0.5))/0.751
      QC=QSC*QRAT
      TW=TW-460.0
 1204 WRITE (2,1205) N,R(N),TW,VRM(N),ZETA(N),BETA(N),QC
 1205 FORMAT (I5,6E19.8)
   90 IF (1.0) 201,201,200
  201 CONTINUE
      END
```

APPENDIX 9.5

The Derivation of the Integral Momentum Equation for the Impingement Region Boundary Layer

The differential element of fluid shown in Figure 9.5.1 will be used as a basis for the derivation. The height of the differential element is greater than or equal to the boundary layer thickness. The derivation follows that of Eckert and Drake (42) for the two-dimensional, incompressible equation. The mass flow into 1-2 is

$$2\pi \int_0^l r\rho v_r \, dy \tag{A-78}$$

and the momentum of the flow entering 1-2 is

$$2\pi \int_0^l r\rho v_r^2 \, dy \tag{A-79}$$

The mass flow leaving 3-4 is

$$2\pi \int_0^l r\rho v_r \, dy + 2\pi \frac{d}{dr}\left\{\int_0^l r\rho v_r \, dy\right\} dr \tag{A-80}$$

and the momentum of the flow out of 3-4 is

$$2\pi \int_0^l r\rho v_r^2 \, dy + 2\pi \frac{d}{dr}\left\{\int_0^l r\rho v_r^2 \, dy\right\} dr \tag{A-81}$$

There is no mass flow or momentum entering 1-3 because of the presence of the flat plate. Therefore, the mass flow

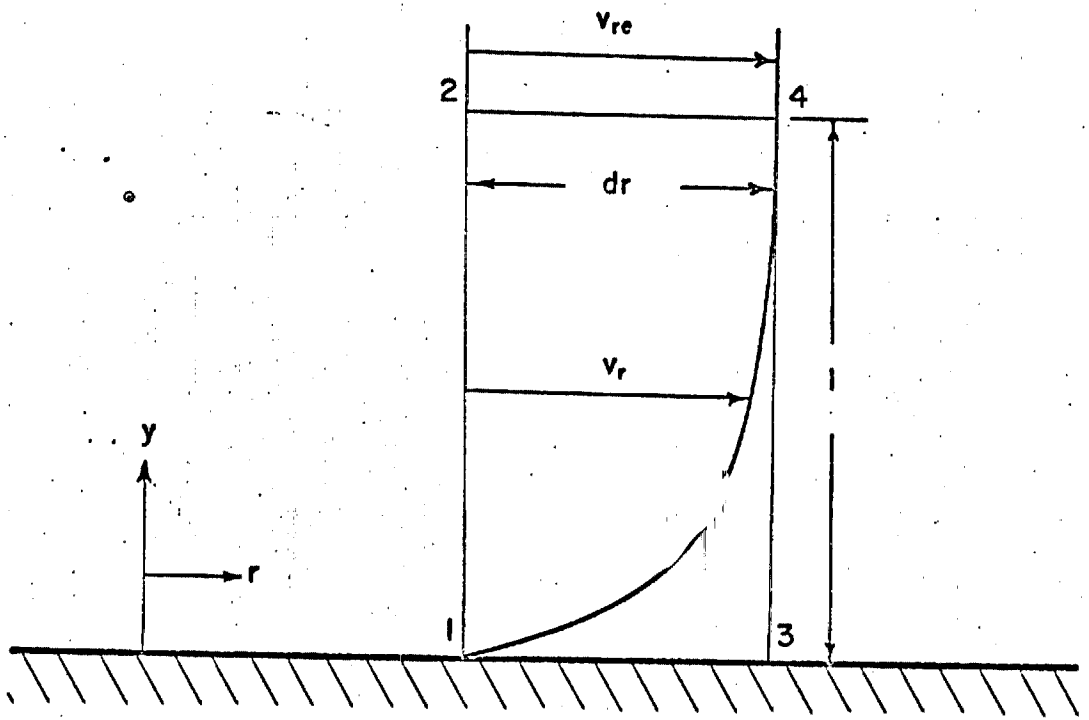

Figure 9.5.1

THE DIFFERENTIAL FLUID ELEMENT

entering 2-4 must be equal to the difference in the mass flow leaving 3-4 and the mass flow entering 1-2, which is

$$2\pi \frac{d}{dr}\left\{\int_o^l r\rho v_r\, dy\right\} dr \qquad \text{(A-82)}$$

Since the velocity at $y=l$ is taken to be v_{re}, the momentum of the flow entering 2-4 is

$$2\pi v_{re} \frac{d}{dr}\left\{\int_o^l r\rho v_r\, dy\right\} dr \qquad \text{(A-83)}$$

Now, setting the momentum into the differential fluid element minus the momentum out of the differential fluid element plus the sum of the forces on the control volume equal to zero, we have

$$-2\pi \frac{d}{dr}\left\{\int_o^l r\rho v_r^2\, dy\right\} dr + 2\pi v_{re} \frac{d}{dr}\left\{\int_o^l r\rho v_r\, dy\right\} dr$$

$$-g_c \tau_w 2\pi r dr + 2\pi r g_c p h - 2\pi h g_c \frac{d}{dr}\{pr\} dr = 0 \qquad \text{(A-84)}$$

Simplifying and letting l equal δ_v, the boundary layer thickness, the integral momentum boundary layer equation becomes:

$$v_{re} \frac{d}{dr}\left\{\int_o^{\delta_v} r\rho v_r\, dy\right\} - \frac{d}{dr}\left\{\int_o^{\delta_v} r\rho v_r^2\, dy\right\}$$

$$= r g_c \tau_w + r \delta_v g_c \frac{dp}{dr} \qquad \text{(A-85)}$$

APPENDIX 9.6

The Calculational Technique for the Impingement Region Boundary Layer Growth and Heat Flux Distribution in the Area Outside the Stagnation Area

9.6.1 Description of the Calculations

The object of this calculational procedure, which was implemented by the computer program listed in section 9.6.3 of this Appendix, was to obtain the impingement region turbulent boundary layer thickness and heat flux distribution in the area outside the stagnation area. The input data for these calculations included the barometric pressure, the static pressure on the plate at the stagnation point, the nozzle to plate distance, the nozzle diameter, and the calculated heat flux at the outer edge of the stagnation area. The measured plate surface temperatures and their axial positions were also input data for these calculations.

To begin the computation, a least squares procedure was used to obtain a third order polynomial for the surface temperature of the plate as a function of temperature. Then, Equations (38), (42), and (24) were used to calculate v_{re}, $\frac{dv_{re}}{dr}$, and $\frac{dp}{dr}$ at the various radial positions in the Runge-Kutta numerical integration formulas (29). These formulas were used repeatedly to obtain W as a function of radial

position. Thus, Equation (53), which defines W, was used to calculate δ_v as a function of radial position.

Beginning with the radial position of the outer edge of the stagnation area, Equation (57) was used to calculate the heat flux versus radial position. These calculations were performed until some radial limit, usually within the wall jet region, was reached. Therefore, the turbulent boundary layer thickness and the heat flux versus radial position in the impingement region outside the stagnation area were calculated.

9.6.2 Computer Program Nomenclature

Indices

N=1,2,3,...,NF--the number of points for the least squares data fit.

Non-subscripted Variables

AP--the ambient or barometric pressure.

BIASK--the constant in the Blasius relationship.

C1, C2, C3--constants of the polynomial for stagnation temperatures on the center-line of the free jet as a function of axial position.

DELR--the length of the increment for the Runge-Kutta solution.

DELTA--δ_v, the boundary layer thickness.

DESR-- δ_v at the outer edge of the boundary layer.

DVRM-- $\frac{dv_{rt}}{dr}$ in the impingement region analysis.

DO--the nozzle diameter.

GMUW--the viscosity of air at the surface temperature of the plate.

GNUW--the kinematic viscosity of air at the surface temperature of the plate.

GMUW--the viscosity of air at the surface temperature of the plate.

HNTOP--the nozzle to plate distance.

INDEX--the number of the experimental run.

NF--the total number of points for the least squares data fit.

PAR1 ⟶ PAR5--the constants of the least squares polynomial.

POWER--"n" in the impingement region analysis.

PPDR-- $\frac{dp}{dr}$ in the impingement region analysis.

PRESS-the static pressure.

QC--the calculated heat flux at some radial position.

QESR--the calculated heat flux at the outer edge of the stagnation area.

R--the radial coordinate.

RESR--the radial position of the outer edge of the stagnation area.

RF--the limiting radial position for the heat flux calculations.

RND--the dimensionless radial coordinate.

ROMS--the density at the edge of the impingement region boundary layer.

ROW--the density of the air at the surface temperature of the plate.

RO--the initial radial position for the Runge-Kutta numerical solution over an increment.

R5--the "half-width" of the pressure distribution on the plate.

STS--the temperature at the edge of the impingement region boundary layer.

TERM1, TERM2, TERM3--the three terms on the right side of Equation (52).

TVHPS--the static pressure on the plate at the stagnation point.

TW--the surface temperature of the plate.

TWESR--the surface temperature of the plate at the outer edge of the stagnation area.

VRM-- v_{re} in the impingement region analysis.

V1, V2, V3, V4--the four constants of the Runge-Kutta numerical solution.

W--a variable defined by Equation (53).

WO--the initial value of W for the Runge-Kutta numerical solution over an increment.

Subscripted Variables

RP(N)--the radial positions of the plate surface temperature measurements.

TP(N)--the measured plate surface temperatures.

9.6.3 Computer Program Listing

```
C     CALCULATION OF THE BOUNDARY LAYER THICKNESS WITH A
C     RUNGE-KUTTA SOLUTION OF THE INTEGRAL MOMENTUM EQUATION
C     AND THE ESTIMATION OF HEAT FLUXES IN THE IMPINGEMENT
C     REGION.
C     INPUT DATA
C     DELR-RADIAL INCREMENT FOR THE RUNGE-KUTTA
C     SOLUTION, NOZZLE DIAMETERS
C     RF-FINAL RADIAL POSITION FOR CALCULATIONS, NOZZLE DIA.
C     BLASK-BLASIUS CONSTANT
C     POWER-RECIPROCAL OF EXPONENT ON VELOCITY POWER PROFILE
C     R5-HALF-WIDTH OF PRESSURE DISTRIBUTION, NOZZLE DIA.
C     AP-AMBIENT PRESSURE,PSIA
C     TWHPS-PLATE PRESSURE AT STAGNATION POINT,PSIG
C     HNTOP-NOZZLE TO PLATE DISTANCE,INCHES
C     C1,C2,C3-PARAMETERS OF LEAST-SQUARE FIT OF STAGNATION
C     TEMPERATURES(DEG. R) VERSUS DISTANCE FROM THE
C     NOZZLE, NOZZLE DIAMETERS
C     DO-NOZZLE DIAMETER,INCHES
C     QESR-HEAT FLUX AT THE END OF THE STAGNATION
C     REGION, BTU/HR.-SQ. FT.
C     NF-NUMBER OF DATA POINTS FOR LEAST-SQUARE FIT
C     INDEX-NUMBER OF EXPERIMENTAL RUN
C     TP-PLATE TEMPERATURE,DEGREES F
C     RP-RADIAL DISTANCE ALONG PLATE,NOZZLE DIAMETERS
C     START,H,FINAL-STARTING VALUE, INCREMENT, AND FINAL
C     VALUE FOR LEAST-SQARES FIT EVALUATION
      DIMENSION TP(90),RP(90),X(90),Y(90),A(5),B(5),C(5),D(5
     X),F(5),BA(5)
     1,CA(5),DA(5),FA(5),CB(5),DB(5),FB(5),DC(5),FC(5),V(90)
     X,V2(90),CYDX
     2(90),D2YDX(90)
    1 READ (1,2) DELR,RF,BLASK,POWER,R5,AP,TWHPS,HNTOP
    2 FORMAT (8F10.0)
      READ (1,112) C1,C2,C3,DO,QESR
  112 FORMAT (5F10.0)
      READ (1,110) NF,INDEX
  110 FORMAT (2I5)
      READ (1,3) (TP(N),RP(N),N=1,NF)
    3 FORMAT (2F10.0)
      READ (1,88) START,H,FINAL
   88 FORMAT (3F10.0)
      WRITE (2,500) INDEX
  500 FORMAT (43H1 THIS CALCULATION IS FOR EXPERIMENTAL RUN
     XI2)
      WRITE (2,600)
  600 FORMAT (69HO PARAMETERS FOR FIT OF WALL TEMPERATURE(DE
     XG. R) VERSUS
     1 DISTANCE(FT.))
```

```
      START=START*CO/12.0
      H=H*DO/12.0
      FINAL=FINAL*CO/12.0
      DC 111 N=1,NF
      TP(N)=TP(N)+460.0
      RP(N)=RP(N)*CO/12.0
      Y(N)=TP(N)
  111 X(N)=RP(N)
      N=NF
      WRITE (2,33)
   33 FCRMAT(81HO              X                    Y
     X       DY/DX
     1                D2Y/DX2     //)
      DC 4 J=1,4
      A(J)=0.0
      B(J)=0.0
      C(J)=0.0
      D(J)=0.0
      F(J)=0.0
      DC 5 I=1,N
      A(J)=A(J)+(X(I)**(J-1))
      B(J)=B(J)+(X(I)**J)
      C(J)=C(J)+(X(I)**(J+1))
      D(J)=D(J)+(X(I)**(J+2))
    5 F(J)=F(J)+(Y(I)*(X(I)**(J-1)))
      IF(A(J)) 4,90,4
    4 CONTINUE
      A(1)=N
      F(1)=0.0
      DC 42 I=1,N
   42 F(1)=F(1)+Y(I)
      DC 6 J=2,4
      BA(J)=(B(J)/A(J))-(B(1)/A(1))
      IF(BA(J)) 7,90,7
    7 CA(J)=(C(J)/A(J))-(C(1)/A(1))
      DA(J)=(D(J)/A(J))-(D(1)/A(1))
    6 FA(J)=(F(J)/A(J))-(F(1)/A(1))
      DC 8 J=3,4
      CB(J)=(CA(J)/BA(J))-(CA(2)/BA(2))
      IF(CB(J)) 9,90,9
    9 DB(J)=(DA(J)/BA(J))-(DA(2)/BA(2))
    8 FB(J)=(FA(J)/BA(J))-(FA(2)/BA(2))
      J=4
      DC(J)=(DB(J)/CB(J))-(DB(3)/CB(3))
      IF(D(J)) 10,90,10
   10 FC(J)=(FB(J)/CB(J))-(FB(3)/CB(3))
      PAR4=FC(4)/DC(4)
      PAR3=(FB(4)-DB(4)*PAR4)/CB(4)
      PAR2=(FA(4)-DA(4)*PAR4-CA(4)*PAR3)/BA(4)
      PAR1=(F(4)-D(4)*PAR4-C(4)*PAR3-B(4)*PAR2)/A(4)
      DC 15 J=1,N
```

```
      V(J)=PAR1+PAR2*X(J)+PAR3*X(J)*X(J)+PAR4*(X(J)**3)-Y(J)
   15 V2(J)=V(J)*V(J)
      SUMV=0.0
      SUMV2=0.0
      DO 16 J=1,N
      SUMV=SUMV+V(J)
   16 SUMV2=SUMV2+V2(J)
      X(1)=START
      I=1
   27 Y(I)=PAR1+PAR2*X(I)+PAR3*X(I)*X(I)+PAR4*(X(I)**3)
      DYDX(I)=PAR2+2.0*PAR3*X(I)+3.0*PAR4*X(I)*X(I)
      D2YDX(I)=2.0*PAR3+6.0*PAR4*X(I)
      I=I+1
      X(I)=X(I-1)+H
      IF(X(I)-FINAL)27,27,28
   28 L=((FINAL-START)/H)+1.0
      IF(L)90,52,52
   52 CONTINUE
      WRITE (2,98) (X(I),Y(I),DYDX(I),D2YDX(I),I=1,L)
   98 FORMAT(1H 4E20.8)
      WRITE (2,99) PAR1,PAR2,PAR3,PAR4,SUMV,SUMV2
   99 FORMAT(6HOPAR1=E18.8/6HOPAR2=E18.8/6HOPAR3=E18.8/6HOPA
     XR4=E18.8/6HO
     1SUMV=E18.8/7HOSUMV2=E17.8//)
      WRITE (2,400)
  400 FORMAT (1COHO              R,N.D.              DELTA,
     XFT.          VRM,FT
     1./SEC.            TW,DEG. F    QC,BTU/HR.-SQ. FT.)
      DELR=DELR*DO/12.0
      RF=RF*DO/12.0
      R5=R5*DO/12.0
      HNTOP=HNTOP/DO
      STS=C1+C2*HNTOP+C3*HNTOP*HNTOP
      RESR=R5*1.15
      IESR=0
      VRMK=2.0*32.2*TVHPS*144.0
      RATIO=(POWER+1.0)*(POWER+2.0)/POWER
      RO=0.0
      WO=0.0
      V1=0.0
      GO TO 24
   38 R=RO
      W=WO
      TW=PAR1+PAR2*R+PAR3*R*R+PAR4*R*R*R
      EPT=-0.694*R*R/(R5*R5)
      PPT=EXPF(EPT)
      PRESS=(AP+PPT*TVHPS)*144.0
      ROW=0.0808*PRESS*530.0/(TW*14.7*144.0)
      ROWS=0.0808*PRESS*530.0/(STS*14.7*144.0)
      VRMX2=VRMK*(1.0-PPT)/ROWS
      VRM=VRMX2**0.5
```

```
      GMUW=0.0C0017*((TW/715.0)**0.5)
      GNUW=GMUW/ROW
      VK14=(GNUW**0.25)
      PPDR=-TVHPS*1.388*R*PPT*144.0/(R5*R5)
      PPTCT=(1.0-PPT)
      VRMCT=VRMK/ROMS
      DVRM=(VRMCT**0.5)*0.694*R*PPT/(R5*R5*(PPTCT**0.5))
      TERM1=(POWER+1.0)*W*DVRM/VRM
      TERM2=BLASK*RATIO*(R**1.25)*(ROW**1.25)*VRM*VK14
      TERM3=RATIO*W*32.2*PPDR/(ROW*VRM*VRM)
      FUNCT=5.0*(TERM1+TERM2+TERM3)/4.0
      V1=FUNCT*DELR
   24 R=RO+DELR/2.0
      W=WO+V1/2.0
      TW=PAR1+PAR2*R+PAR3*R*R+PAR4*R*R*R
      EPT=-0.694*R*R/(R5*R5)
      PPT=EXPF(EPT)
      PRESS=(AP+PPT*TVHPS)*144.0
      ROW=0.0808*PRESS*530.0/(TW*14.7*144.0)
      ROMS=0.0808*PRESS*530.0/(STS*14.7*144.0)
      VRMX2=VRMK*(1.0-PPT)/ROMS
      VRM=VRMX2**0.5
      GMUW=0.CC0017*((TW/715.0)**0.5)
      GNUW=GMUW/ROW
      VK14=(GNUW**0.25)
      PPDR=-TVHPS*1.388*R*PPT*144.0/(R5*R5)
      PPTCT=(1.0-PPT)
      VRMCT=VRMK/ROMS
      DVRM=(VRMCT**0.5)*0.694*R*PPT/(R5*R5*(PPTCT**0.5))
      TERM1=(POWER+1.0)*W*DVRM/VRM
      TERM2=BLASK*RATIO*(R**1.25)*(ROW**1.25)*VRM*VK14
      TERM3=RATIO*W*32.2*PPDR/(ROW*VRM*VRM)
      FUNCT=5.0*(TERM1+TERM2+TERM3)/4.0
      V22=FUNCT*DELR
      W=WO+V22/2.0
      TW=PAR1+PAR2*R+PAR3*R*R+PAR4*R*R*R
      EPT=-0.694*R*R/(R5*R5)
      PPT=EXPF(EPT)
      PRESS=(AP+PPT*TVHPS)*144.0
      ROW=0.0808*PRESS*530.0/(TW*14.7*144.0)
      ROMS=0.0808*PRESS*530.0/(STS*14.7*144.0)
      VRMX2=VRMK*(1.0-PPT)/ROMS
      VRM=VRMX2**0.5
      GMUW=0.CC0017*((TW/715.0)**0.5)
      GNUW=GMUW/ROW
      VK14=(GNUW**0.25)
      PPDR=-TVHPS*1.388*R*PPT*144.0/(R5*R5)
      PPTCT=(1.0-PPT)
      VRMCT=VRMK/ROMS
      DVRM=(VRMCT**0.5)*0.694*R*PPT/(R5*R5*(PPTCT**0.5))
      TERM1=(POWER+1.0)*W*DVRM/VRM
```

```
      TERM2=BLASK*RATIO*(R**1.25)*(ROW**1.25)*VRM*VK14
      TERM3=RATIO*W*32.2*PPDR/(ROW*VRM*VRM)
      FUNCT=5.0*(TERM1+TERM2+TERM3)/4.0
      V3=FUNCT*DELR
      R=RO+DELR
      W=WO+V3
      TW=PAR1+PAR2*R+PAR3*R*R+PAR4*R*R*R
      EPT=-0.694*R*R/(R5*R5)
      PPT=EXPF(EPT)
      PRESS=(AP+PPT*TVHPS)*144.0
      ROW=0.0808*PRESS*530.0/(TW*14.7*144.0)
      ROMS=0.0808*PRESS*530.0/(STS*14.7*144.0)
      VRMX2=VRMK*(1.0-PPT)/ROMS
      VRM=VRMX2**0.5
      GMUW=0.CC0017*((TW/715.0)**0.5)
      GNUW=GMUW/ROW
      VK14=(GNUW**0.25)
      PPDR=-TVHPS*1.388*R*PPT*144.0/(R5*R5)
      PPTCT=(1.0-PPT)
      VRMCT=VRMK/ROMS
      DVRM=(VRMCT**0.5)*0.694*R*PPT/(R5*R5*(PPTCT**0.5))
      TERM1=(POWER+1.0)*W*DVRM/VRM
      TERM2=BLASK*RATIO*(R**1.25)*(ROW**1.25)*VRM*VK14
      TERM3=RATIO*W*32.2*PPDR/(ROW*VRM*VRM)
      FUNCT=5.0*(TERM1+TERM2+TERM3)/4.0
      V4=FUNCT*DELR
      DELW=(V1+2.0*V22+2.0*V3+V4)/6.0
      W=WO+DELW
      R=RO+DELR
      IF (W) 201,201,202
  201 WRITE (2,203)
  203 FORMAT (11HONEGATIVE W)
      GO TO 90
  202 CONTINUE
      W45=W**0.8
      DELTA=W45/(ROW*VRM*R)
      IF (IESR) 299,300,299
  300 IF (RESR-R) 301,301,302
  302 TW=TW-460.0
      RND=R*12.0/DO
      WRITE (2,35) RND,DELTA,VRM,TW
   35 FORMAT (4E20.8)
      GO TO 303
  301 IESR=1
      TWESR=TW
      DESR=DELTA
  299 QC=DESR*(STS-TW)*QESR/(DELTA*(STS-TWESR))
      TW=TW-460.0
      RND=R*12.0/DO
      WRITE (2,304) RND,DELTA,VRM,TW,QC
  304 FORMAT (5E20.8)
```

```
303 WC=W
    RC=R
    IF (R-RF) 36,90,90
 36 GC TO 38
 90 IF (1.0) 39,39,1
 39 CCNTINUE
    END
```

APPENDIX 9.7

Estimates of the Experimental Errors

9.7.1 Static Pressure Measurements

The static pressure taps in the plate were designed according to the method of Rayle (37) to reduce the errors induced by their presence. Although there was no calibration technique available to check the pressure tap measurements, it was felt that the measurements were accurate to the limit with which the height of the mercury and oil columns could be read from the manometer board. Thus, the errors in the static pressure readings varied with the magnitude of the gauge pressure, but they were always less than 2 to 3 per cent of the stagnation point gauge pressures.

9.7.2 Heat Flux Measurements

A quick calibration check of two heat flux probes was made with a guarded plate heater. Although the heat flux levels for the calibration check were low (around 1200 BTU/hr.-ft.^{2}) because of the guarded plate heater used, the heat fluxes measured by the probes were within $\pm$10 per cent of the value calculated from the wattmeter readings of the guarded plate assemly. It was felt that the agreement of the calibration check might have been even better for higher heat fluxes. This is because the temperature difference

across the probes would have been higher and thus would not have been affected as much by thermocouple errors. In any event, the heat flux measurements are probably accurate within $\pm$10 per cent.

9.7.3 Total Head Probe Measurements

Again, there was no good calibration check for the total head pressure measurements. The total head probes were designed, using an analysis based upon the potential flow solution for flow around a cylinder, so that errors in the total head pressure because of their presence would be less than 2 to 3 per cent. However, much higher velocities were used in the design analysis than were actually measured, and, therefore, the errors are probably much smaller.

The errors in the total head pressure measurements in the boundary layer of the wall jet can only be estimated. Usually, for measurements near a wall, the total pressures appear to have a larger value than they should (44). These errors may be compensated for by shifting the measured total head pressure curve by a fixed amount which depends upon the probe geometry. This shift factor, for the probes used here, was about 0.001 to 0.002 inches (44). This correction was neglected because the errors involved in locating the probe were of the same order of magnitude.

Total head probe measurements were reproducible within 2 to 3 per cent. Axial velocity and temperature decay data from three experimental runs with approximately the same conditions are plotted in Figure 9.7.1. Also, the Kiel probe and the standard total head probe measured the same total head pressure at the same location in the flow field. Figure 9.7.2 shows a plot of total head pressure and stagnation temperature across the entire width of the jet to check the assumed condition of angular symmetry.

9.7.4 Stagnation Temperature Measurements

No calibration check of the stagnation temperature measurements was made except to note the fact that the stagnation temperatures measured with the probes agreed with those measured inside the plenum chamber of the nozzle. The combination of conduction loss errors, radiation loss errors, flow disturbance errors, and recovery factor errors was estimated to be less than 5 per cent of the difference between the temperature measured and the ambient temperature (38), (39). It was not possible to estimate the flow disturbance errors in the measurement of the wall jet boundary layer temperature variation, although they were undoubtedly higher than the comparable total head pressure errors.

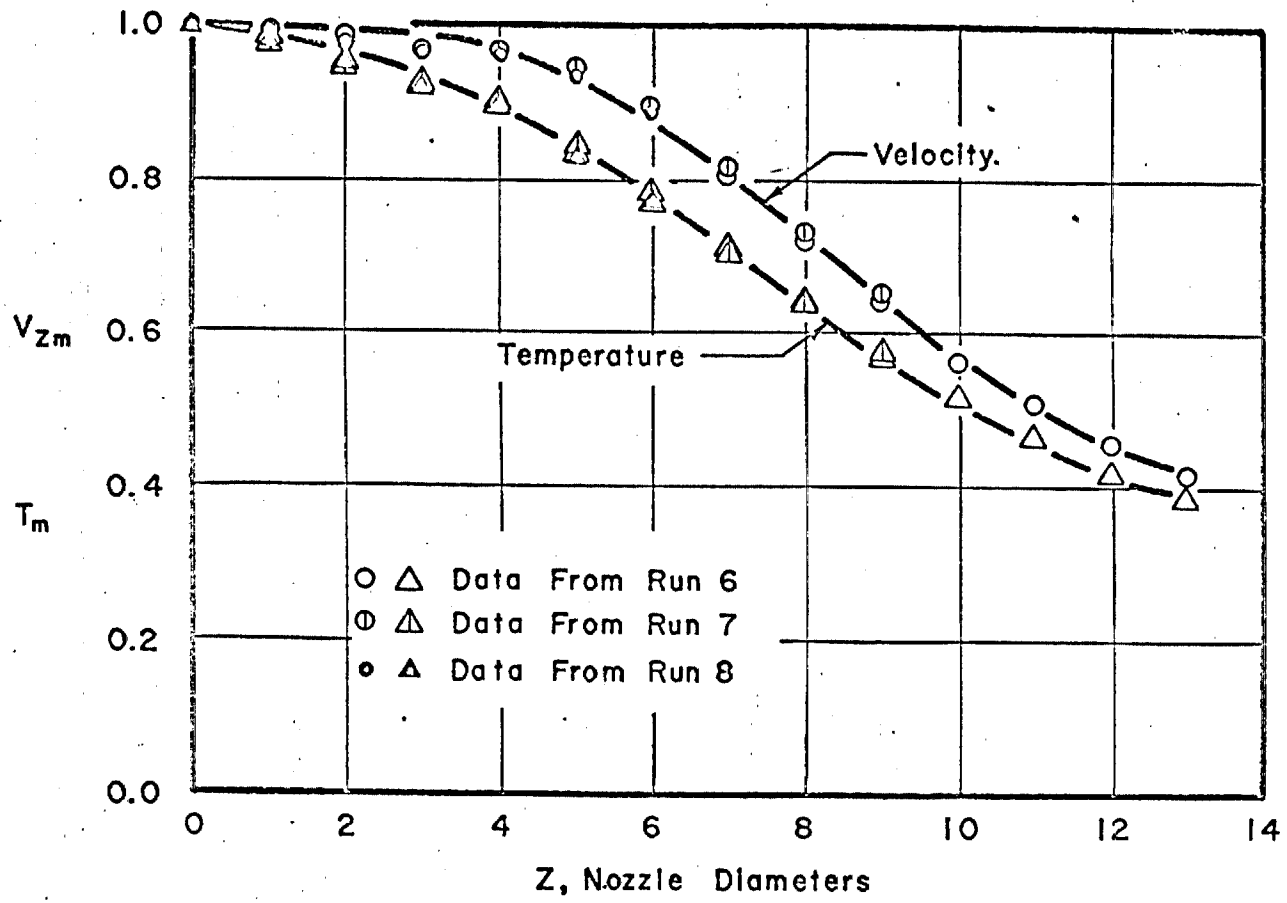

Figure 9.7.1

THE ABILITY TO REPRODUCE THE AXIAL DECAY DATA

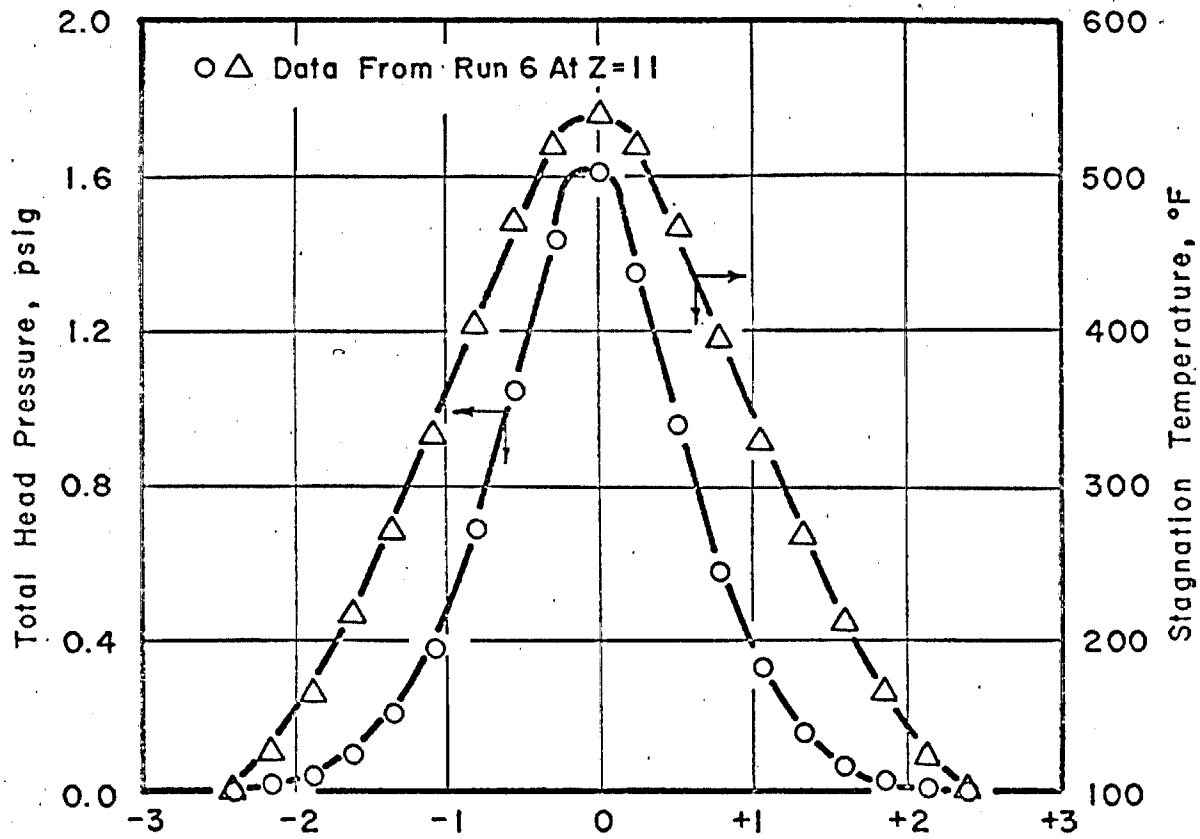

Figure 9.7.2

THE CHECK OF ANGULAR SYMMETRY

APPENDIX 9.8

Data Reduction Techniques

9.8.1 The Static Pressure and Heat Flux Measurements

The static pressure and heat flux data were the first to be reduced. The radial positions of the static pressure taps were tabulated in terms of nozzle diameters. The pressures were converted from inches of oil or inches of mercury to psig. Dimensionless pressure ratios ($\frac{\Delta p}{\Delta p_c}$) were also calculated.

To calculate the heat fluxes from the raw data, the e.m.f.'s of the thermocouples were converted to degrees F. Standard thermocouple-e.m.f. curves were used for this conversion because calibration of the thermocouples against standard thermometers revealed that the error introduced by doing this was never more than 1.5°F. Then, the temperatures at the three points of the heat flux probes were plotted against their axial position on the rod. If this plot was approximately a straight line, indicating a one-dimensional heat transfer, the heat fluxes were calculated. These heat flux plots never varied more than several per cent from a straight line.

The heat fluxes were calculated by subtracting the temperature of the probe at a depth of 3/8 inches from the

temperature at the surface of the probe and dividing the difference by 3/8 inches to get the temperature gradient. This gradient was then multiplied by the thermal conductivity of Inconel at the surface temperature of the probe (see Figure 9.8.1 for the thermal conductivity of Inconel versus temperature) to obtain the heat flux at that point. The temperatures of the thermocouples with the greatest distance separating them were used to calculate the gradient because it was felt that the greatest error involved was the error in the measurement of the distance between thermocouples on the probe.

9.8.2 The Free Jet and Wall Jet Probe Measurements

The total head pressures and stagnation temperatures measured with the free jet and wall jet probes were converted into velocities and static temperatures with a computer program. The input data for the program included the total head pressures and stagnation temperatures measured by the probes, the ambient temperature, and the barometric pressure. In the program, the Mach number of the flow was calculated from the ratio of the stagnation pressure to the static pressure. Then, the recovery ratio was determined (see Figure 9.8.2 for a plot of recovery ratio versus Mach number for the stagnation temperature probes), and the

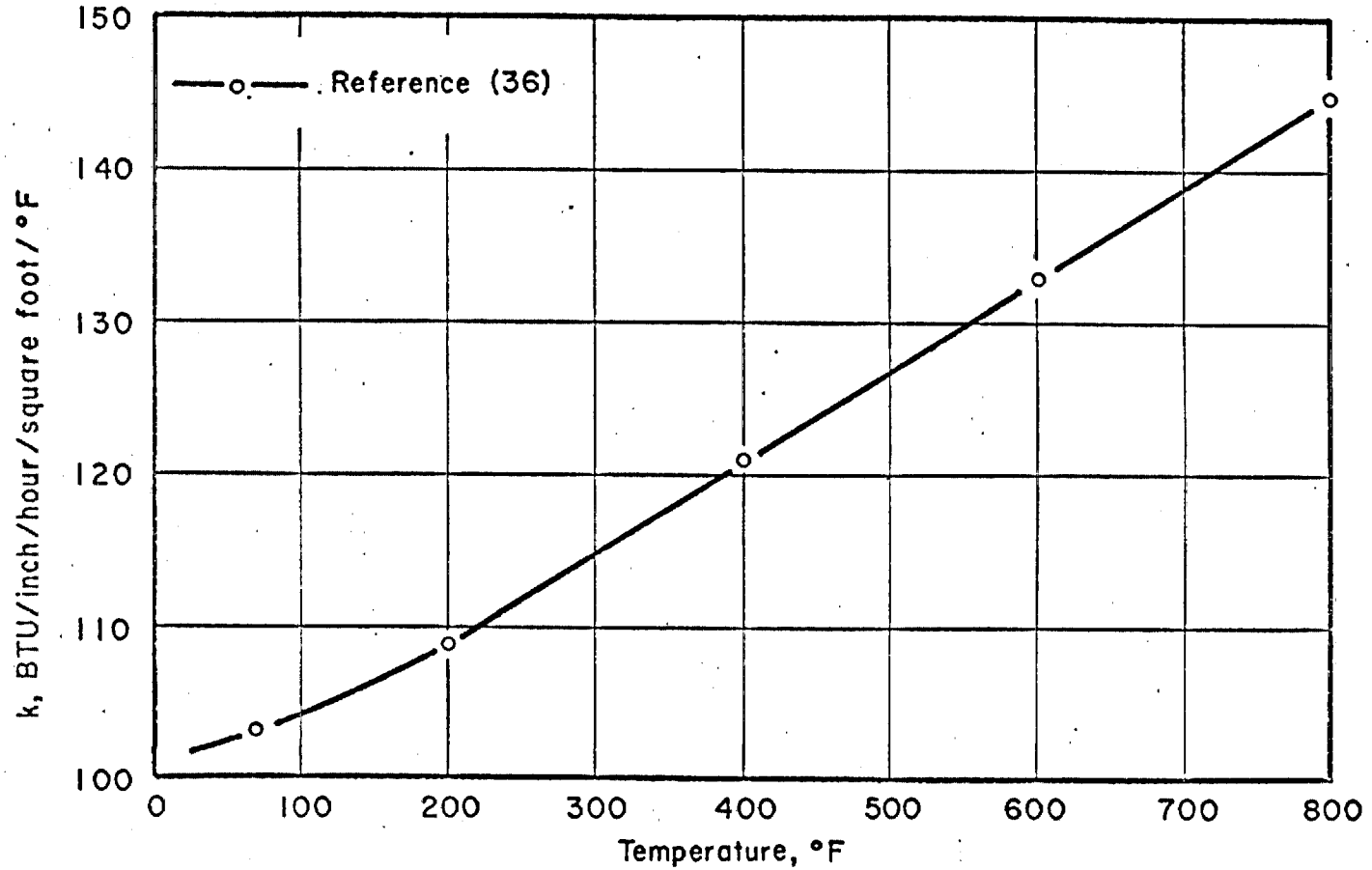

Figure 9.8.1

THERMAL CONDUCTIVITY OF INCONEL AS A FUNCTION OF TEMPERATURE

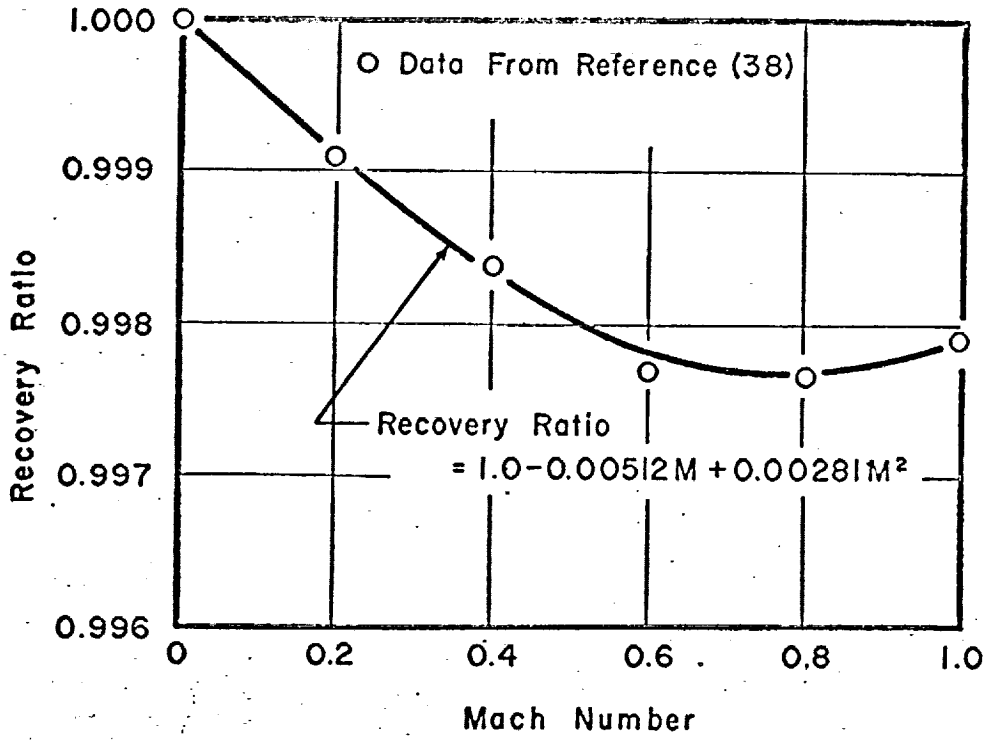

Figure 9.8.2

THE RECOVERY RATIO AS A FUNCTION OF MACH NUMBER

static temperature was calculated from the Mach number and the recovery ratio. The recovery ratio was unity for the first measured quantities which were the stagnation temperature and total head pressure in the plenum chamber of the nozzle. The output of program included velocities and temperatures in both dimensionless and dimensional forms and the Mach number.

The variation of physical properties of the flow was also considered in the program. Figure 9.8.3 shows a plot of C_p as a function of temperature. The computer program which was used for these calculations is listed in the section 9.8.4 of this Appendix.

9.8.3 Computer Nomenclature

Indices

J--1,2,3,...,N-- number of data points.

Nonsubscripted Variables

AP--ambient or barometric pressure.

CPRAT--the heat capacity ratio.

INDEX--the number of the experimental run.

N--the total number of data points.

RRAT--the recovery ratio.

TA--the ambient temperature.

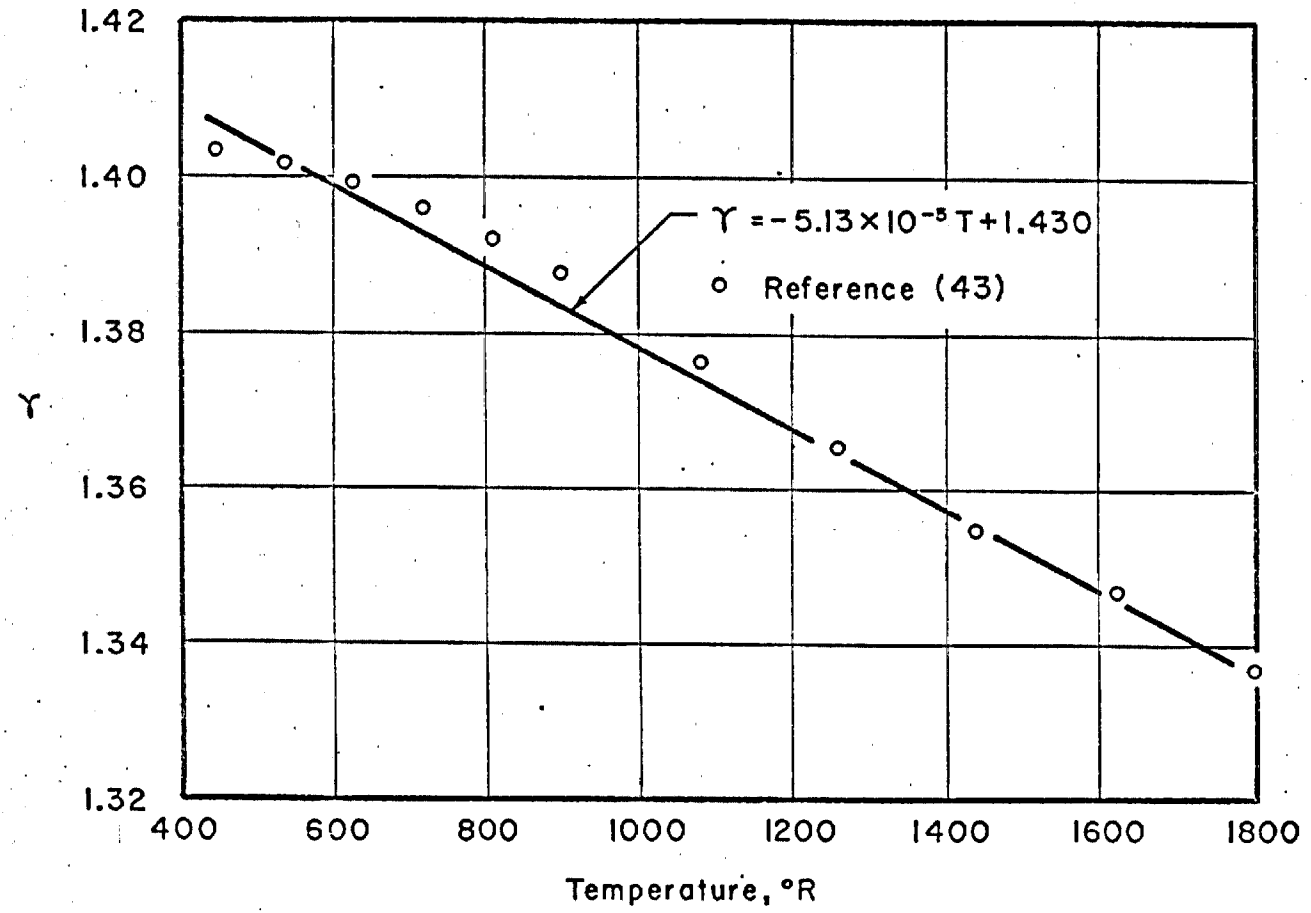

Figure 9.8.3

HEAT CAPACITY RATIO OF AIR AS A FUNCTION OF TEMPERATURE

Subscripted Variables

DELP(J)--the measured total head pressures.

PTERM(J)--the pressure ratios.

SSN(J)--the Mach number.

STAGT(J)--the measured stagnation temperatures.

T(J)--the dimensionless static temperatures.

TDEGF(J), TDEGR(J)--the static temperatures.

VEL(J)--the velocities.

VZ(J)--the dimensionless velocities.

9.8.4 Computer Program Listing

```
C     PROGRAM TO CALCULATE VELOCITIES AND TEMPERATURES FROM
C     TOTAL HEAD PRESSURE AND STAGNATION TEMPERATURE DATA,
C     BAROMETRIC PRESSURE, AND AMBIENT TEMPERATURE.
C     OUTPUT INCLUDES VELOCITIES AND TEMPERATURES IN BOTH
C     DIMENSIONAL AND DIMENSIONLESS FORMS.
C     INPUT DATA
C     N-NUMBER OF DATA POINTS
C     TA-AMBIENT TEMPERATURE, DEG. F
C     AP-AMBIENT PRESSURE, PSIA
C     DELP-MEASURED VELOCITY HEAD PRESSURE, PSIG
C     STAGT-MEASURED STAGNATION TEMPERATURES, DEG. F
      DIMENSION STAGT(100),DELP(100),SSNX2(100),SSN(100),VE
     XL(100),VZ(10
     10),TFDEG(100),PTERM(100),T(100),TDEGR(100)
  102 READ (1,1) INDEX,N,TA,AP
    1 FORMAT (2I5,2F10.0)
      READ (1,2) (DELP(J),STAGT(J),J=1,N)
    2 FORMAT (2F10.0)
      WRITE (2,94) INDEX
   94 FORMAT (43H1 THIS CALCULATION IS FOR EXPERIMENTAL RUN
     XI2)
      WRITE (2,5)
    5 FORMAT (110HO          DELP          STAGT   VEL,
     XFT./SEC.
     1    VZ   TFDEG,DEG. F              T            SSN
     X J)
      TA=TA+460.0
      DO 3 J=1,N
      STAGT(J)=STAGT(J)+460.0
      CPRAT=1.430-0.0000513*STAGT(J)
      Z=CPRAT-1.0
      RATIO=Z/CPRAT
      PTERM(J)=(DELP(J)/AP)+1.0
      SSNX2(J)=2.0*((PTERM(J)**RATIO)-1.0)/Z
      SSN(J)=SSNX2(J)**0.5
      IF(J-1) 6,6,7
    6 RRAT=1.0
      GO TO 8
    7 RRAT=1.0+0.00281*SSNX2(J)-0.00512*SSN(J)
    8 TDEGR(J)=STAGT(J)/((1.0+Z*SSNX2(J)/2.0)*RRAT)
      T(J)=(TDEGR(J)-TA)/(TDEGR(1)-TA)
      VEL(J)=SSN(J)*49.02*(TDEGR(J)**0.5)
      VZ(J)=VEL(J)/VEL(1)
      TFDEG(J)=TDEGR(J)-460.0
      STAGT(J)=STAGT(J)-460.0
      WRITE (2,4) DELP(J),STAGT(J),VEL(J),VZ(J),TFDEG(J),T(J
     X),SSN(J),J
    4 FORMAT (7F15.8,I5)
```

```
  3 CCNTINUE
    IF (1.0) 101,101,102
101 CCNTINUE
    END
```

APPENDIX 9.9

Experimental Data

The reduced data for the experimental runs are tabulated in this Appendix.

Table 9.9.1

The Static Pressure Distribution on the Plate

Run 3 (D=0.250 inches)

Radial Position (Nozzle diameters)	Pressure (psig)	$\frac{\Delta p}{\Delta p_s}$
0.000	0.7520	1.000
1.248	0.3765	0.501
2.248	0.1076	0.143
3.248	0.314	0.042
4.248	0.0141	0.019
5.248	0.0127	0.017
7.248	0.0083	0.011
9.248	0.0061	0.008
11.248	0.0047	0.006
13.248	0.0029	0.004

Run 4 (D=0.250 inches)

Radial Position (nozzle diameters)	Pressure (psig)	$\frac{\Delta p}{\Delta p_s}$
0.000	1.552	1.000
1.238	0.723	0.466
2.248	0.184	0.119
3.248	0.056	0.036
4.248	0.026	0.017
5.248	0.026	0.017
7.248	0.013	0.008
9.248	0.008	0.005
11.248	0.005	0.003
13.248	0.005	0.003

(Table 9.9.1 continued)

Run 5 (D=0.250 inches)

Radial Position (nozzle diameters)	Pressure (psig)	$\frac{\Delta p}{\Delta P_s}$
0.000	1.189	1.000
1.248	0.578	0.486
2.248	0.157	0.132
3.248	0.047	0.040
4.248	0.020	0.017
5.248	0.018	0.015
7.248	0.011	0.009
9.248	0.007	0.006
11.248	0.004	0.003
13.248	0.004	0.003

Run 6 (D=0.375 inches)

Radial Position (nozzle diameters	Pressure (psig)	$\frac{\Delta p}{\Delta P_s}$
0.000	0.872	1.000
0.832	0.642	0.716
1.499	0.308	0.353
2.165	0.133	0.153
2.832	0.048	0.055
3.499	0.025	0.029
4.832	0.015	0.017
6.165	0.011	0.013
7.499	0.008	0.009
8.832	0.005	0.006

Run 7 (D=0.375 inches)

Radial Position (nozzle diameters)	Pressure (psig)	$\frac{\Delta p}{\Delta P_s}$
0.000	1.557	1.000
0.832	0.877	0.563
1.499	0.287	0.184
2.165	0.089	0.057
2.835	0.031	0.020
3.499	0.026	0.017
4.832	0.014	0.009

(Table 9.9.1 continued)

Radial Position (nozzle diameters)	Pressure (psig)	$\frac{\Delta p}{\Delta p_s}$
6.165	0.009	0.006
7.499	0.005	0.003
8.832	0.003	0.002

Run 8 (D=0.375 inches)

Radial Position (nozzle diameters)	Pressure (psig)	$\frac{\Delta p}{\Delta p_s}$
0.000	3.487	1.000
0.832	0.972	0.279
1.499	0.165	0.047
2.165	0.069	0.020
2.835	0.033	0.009
3.499	0.029	0.008
4.832	0.010	0.003
6.165	0.006	0.002
7.499	0.003	0.001
8.832	0.002	0.001

Run 9 (D=0.250 inches)

Radial Position (nozzle diameters)	Pressure (psig)	$\frac{\Delta p}{\Delta p_s}$
0.000	1.351	1.000
1.248	0.700	0.518
2.248	0.188	0.139
3.248	0.053	0.039
4.248	0.021	0.016
5.248	0.019	0.014
7.248	0.009	0.007
9.248	0.005	0.004
11.248	0.004	0.003
13.248	0.003	0.002

(Table 9.9.1 continued)

Run 10 (D=0.250 inches)

Radial Position (nozzle diamters)	Pressure (psig)	$\frac{\Delta p}{\Delta p_s}$
0.000	1.385	1.000
1.248	0.655	0.473
2.248	0.163	0.118
3.248	0.046	0.033
4.248	0.020	0.014
5.248	0.018	0.013
7.248	0.008	0.006
9.248	0.004	0.003
11.248	0.002	0.001
13.248	0.001	0.001

Table 9.9.2

The Heat Flux and Surface Temperature Distribution

Run 3 (D=0.250 inches)

Radial Position (nozzle diameters)	Heat Flux (BTU/hr.-ft.^{2})	Surface Temperature (^oF)
0.00	20,214	255.5
2.40	14.030	223.8
5.36	7,065	176.4
9.24	2,444	135.8
14.72	741	115.4
14.72	943	117.0
24.00	265	105.6

Run 4 (D=0.250 inches)

Radial Position (nozzle diameters)	Heat Flux (BTU/hr.-ft.^{2})	Surface Temperature (^oF)
0.00	24,472	284.7
2.40	18,006	250.4
5.36	8,331	190.0
9.24	3,044	141.6
14.72	895	119.3
14.72	1,000	120.8
24.00	293	108.4

Run 5 (D=0.250 inches)

Radial Position (nozzle diameters)	Heat Flux (BTU/hr.-ft.^{2})	Surface Temperature (^oF)
0.00	23,623	277.8
2.40	17,170	244.2
5.36	7,704	186.5
9.24	2,883	142.0
14.72	941	120.3
14.72	1,051	121.7
24.00	279	109.8

Table 9.9.2 (continued)

Run 6 (D=0.375 inches)

Radial Position (nozzle diameters)	Heat Flux (BTU/hr.-ft.^{2})	Surface Temperature ($^\circ$F)
0.000	18,919	265.6
1.600	15,639	246.2
3.573	9,648	206.1
6.160	5,094	168.2
9.813	1,715	137.0
16.000	524	122.5

Run 7 (D=0.375 inches)

Radial Position (nozzle diameters)	Heat Flux (BTU/hr.-ft.^{2})	Surface Temperature ($^\circ$F)
0.000	41,992	366.2
1.600	28,601	313.9
3.573	12,956	235.0
6.160	5,245	176.4
9.813	1,666	141.0
9.813	1,726	143.4
16.000	435	126.8

Run 8 (D=0.375 inches)

Radial Position (nozzle diameters)	Heat Flux (BTU/hr.-ft.^{2})	Surface Temperature ($^\circ$F)
0.000	77,578	545.6
1.600	45,905	408.2
3.573	15,029	258.0
6.160	5,601	183.6
9.813	1,883	147.3
9.813	2,035	150.23
16.000	289	130.93

Table 9.9.2 (continued)

Run 9 (D=0.250 inches)

Radial Position (nozzle diameters)	Heat Flux (BTU/hr.-ft.^{2})	Surface Temperature (^{o}F)
0.00	32,576	322.9
2.40	20,620	270.3
5.36	9,726	205.1
9.24	3,614	156.0
14.72	1,195	131.2
14.72	1,209	131.3
24.00	336	119.6

Run 10 (D=0.250 inches)

Radial Position (nozzle diameters)	Heat Flux (BTU/hr.-ft.^{2})	Surface Temperature (^{o}F)
0.00	20,419	250.2
2.40	13,701	213.0
5.36	6,012	165.6
9.24	2,147	130.8
14.72	818	113.4
14.72	819	113.9
24.00	292	105.2

Table 9.9.3

The Axial Variationof Free Jet Velocity and Temperature

Run 3 (D=0.250 inches)

Axial Position (nozzle diameters)	V_{Zm}	T_m
0.0	1.000	1.000
1.0	0.997	1.002
2.0	0.990	0.991
3.0	0.979	0.948
4.0	0.954	0.868
5.0	0.897	0.781
6.0	0.829	0.708

Run 4 (D=0.250 inches)

Axial Position (nozzle diameters)	V_{Zm}	T_m
0.0	1.000	1.000
1.0	1.013	1.038
2.0	1.018	1.033
3.0	1.005	1.008
4.0	0.995	0.960
5.0	0.959	0.889
6.0	0.895	0.821
7.0	0.829	0.747
8.0	0.744	0.686
9.0	0.667	0.663
10.0	0.605	0.581
11.0	1.544	0.530
12.0	0.488	0.485

Run 5 (D=0.250 inches)

Axial Position (nozzle diameters)	V_{Zm}	T_m
0.0	1.000	1.000
1.0	0.993	0.979
2.0	0.989	0.970

Table 9.9.3 (continued)

Axial Position (nozzle diameters)	V_{zm}	T_m
3.0	0.989	0.951
4.0	0.973	0.911
5.0	0.940	0.851
6.0	0.882	0.783
7.0	0.810	0.715
8.0	0.728	0.655
9.0	0.648	0.600
10.0	0.588	0.549
11.0	0.529	0.504
12.0	0.478	0.460

Run 6 (D=0.375 inches)

Axial Position (nozzle diameters)	V_{zm}	T_m
0.0	1.000	1.000
1.0	0.989	0.980
2.0	0.983	0.946
3.0	0.968	0.918
4.0	0.963	0.984
5.0	0.941	0.838
6.0	0.884	0.767
7.0	0.802	0.702
8.0	0.716	0.634
9.0	0.636	0.571
10.0	0.565	0.525
11.0	0.506	0.464
12.0	0.455	0.420
13.0	0.413	0.386

Table 9.9.3 (continued)

Run 7 (D=0.375 inches)

Axial Position (nozzle diameters)	V_{Zm}	T_m
0.0	1.000	1.000
1.0	0.995	0.976
2.0	0.985	0.949
3.0	0.979	0.923
4.0	0.967	0.899
5.0	0.949	0.845
6.0	0.897	0.777
7.0	0.814	0.700
8.0	0.733	0.638
9.0	0.649	0.576

Run 8 (D=0.375 inches)

Axial Position (nozzle diameters)	V_{Zm}	T_m
0.0	1.000	1.000
1.0	0.988	0.979
2.0	0.978	0.951
3.0	0.967	0.919
4.0	0.962	0.901
5.0	0.935	0.833
6.0	0.888	0.778

Run 9 (D=0.250 inches)

Axial Position (nozzle diameter)	V_{Zm}	T_m
0.0	1.000	1.000
1.0	0.995	0.982
2.0	0.987	0.956
3.0	0.982	0.941
4.0	0.972	0.910
5.0	0.945	0.855
6.0	0.888	0.787
7.0	0.811	0.728
8.0	0.727	0.665

Table 9.9.3 (continued)

Axial Position (nozzle diameter)	V_{Zm}	T_m
9.0	0.656	0.610
10.0	0.588	0.561
11.0	0.526	0.505
12.0	0.474	0.461

Run 10 (D=0.250 inches)

Axial Position (nozzle diameter)	V_{Zm}	T_m
0.0	1.000	1.000
1.0	1.008	1.008
2.0	1.002	0.984
3.0	0.995	0.972
4.0	0.989	0.937
5.0	0.964	0.888
6.0	0.913	0.821
7.0	0.846	0.754
8.0	0.762	0.697
9.0	0.688	0.642
10.0	0.623	0.588
11.0	0.563	0.540
12.0	0.512	0.499

Table 9.9.4

The Radial Variation of Free Jet Velocity and Temperature

Run 3 (D=0.250 inches)

Axial Position (nozzle diameters)	Radial Position (nozzle diameters)	V_z	T
1.0	0.000	1.003	1.012
	0.120	1.006	1.011
	0.240	1.000	0.997
	0.360	0.985	0.942
	0.480	0.805	0.767
	0.600	0.268	0.628
	0.720	0.000	0.361
4.0	0.000	0.955	0.864
	0.200	0.900	0.808
	0.400	0.699	0.694
	0.600	0.456	0.550
	0.800	0.249	0.373
	1.000	0.129	0.230
	1.200	0.000	0.123
8.0	0.000	0.689	0.583
	0.240	0.638	0.561
	0.480	0.514	0.505
	0.720	0.373	0.415
	0.960	0.254	0.320
	1.200	0.168	0.243
	1.440	0.087	0.170
	1.680	0.048	0.096
	1.920	0.000	0.054
11.0	0.000	0.496	0.444
	0.320	0.455	0.427
	0.640	0.357	0.373
	0.960	0.255	0.306
	1.280	0.166	0.227
	1.600	0.100	0.158
	1.920	0.048	0.105
	2.240	0.000	0.055

Table 9.9.4 (continued)

Run 4 (D=0.250 inches)

Axial Position (nozzle diameters)	Radial Position (nozzle diameters)	V_z	T
4.0	0.000	0.995	0.960
	0.200	0.944	0.909
	0.400	0.721	0.788
	0.600	0.453	0.629
	0.800	0.230	0.411
	1.000	0.086	0.244
	1.200	0.035	0.105
	1.400	0.000	0.048
8.0	0.000	0.744	0.686
	0.240	0.662	0.672
	0.480	0.486	0.597
	0.720	0.337	0.479
	0.960	0.209	0.357
	1.200	0.123	0.253
	1.440	0.064	0.166
	1.680	0.035	0.098
	1.920	0.000	0.047
11.0	0.000	0.541	0.530
	0.320	0.489	0.508
	0.640	0.372	0.437
	0.960	0.256	0.346
	1.280	0.166	0.252
	1.600	0.098	0.174
	1.920	0.050	0.109
	2.240	0.000	0.056

Run 5 (D=0.250 inches)

Axial Position (nozzle diameters)	Radial Position (nozzle diameters)	V_z	T
4.0	0.000	0.972	0.912
	0.120	0.961	0.892
	0.240	0.894	0.845
	0.360	0.768	0.773
	0.480	0.606	0.692
	0.600	0.441	0.592
	0.720	0.303	0.483

Table 9.9.4 (continued)

Axial Position (nozzle diameters)	Radial Position (nozzle diameters)	V_z	T
	0.840	0.198	0.365
	0.960	0.119	0.285
	1.080	0.066	0.210
	1.200	0.000	0.111
8.0	0.000	0.728	0.653
	0.240	0.664	0.634
	0.480	0.487	0.565
	0.720	0.344	0.460
	0.960	0.214	0.340
	1.200	0.127	0.241
	1.440	0.069	0.152
	1.680	0.038	0.093
	1.920	0.000	0.042
11.0	0.000	0.529	0.504
	0.320	0.476	0.480
	0.640	0.374	0.413
	0.960	0.257	0.321
	1.280	0.170	0.250
	1.600	0.098	0.159
	1.920	0.055	0.101
	2.240	0.037	0.051
	2.560	0.000	0.019

Run 6 (D=0.375 inches)

Axial Position (nozzle diameters)	Radial Position (nozzle diameters)	V_z	T
4.0	0.000	0.965	0.893
	0.107	0.958	0.883
	0.213	0.925	0.844
	0.320	0.826	0.783
	0.427	0.673	0.707
	0.533	0.502	0.608
	0.640	0.359	0.510
	0.747	0.242	0.383
	0.853	0.147	0.277
	0.960	0.085	0.193
	1.067	0.047	0.115
8.0	0.000	0.716	0.634
	0.187	0.678	0.617

Table 9.9.4 (continued)

Axial Position (nozzle diameters)	Radial Position (nozzle diameters)	V_z	T
	0.373	0.573	0.567
	0.560	0.442	0.484
	0.747	0.333	0.399
	0.933	0.236	0.314
	1.120	0.159	0.233
	1.307	0.096	0.164
	1.493	0.066	0.111
	1.680	0.032	0.060
11.0	0.000	0.506	0.464
	0.267	0.469	0.448
	0.533	0.389	0.400
	0.800	0.301	0.333
	1.067	0.218	0.264
	1.333	0.148	0.200
	1.600	0.095	0.141
	1.867	0.065	0.090
	2.133	0.044	0.049
	2.400	0.000	0.021

Run 7 (D=0.375 inches)

Axial Position (nozzle diameters)	Radial Position (nozzle diameters)	V_z	T
4.0	0.000	0.969	0.899
	0.107	0.963	0.887
	0.213	0.933	0.848
	0.320	0.836	0.787
	0.427	0.679	0.705
	0.533	0.510	0.616
	0.640	0.358	0.506
	0.747	0.238	0.399
	0.853	0.143	0.290
	0.960	0.078	0.207
	1.067	0.000	0.124
6.0	0.000	0.897	0.777
	0.160	0.848	0.748
	0.320	0.727	0.678
	0.480	0.560	0.584
	0.640	0.407	0.482

Table 9.9.4 (continued)

Axial Position (nozzle diameters)	Radial Position (nozzle diameters)	V_z	T
	0.800	0.275	0.373
	0.960	0.179	0.276
	1.120	0.097	0.179
	1.280	0.057	0.106
	1.440	0.044	0.052
	1.600	0.000	0.022
8.0	0.000	0.733	0.638
	0.267	0.643	0.606
	0.533	0.471	0.501
	0.800	0.309	0.371
	1.067	0.170	0.260
	1.333	0.096	0.156
	1.600	0.045	0.075
	1.867	0.031	0.028
	2.133	0.000	0.011

Run 8 (D=0.375 inches)

Axial Position (nozzle diameters)	Radial Position (nozzle diameters)	V_z	T
3.0	0.000	0.968	0.919
	0.120	0.965	0.908
	0.240	0.947	0.874
	0.360	0.851	0.808
	0.480	0.635	0.699
	0.600	0.404	0.559
	0.720	0.225	0.410
	0.840	0.110	0.264
	0.960	0.024	0.151
	1.080	0.000	0.067
5.0	0.000	0.935	0.833
	0.160	0.902	0.806
	0.320	0.772	0.724
	0.480	0.596	0.632
	0.640	0.407	0.501
	0.800	0.260	0.380
	0.960	0.152	0.265
	1.120	0.073	0.167
	1.280	0.023	0.095

Table 9.9.4 (continued)

Run 9 (D=0.250 inches)

Axial Position (nozzle diameters)	Radial Position (nozzle diameters)	V_z	T
4.0	0.000	0.972	0.910
	0.140	0.957	0.887
	0.280	0.862	0.821
	0.420	0.692	0.731
	0.560	0.406	0.628
	0.700	0.318	0.486
	0.840	0.189	0.356
	0.980	0.096	0.244
	1.120	0.027	0.150
	1.260	0.000	0.059
8.0	0.000	0.728	0.664
	0.240	0.659	0.642
	0.480	0.521	0.558
	0.720	0.360	0.446
	0.960	0.238	0.331
	1.200	0.140	0.228
	1.440	0.070	0.144
	1.680	0.040	0.081
	1.920	0.000	0.033
11.0	0.000	0.526	0.505
	0.320	0.476	0.480
	0.640	0.367	0.412
	0.960	0.254	0.323
	1.280	0.174	0.236
	1.600	0.112	0.161
	1.920	0.065	0.088
	2.240	0.039	0.041
	2.560	0.017	0.017
	2.880	0.000	0.008

Table 9.9.4 (continued)

Run 10 (D=0.250 inches)

Axial Position (nozzle diameters)	Radial Position (nozzle diameters)	V_z	T
4.0	0.000	0.983	0.938
	0.140	0.972	0.920
	0.280	0.889	0.857
	0.420	0.710	0.770
	0.560	0.500	0.649
	0.700	0.319	0.524
	0.840	0.196	0.368
	0.980	0.100	0.255
	1.120	0.048	0.149
	1.260	0.000	0.077
8.0	0.000	0.762	0.697
	0.240	0.688	0.672
	0.480	0.540	0.591
	0.720	0.384	0.470
	0.960	0.250	0.349
	1.200	0.156	0.237
	1.440	0.080	0.149
	1.680	0.046	0.076
	1.920	0.000	0.027
11.0	0.000	0.563	0.540
	0.320	0.513	0.515
	0.640	0.404	0.443
	0.960	0.278	0.348
	1.280	0.194	0.253
	1.600	0.118	0.165
	1.920	0.065	0.092
	2.240	0.040	0.041
	2.560	0.028	0.013
	2.880	0.000	0.005

Table 9.9.5

The Variation of Velocity and Temperature in the Wall Jet

Run 3 (D=0.250 inches)

Radial Position (nozzle diameters)	Distance Above Plate (inches)	Velocity (ft./sec.)	Temperature (^{o}F)
4.0	0.000	0.00	200.0
	0.010	262.76	285.0
	0.060	203.20	165.2
	0.110	123.21	232.1
	0.160	65.51	189.8
	0.210	20.78	151.0
	0.260	0.00	124.0
	0.310	0.00	97.0
6.0	0.000	0.00	168.0
	0.010	181.92	229.8
	0.060	164.97	228.2
	0.110	112.34	209.2
	0.160	59.14	184.9
	0.210	0.00	153.0
	0.260	0.00	118.0
	0.310	0.00	96.0
8.0	0.000	0.00	146.0
	0.010	126.55	188.0
	0.060	126.65	189.0
	0.110	105.01	181.4
	0.160	72.13	171.8
	0.210	45.45	166.0
	0.260	0.00	137.0
	0.310	0.00	118.0
	0.360	0.00	110.0
10.0	0.000	0.00	132.0
	0.010	95.92	160.5
	0.060	101.68	167.4
	0.110	90.38	159.6
	0.160	74.11	153.7
	0.210	56.17	148.9
	0.260	37.44	136.0
	0.310	23.50	127.0
	0.360	0.00	114.0
	0.410	0.00	102.0
	0.460	0.00	94.0

Table 9.9.5 (continued)

Run 4 (D=0.250 inches)

Radial Position (nozzle diameters)	Distance Above Plate (inches)	Velocity (ft./sec.)	Temperature (^{o}F)
4.0	0.000	0.00	217.1
	0.010	371.86	295.7
	0.040	333.37	289.8
	0.070	258.55	269.2
	0.100	183.32	248.7
	0.130	124.07	221.1
	0.160	74.34	192.7
	0.190	38.39	167.0
	0.220	0.00	143.0
	0.250	0.00	122.0
6.0	0.000	0.00	178.2
	0.010	251.42	237.4
	0.060	229.03	236.3
	0.110	155.78	224.4
	0.160	77.85	200.7
	0.210	0.00	168.0
	0.260	0.00	134.0
	0.310	0.00	108.0
8.0	0.000	0.00	152.8
	0.010	174.90	192.9
	0.060	175.04	193.9
	0.110	141.62	187.7
	0.160	97.89	177.5
	0.210	48.40	162.9
	0.260	0.00	144.0
	0.310	0.00	124.0
	0.360	0.00	124.0
	0.410	0.00	97.0
10.0	0.000	0.00	136.3
	0.010	129.00	167.9
	0.060	137.59	170.8
	0.110	121.99	168.1
	0.160	97.54	163.5
	0.210	70.24	157.8
	0.260	44.71	147.9
	0.310	16.74	137.0
	0.360	0.00	135.0
	0.410	0.00	113.0
	0.460	0.00	103.0
	0.510	0.00	95.0

Table 9.9.5 (continued)

Run 5 (D=0.250 inches)

Radial Position (nozzle diameters)	Distance Above Plate (inches)	Velocity (ft./sec.)	Temperature (°F)
4.0	0.000	0.00	213.0
	0.010	334.76	288.7
	0.040	316.83	289.6
	0.070	248.31	278.6
	0.100	185.43	260.7
	0.130	126.59	245.0
	0.160	81.24	213.0
	0.190	49.09	288.7
	0.220	24.01	289.6
	0.250	0.00	278.6
	0.280	0.00	260.7
	0.310	0.00	245.0
6.0	0.000	0.00	177.7
	0.010	227.91	230.3
	0.050	222.23	232.5
	0.090	175.79	221.9
	0.130	120.21	210.1
	0.170	64.05	188.8
	0.210	12.07	162.0
	0.250	0.00	135.0
	0.290	0.00	114.0
	0.330	0.00	98.0
8.0	0.000	0.00	153.4
	0.010	160.99	189.3
	0.060	162.38	189.2
	0.110	136.24	185.8
	0.160	96.93	1775.
	0.210	57.76	159.9
	0.260	20.56	142.0
	0.310	0.00	123.0
	0.360	0.00	107.0
	0.410	0.00	96.0
10.0	0.000	0.00	136.7
	0.010	120.24	165.1
	0.060	125.19	167.0
	0.110	113.30	164.2
	0.160	92.44	159.5
	0.210	68.77	152.8

Table 9.9.5 (continued)

Radial Position (nozzle diameters)	Distance Above Plate (inches)	Velocity (ft./sec.)	Temperature (^{o}F)
	0.260	47.51	142.9
	0.310	26.31	132.0
	0.360	0.00	120.0
	0.410	0.00	110.0
	0.460	0.00	98.0

Run 6 (D=0.375 inches)

Radial Position (nozzle diameters)	Distance Above Plate (inches)	Velocity (ft./sec.)	Temperature (^{o}F)
4.0	0.000	0.00	199.0
	0.010	273.39	279.6
	0.050	268.88	275.8
	0.090	223.46	262.5
	0.130	171.71	247.0
	0.170	123.34	226.1
	0.210	85.86	204.6
	0.250	54.99	180.9
	0.290	27.02	159.0
	0.330	0.00	140.0
	0.370	0.00	122.0
	0.410	0.00	109.0
6.0	0.000	0.00	170.1
	0.010	183.34	223.7
	0.060	186.93	221.6
	0.110	160.72	217.3
	0.160	123.94	205.1
	0.210	83.95	289.6
	0.260	45.64	170.9
	0.310	0.00	149.0
	0.360	0.00	130.0
	0.410	0.00	113.0
8.0	0.000	0.00	151.2
	0.010	128.25	181.0
	0.060	134.08	181.8
	0.110	128.07	185.0
	0.160	113.49	183.2
	0.210	91.73	177.5
	0.260	70.17	172.8
	0.310	50.01	163.9

Table 9.9.5 (continued)

Radial Position (nozzle diameters)	Distance Above Plate (inches)	Velocity (ft./sec.)	Temperature (°F)
	0.360	29.50	155.0
	0.410	0.00	145.0
	0.460	0.00	132.0
	0.510	0.00	122.0
	0.560	0.00	113.0
	0.610	0.00	103.0
10.0	0.000	0.00	136.7
	0.010	98.12	159.4
	0.070	101.84	160.4
	0.130	102.80	163.4
	0.190	94.49	161.5
	0.250	80.99	158.7
	0.310	65.93	154.8
	0.370	50.91	150.9
	0.430	35.73	142.0
	0.490	23.63	133.0
	0.550	11.75	126.0
	0.610	0.00	117.0
	0.670	0.00	108.0
	0.730	0.00	101.0

Run 7 (D=0.375 inches)

Radial Position (nozzle diameters)	Distance Above Plate (inches)	Velocity (ft./sec.)	Temperature (°F)
4.0	0.000	0.00	218.5
	0.010	303.91	318.3
	0.040	289.09	320.6
	0.070	260.04	313.2
	0.100	211.03	299.9
	0.130	158.67	284.4
	0.160	105.14	263.4
	0.190	57.25	236.9
	0.220	0.00	208.0
	0.250	0.00	178.0
	0.280	0.00	150.0
	0.310	0.00	129.0
6.0	0.000	0.00	178.5
	0.010	182.02	233.7

Table 9.9.5 (continued)

Radial Position (nozzle diameters)	Distance Above Plate (inches)	Velocity (ft./sec.)	Temperature (°F)
	0.050	186.50	237.6
	0.090	167.60	233.1
	0.030	141.11	227.7
	0.170	107.72	217.3
	0.210	72.96	206.8
	0.250	39.10	191.0
	0.290	0.00	172.0
	0.330	0.00	155.0
	0.370	0.00	137.0
	0.410	0.00	122.0
8.0	0.000	0.00	156.8
	0.010	125.44	192.0
	0.060	127.35	193.0
	0.110	125.03	194.0
	0.160	111.29	192.3
	0.210	93.70	185.5
	0.260	71.38	178.8
	0.310	51.53	168.9
	0.360	29.46	157.0
	0.410	0.000	146.0
	0.460	0.00	133.0
	0.510	0.00	122.0
	0.560	0.00	112.0
10.0	0.000	0.00	140.7
	0.010	90.31	172.6
	0.060	98.31	174.4
	0.110	95.17	173.5
	0.160	86.04	171.6
	0.210	74.88	169.7
	0.260	62.85	163.8
	0.310	52.47	157.9
	0.360	39.69	151.0
	0.410	23.78	143.0
	0.460	0.00	135.0
	0.510	0.00	128.0
	0.560	0.00	119.0
	0.610	0.00	111.0

Table 9.9.5 (continued)

Run 8 (D=0.375 inches)

Radial Position (nozzle diameters)	Distance Above Plate (inches)	Velocity (ft./sec.)	Temperature (^{o}F)
4.0	0.000	0.00	240.0
	0.010	306.83	334.2
	0.040	298.88	335.6
	0.070	253.21	324.5
	0.100	196.01	307.4
	0.130	136.11	285.9
	0.160	82.37	256.7
	0.170	21.98	221.0
	0.220	0.00	183.0
	0.250	0.00	156.0
	0.280	0.00	130.0
	0.310	0.00	117.0
	0.340	0.00	107.0
6.0	0.000	0.00	186.0
	0.010	175.56	242.9
	0.050	178.61	244.8
	0.090	162.14	245.3
	0.130	133.51	238.9
	0.170	104.31	227.4
	0.210	71.50	215.8
	0.250	37.41	198.0
	0.290	0.00	181.0
	0.330	0.00	160.0
	0.370	0.00	141.0
	0.410	0.00	125.0
	0.450	0.00	114.0
8.0	0.000	0.00	161.0
	0.010	117.82	201.2
	0.060	124.96	202.0
	0.110	114.66	203.2
	0.160	98.32	200.5
	0.210	81.53	188.9
	0.310	36.86	179.0
	0.360	0.00	154.0
	0.460	0.00	142.0
	0.510	0.00	126.0
	0.560	0.00	116.0
	0.610	0.00	107.0

Table 9.9.5 (continued)

Radial Position (nozzle diameters)	Distance Above Plate (inches)	Velocity (ft./sec.)	Temperature (°F)
10.0	0.000	0.00	148.0
	0.010	94.99	177.5
	0.070	95.06	178.5
	0.130	95.78	177.5
	0.190	90.05	176.6
	0.250	80.05	171.7
	0.310	68.68	164.8
	0.370	52.59	156.9
	0.430	39.68	147.0
	0.490	26.53	137.0
	0.550	11.76	127.0
	0.610	0.00	117.0

Run 9 (D=0.250 inches)

Radial Position (nozzle diameters)	Distance Above Plate (inches)	Velocity (ft./sec.)	Temperature (°F)
4.0	0.000	0.00	233.0
	0.010	350.92	331.9
	0.040	319.48	332.6
	0.070	249.44	314.4
	0.100	179.02	290.9
	0.130	110.19	263.3
	0.160	65.68	230.8
	0.190	28.07	197.0
	0.220	0.00	166.0
	0.250	0.00	144.0
	0.280	0.00	123.0
	0.310	0.00	110.0
6.0	0.000	0.00	195.0
	0.010	240.18	265.9
	0.045	234.06	266.1
	0.080	208.53	259.0
	0.115	158.78	246.3
	0.150	107.82	232.3
	0.185	56.75	210.9
	0.220	0.00	181.0
	0.255	0.00	163.0
	0.290	0.00	134.0

Table 9.9.5 (continued)

Radial Position (nozzle diameters)	Distance Above Plate (inches)	Velocity (ft./sec.)	Temperature (°F)
	0.325	0.00	117.0
	0.360	0.00	104.0
8.0	0.000	0.00	169.0
	0.010	166.99	214.1
	0.050	163.61	218.2
	0.090	141.85	217.7
	0.130	112.90	213.2
	0.170	75.64	202.7
	0.210	45.05	190.9
	0.250	0.00	175.0
	0.290	0.00	156.0
	0.330	0.00	139.0
	0.370	0.00	127.0
	0.410	0.00	113.0
	0.450	0.00	103.0
10.0	0.000	0.00	150.0
	0.010	122.03	188.1
	0.060	124.73	190.0
	0.110	109.95	187.3
	0.160	86.71	180.6
	0.210	62.74	171.8
	0.260	36.62	162.0
	0.310	0.00	146.0
	0.360	0.00	133.0
	0.410	0.00	120.0
	0.460	0.00	109.0
	0.510	0.00	102.0

Run 10 (D=0.250 inches)

Radial Position (nozzle diameters)	Distance Above Plate (inches)	Velocity (ft./sec.)	Temperature (°F)
4.0	0.000	0.00	184.0
	0.010	319.94	249.4
	0.040	300.27	243.4
	0.070	238.19	228.9
	0.100	169.90	214.1
	0.130	109.91	191.3
	0.160	67.18	167.8

Table 9.9.5 (continued)

Radial Position (nozzle diameters)	Distance Above Plate (inches)	Velocity (ft./sec.)	Temperature (°F)
	0.190	31.36	146.0
	0.220	0.00	127.0
	0.250	0.00	110.0
	0.280	0.00	100.0
6.0	0.000	0.00	160.0
	0.010	221.80	212.5
	0.040	221.98	207.5
	0.070	198.20	204.3
	0.100	160.90	194.3
	0.130	119.41	181.1
	0.160	76.36	168.7
	0.190	37.63	151.0
	0.220	0.00	130.0
	0.250	0.00	116.0
	0.280	0.00	103.0
8.0	0.000	0.00	140.0
	0.010	151.91	175.5
	0.050	161.91	176.3
	0.090	147.54	171.6
	0.130	123.95	166.0
	0.170	94.18	157.5
	0.210	62.75	146.8
	0.250	33.24	136.0
	0.290	0.00	123.0
	0.330	0.00	110.0
	0.370	0.00	100.0
	0.410	0.00	97.0

10. BIBLIOGRAPHY

1. Abramovich, G. N., "Turbulent Jets Theory," Translation Report No. AD 283858, Armed Services Technical Information Agency, 1962.

2. Corrsin, S. and Uberoi, M. S., "Further Experiments on the Flow and Heat Transfer in a Heated Turbulent Air Jet," National Advisory Committee for Aeronautics Technical Note No. 1865, 1949.

3. Hinze, J. O. and Vander Hegge Zijnen, B. G., "Transfer of Heat and Matter in the Turbulent Mixing Zone of an Axially Symmetrical Jet," Applied Scientific Research, Section A, Vol. 1, (435-461) 1949.

4. Tollmien, W., "Calculation of Turbulent Expansion Processes," National Advisory Committee for Aeronautics Technical Memorandum No. 1085, September 1945.

5. Schlichting, H., "Boundary Layer Theory," McGraw-Hill Book Company, Inc., New York, 1955.

6. Kleinstein, G., "Mixing in Turbulent Axially Symmetric Free Jets," Journal of Spacecraft and Rockets, Vol. 1, No. 4, (403-408), July-August 1964.

7. Warren, W. R., "An Analytical and Experimental Study of Compressible Free Jets," PhD Thesis, Princeton University, 1957.

8. Pai, S. I., "Axially Symmetrical Jet Mixing of a Compressible Fluid," Quarterly of Applied Mathematics, Vol. 10, No. 2 (141-148), 1952.

9. Szablewski, W., "Turbulente Vermischung Runder Kaltluftstrahlen Mit Umgebender Ruhender Heissluft," International Journal of Heat and Mass Transfer, Vol. 6, (739-754), August 1963.

10. Cohen, N. S., "Additional Pyrogen Igniter Jet Flow Studies, 1. Analytical Developments," Report TM1SRO, Aerojet-General Corporation, Sacramento, California, June 1964.

11. Abbott, M. R., "Axially Symmetric Steady Motion of a Viscous Incompressible Fluid: Some Numerical Experiments," Computer Journal, Vol. 7, (47-53), April 1964.

12. Lapidus, L., "Digital Computation for Chemical Engineers," McGraw-Hill Book Company, Inc., New York, (254-255), 1962.

13. Wegstein, J. H., "Accelerating Convergence of Iterative Processes," Communications of the Association for Computing Machinery, Vol. 1, No. 6, (9-13), June 1958.

14. Hwang, C. L. and Fan, L. T., "Finite Difference Analysis of Forced-Convection Heat Transfer in Entrance Region of a Flat Rectangular Duct,"Applied Scientific Research, Section A, Vol. 13, (401-422), 1965.

15. Perry, K. P., "Heat Transfer by Convection from a Hot Gas Jet to a Plane Surface," Proceedings of the Institute of Mechanical Engineers, Vol. 168, (775-784), 1954.

16. Vickers, J. M. F., "Heat Transfer Coefficients Between Fluid Jets and Normal Surfaces," Industrial and Engineering Chemistry, Vol. 51, No. 8, (967-972), August 1959.

17. Kezios, S. P., "Heat Transfer in the Flow of a Cylindrical Air Jet Normal to an Infinite Plane," PhD Thesis, Illinois Institute of Technology, 1956.

18. Schauer, J. J. and Eustis, R. H., "The Flow Development and Heat Transfer Characteristics of Plane Turbulent Impinging Jets," Technical Report No. 3, Department of Mechanical Engineering, Stanford University, October 1963.

19. Van der Hegge Zijnen, B. G., "Measurements of the Velocity Distribution in a Plane Turbulent Jet of Air," Applied Scientific Research, Section A, Vol. 7, (256-277), 1958.

20. Snedecker, R. S. and Donaldson, C. duP., "Experiments on Free and Impinging Underexpanded Jets from a Convergent Nozzle," Report No. AD 461622, Defense Documentation Center for Scientific and Technical Information, 1964.

21. Strand, T., "On the Theory of Normal Ground Impingement of Axi-Symmetrical Jets in Inviscid Incompressible Flow," American Institute of Aeronautics and Astronautics Paper No. 64-424, First American Institute of Aeronautics and Astronautics Annual Meeting, Washington, June 1964.

22. Slezkin, N. A., "On the Impingement of a Plane Gaseous Jet onto an Infinite Wall," (In Russian), Institute of Mechanics Academy of Sciences, Union of Socialist Soviet Republics Applied Mathematics and Mechanics, Vol. 16, 1952.

23. Leclerc, A., "Deviation d'un Jet Liquide par une Plaque Normale a son Axe," Houille Blanche, (816-821), 1950.

24. Schrader, H., "Trocknung feuchter Oberflachen mittels Warmluftstrahlen. Stromungsvorgange und Stoffubertragung," Forschung Auf Dem Gebiete Des Ingenieur-Wesens, Vol. 27, (64), 1961.

25. Tani, I. and Komatsu, Y., "Impingement of a Round Jet on a Flat Surface," Proceedings of the Eleventh International Congress of Applied Mechanics, Munich, (672-676), August 1964.

26. Kemp, N. H., Rose, P. H., and Detra, R. W., "Laminar Heat Transfer Around Blunt Bodies in Dissociated Air," Journal of the Aero-Space Sciences, Vol. 26, (421-430), July 1959.

27. Fay, J. A. and Riddell, F. R., "Theory of Stagnation Point Heat Transfer in Dissociated Air," Journal of the Aeronautical Sciences, Vol. 25, No. 2, (73-85), February 1958.

28. Lees, L., "Laminar Heat Transfer Over Blunt-Nosed Bodies at Hypersonic Flight Speeds," Jet Propulsion, Vol. 26, No. 4, (259-269), April 1956.

29. Scarborough, J. B., "Numerical Mathematical Analysis," The John Hopkins Press, Baltimore, 1958.

30. Prandtl, L., "Uber den Reibungswiderstand Stromender Luft," Aerodynamischen Versuchsanstalt Gottingen, III Lieferung, Munchen-Berlin, 1927.

31. Foerthmann, E., "Turbulent Jet Expansion," National Advisory Committee for Aeronautics Technical Memorandum 789, March 1936.

32. Reichardt, H., "Gesetzmassigkeiten der freien Turbulenz," Verein Deutscher Ingenieure-Forschung sheft 414, Verein Deutscher Ingenieure-Verlag, Berlin, 1942.

33. Anderson, J. E., and Stresion, E. F., "Heat Transfer From Flames Impinging on Flat and Cylindrical Surfaces," Transactions of the American Society of Mechanical Engineers, Series C - Journal of Heat Transfer, Vol. 85, No. 1, (49-54), February 1963.

34. Gardon, R. and Akfirat, J. C., "The Role of Turbulence in Determining the Heat-Transfer Characteristics of Impinging Jets," International Journal of Heat and Mass Transfer, Vol. 8, (1261-1272), 1965.

35. Smirov, V. A., Verevochkin, G. E., and Brdlich, P. M., "Heat Transfer Between a Jet and a Held Plate Normal to Flow," International Journal of Heat and Mass Transfer, Vol. 2 (1-7), 1961.

36. "Engineering Properties of Inconel Alloy 600," Technical Bulletin T-7, Huntington Alloys Products Division, The International Nickel Company, Inc., Huntington, West Virginia, 1962.

37. Rayle, R. E., "An Investigation of the Influence of Orifice Geometry on Static Pressure Measurements," MS Thesis, Massachusetts Institute of Technology, 1949.

38. Stickney, T. M., "Recovery and Time-Response Characteristics of Six Thermocouple Probes in Subsonic and Supersonic Flow," National Advisory Committee for Aeronautics, Technical Note 3455, July 1955.

39. "Thermocouples for High Accuracy Gas Temperature Measurements," Product Information Report No. 3.13, Aero Research Instruments, Chicago, Illinois, 1962.

40. Kiel, G., "Total Head Meter with Small Sensitivity to Yaw," National Advisory Committee for Aeronautics, Technical Memorandum 775, 1936.

41. Bird R., Steward, W. E., and Lightfoot, E. N., "Transport Phenomena," John Wiley and Sons, Inc., New York, 1960.

42. Eckert, E. R. G., and Drake, R. M., "Heat and Mass Transfer," McGraw-Hill Book Company, Inc., New York, 1959.

43. Hilsenrath, J., et. al., "Tables of Thermal Properties of Gases," National Bureau of Standards Circular 546, United States Government Printing Office, Washington, November 1955.

44. "United Sensor and Control Corporation Catalogue," United Sensor and Control Corporation, East Hartford, Connecticut, 1965.

11. Vita

Biographical items on the author of the dissertation.

Mr. J. F. Tomich:

1) Born November 23, 1940.

2) Attended Belleville Junior College September 1958 to June 1960.

3) Attended Washington University September 1960 to June 1962. Received Bachelor of Science in Chemical Engineering June 1962.

4) Chemical Engineer, Monsanto Company, Summer 1961 and 1962.

5) Attended Washington University September 1962 to present date. Awarded Washington University Graduate Fellowship in the academic year 1962-1963. National Aeronautics and Space Administration Trainee in the academic years 1963-1964, 1964-1965, and 1965-1966.

6) Chemical Engineer, Monsanto Company, Summer 1963.

7) Membership in Professional Societies: Alpha Chi Sigma, Sigma Xi, Tau Beta Pi.

January, 1967

SEVER INSTITUTE OF TECHNOLOGY
Doctor of Science Degree

DISSERTATION ACCEPTANCE

Three copies of this form must be turned in to the Sever Office not later than January 15 or May 15 of the proper semester. In addition, the Chairman of the Doctoral Committee and two additional members of the Sever faculty, including the supervisor, if different from the Chairman of the Doctoral Committee, will present in writing separate dissertation reports, or one common report, to the Director. The reports are attached to this form.

Date September 14, 1966

The dissertation of John F. Tomich

entitled HEAT AND MOMENTUM TRANSFER FROM COMPRESSIBLE TURBULENT JETS OF HOT AIR IMPINGING NORMALLY ON A SURFACE

has been examined by the undersigned committee of three faculty members and has received full approval for acceptance in partial fulfillment of the requirements for the degree, Doctor of Science.

format O.K. JMD

Signed Eric Weger
Chairman of Doctoral Committee

Committee:
J. M. Swanson
James E. Nelson